A thesis submitted in the fulfilment of the requirement of the Degree of Doctor Philosophiae

in the

Doctoral School of Science and Engineering

From the University of Cergy-Pontoise

and

Department of Chemistry, Faculty of Science

From the University of the Western Cape

Speciality: Physical and Analytical Chemistry

Metallic nanoparticles with polymeric shell: A multifunctional platform for application to biosensor

Presented by

Xolani Terrance Ngema

On the 30 March 2018 before the jury composed of:

President, Referee:	Prof Fethi Bedioui	UTCBS, Université Paris Descartes
Referee:	Dr Guillaume Herlem	NIT, Université de Franche-Comté
Examiners:	Dr Nicole Jaffrezic	ISA,Villeurbane
	Dr Alain Pailleret	LISE, Université Pierre et Marie CURIE
Thesis supervisors:	Prof Priscilla Baker	SensorLab, University of the Western Cape
	Prof Pierre-Henri Aubert	LPPI, Université de Cergy-Pontoise
Co-supervisors:	Dr Fanelwa Ajayi	SensorLab, University of the Western Cape
	Dr Philippe Banet	LPPI, Université de Cergy-Pontoise

ACKNOWLEGDEMENTS

I would like to acknowledge the University of the Western Cape, Science Faculty, Department of Chemistry, SensorLab (South Africa) and the University of Cergy-Pontoise, Science and Engineering, Laboratoire de Physico-chimie des Polymères et des Interfaces (France) for granting me the opportunity to persue my Doctoral degree and providing all the necessary equipment and materials required for my research. I would also like to acknowledge the President of the Université Paris Seine, Mrs Anne-Sophie Barthez, and the Deputy Vice Chancellor Research and Innovation of the University of the Western Cape Prof Jose Frantz, for approving the joint supervision of this thesis.

Supervisors: Prof Pierre-Henri Aubert, Prof Priscilla Baker, Dr Philippe Banet and Dr Fanelwa Ajayi, thank you so much for your patience and believing in me, always giving all your academic guidance and shape to this research project.

To my beloved mother Zanele Nxumalo, thank you so much for your support, love and always trusting my decisions. To my grandmothers Ntombana Ngema and Betina Simelane thank you for your prayers and always pouring words of wisdom into my life. To my family and friends, thank you for your support and always believing in me.

SensorLab Colleagues: Thank you for your contribution to this work and your support is highly valued.

LPPI colleagues: Thank you for welcoming me with your warm hands and making my stay in France pleasant.

LIST OF PUBLICATIONS

Xolani Terrance Ngema, Meryck Ward, Siyabulela Hamnca, Priscilla Gloria Lorraine Baker, Emmanuel Iheanyichukwu Iwuoha. Spectro-Electrochemical of Detection Anthracene at Electrodeposited Polyamic Acid Thin Films. Journal of Nano Research, 44, 63-78 (2016)

Francis N. Muya, **Xolani Terrance Ngema**, Priscilla G. L. Baker Priscilla Gloria Lorraine Baker, Emmanuel Iheanyichukwu Iwuoha. Sensory Properties of Polysulfone Hydrogel for Electro-Analytical Profiling of Vanadium and Selenium in Aqueous Solutions. Journal of Nano Research, 44, 142-157 (2016)

Siyabulela Hamnca, Meryck Ward, **Xolani Terrance Ngema**, Priscilla Baker, Emmanuel Iheanyichukwu Iwuoha. Development of Graphenated Polyamic Acid Sensors for Electroanalytical Detection of Anthracene. Journal of Nano Research, 43, 11-22 (2016)

Lucian-Gabriel Zamfir, Lucian Rotariu, Virgil Emanuel Marinescu, **Xolani T. Simelane**, Priscilla G.L. Baker, Emmanuel I. Iwuoha, Camelia Bala. Non-enzymatic polyamic acid sensors for hydrogen peroxide detection. Sensors and Actuators B: Chemical, 226, 525-533 (2016)

TABLE OF CONTENTS

LIST OF FIGURES

LIST OF TABLES

LIST OF ABBREVIATION

A60 – Mycobacterium bovis antigen complex

Ab – Antibody

AFM – Atomic force microscopy

Ag – Antigen

Ag85B – Antigen 85B Mycobacterium

AgNPs – Silver nanoparticles

CFP-10 – 10-kDa culture filtrate protein

CV – Cyclic voltammetry

CYP – Cytochrome P450 enzyme

CYP2E1 – Cytochrome P450-2E1 enzyme

DPV – Differential pulse voltammetry

DR – Drug-resistant

DR-TB – Drug-resistant tuberculosis

DST – Drug Susceptibility Testing

ELISA – Enzyme-linked immunosorbent assay

ESTAT6 – 6-kDa early secretory antigenic target

ETH – Ethambutol

GCE – Glassy carbon electrode

HIV – Human immunodeficiency virus

HRP – Horseradish peroxide

LAM – Lipoarabinomannan

MDR – Multidrug-resistant

MDR-TB – Multidrug-resistant tuberculosis

MGIT – Mycobacteria growth indicator tube

MTB – Mycobacterium tuberculosis

MTBC – Mycobacterium tuberculosis complex

PAA – Polyamic acid

PPy – Polypyrrole

QFT – Quantiferon

RIF – Rifampicin

SEM – Scanning electron microscopy

SWV – Square wave voltammetry

TAT – Turnaround time

TB – Tuberculosis

TMB – 3,3'5,5'-tetramethylbenzidine

WHO – World Health Organization

XDR – Extensively drug-resistant

XDR-TB – Extensively drug-resistant tuberculosis

General Introduction

This research work focuses on advances, directions and strategies in the development of a simple, cheap and ultra-sensitive electrochemical immunosensor and biosensor for the detection of the tuberculosis disease and anti-tuberculosis drugs. Tuberculosis (TB) is a potentially serious infectious disease that mainly affects the lungs. Many strains of tuberculosis resist most of the drugs used to treat the disease. People with active tuberculosis are required to take several types of medications for 6 to 9 months to eradicate the infection and prevent development of drug resistance. One more reason tuberculosis remains a major problem is the increase in drug-resistant strains of the bacterium. However, the drug-resistant strains are man-made. The treatment of the disease is provided with information, supervision and support to the patient by a health worker or trained volunteer. Without such support, treatment adherence can be difficult and the disease can spread in which some result in drug-resistant strains. It is also widely recognised that the poorer the community, the greater the likelihood of being infected with the TB disease. A lack of basic health services, poor nutrition and inadequate living conditions all contribute to the spread of TB. Therefore, cheaper methods of detecting tuberculosis and drug-resistant strains are needed. To achieve this, biomarkers can be used for diagnosis of the disease since other sources have major variants in combination with clinical methods of disease detection and treatment. These biomarkers can allow the monitoring of the disease by revealing their biological states. Electrochemistry methods may offer a novel way to detect airbone particles containing tuberculosis disease. The electrochemical methods such as cyclic voltammetry (CV), square wave voltammetry (SWV) and differential pulse voltammetry are famously used for the development of electrochemical devices such as immunosensors and biosensors. The electrochemical techniques are essential for the characterization of the electroactive species, the study of the electrochemical reactions and direct electron transfer of enzymes at the electrode surfaces as well as in the detection of analytes by incorporation of biological recognition elements such as enzymes, antibodies/antigens etc. Different biological elements may be combined with different kinds of transducers provided that the reaction of biological element with the substrate can be monitored. On the basis of the transducing element, biosensors are broadly classified as electrochemical immunosensors, enzyme electrodes and microbial electrodes depending on whether an antibody, an enzyme, or microbe is used as the principal biological constituent of the recognition layer. Nanoparticles are also an important aspect in the development of biosensors. And using nanoparticles, improvements are being seen in the sensitivity and

performance of the biosensors. Hence, nanoparticles will be used as part of the transducer for biosensor development.

Chapter one presents the history of tuberculosis (TB), the introduction into what tuberculosis is and the impact of the spread of TB has on human beings. It also highlights the various strategies used for the detection of biomarkers for tuberculosis such as enzyme-linked immunosorbent assay (ELISA). The current TB diagnostic tools used in health care departments are also highlighted in this chapter. The electrochemical sensors developed for detection of tuberculosis and their respective performances are also motioned. The electrochemical sensors based on cytochrome P450 enzymes recognition events are described based on different output signals. This section also entails the use of the nanoparticles for cytochrome P450-based biosensor development.

Chapter two presents the characterization of immunosensor platforms and detection of *Mycobacterium tuberculosis* using indirect ELISA method and electrochemical immunosensor.

Chapter three presents the characterization of polyamic acid and polyprrole thin films and polyamic acid and polypyrrole composites platforms.

Chapter four presents the immobilization of cytochrome P450 enzyme on polyamic acid and polyprrole thin films and polyamic acid and polypyrrole composites platforms and the detection of anti-TB drugs (ethambutol and rifampicin).

Chapter five presents the combined conclusion of the thesis work with recommendations and future work.

Annex presents the experimental work done for the development of electrochemical immunosensor and biosensor for the detection of tuberculosis and anti-TB drugs, respectively. It also gives a description on the electrochemical and analytical techniques used for the characterization of the electrochemical immunosensor and biosensor platforms.

Chapter One

This chapter gives a brief background on the latest statistics of individuals infected by tuberculosis, history of tuberculosis (TB), transmission of tuberculosis, diagnostic methods for tuberculosis, ELISA protocols, TB antigens commonly used for ELISA, first-line anti-TB drugs, drug-resistance, and electrochemical sensors for TB detection and drug-resistance. The problem statement gives the limitations of using the available diagnostic methods and how crucial it is to have cheap diagnostic systems that can detect and monitor tuberculosis and multidrug-resistance. The research project framework give details about how the immunosensor and biosensor strategies will be developed for the detection of tuberculosis and anti-TB drugs, respectively.

1.1 Introduction

Nowadays, the analysis and the detection of tuberculosis (TB) pathogen, as well as prevention, early treatment and therapy of the disease are significantly important for better health care. Six million cases of TB were reported in 2014 which included those being infected with HIV as well [1]. The global health report of 2015 estimated that over 9.6 million people developed TB and 1.5 million died from the infectious disease of which 12 % were co-infected with HIV [2]. From the total numbers, 5.4 million were men, 3.2 million were women and approximately 1 million were children. The consequence of this shows that 37 % of the new cases went undiagnosed and therefore, these cases were not reported. An astonishing number of 1.2 million new cases of TB co-infected with HIV was reported of which 75 % were reported for the African continent. In South Africa, about 0.8% of the population of about 54 million develop active TB disease each year [3]. The number of undiagnosed cases comes with certain errors, due to the diagnostic systems are not yet fully in place (in the poorer or developing countries). A large number of TB cases are left unknown without any reporting and results in no treatment. There are various methods of combing the collective information on the degree of the spread of this disease. The main methods used to predict or estimate TB incidence are based on case notifications through expert opinion, prevalence survey, case notifications through standard adjustments and capture-recapture. Most of the poor countries and developing countries utilize case notifications data and combining expert opinions on the detection gaps. This provides a reasonable estimation of TB incidences. When this information from the different parts of the world is combined, it shows that the various regions have different strains of the bacteria.

1.2 Tuberculosis History

Tuberculosis (TB) is an airborne disease caused by *Mycobacterium tuberculosis* (MTB) that usually affects the lungs leading to severe coughing, fever and chest pains. The other four closely related mycobacteria responsible for tuberculosis are: *Mycobacterium bovis* (*M. bovis*), *Mycobacterium africanum* (*M. africanum*), *Mycobacterium microti* (*M. microti*) and *Mycobacterium. Canetti* (*M. Canetti*) [4]. According to the study of *Mycobacterium tuberculosis* complex DNA from an extinct Bison dated 1700 years before the present by Rothschild and co-workers, it is believed that *Mycobacterium tuberculosis* organisms were widespread in bovids that immigrated to North America over the Bering Strait connection and widespread during the late Pleistocene [5]. The Holarctic distribution (which is the terrestrial ecozone that

encompasses the majority of habitats found throughout the northern continents of the world) and bovids were suspected as the likely vector and reservoir for dispersion of tuberculosis. Therefore, since cattle were suspected to be infected with tuberculosis, contaminated milk was regarded as a major transmission route to humans. *Mycobacterium bovis* was then regarded as a pathogen that may penetrate the gastrointestinal mucosa or invade the lymphatic tissue of the oropharynx when ingested in milk from diseased cows [6]. The human infection with *M. bovis* decreased significantly in developed countries as a result of the pasteurization of milk and effective TB control amongst cattle. Infection with the other organisms is relatively rare. In other studies, the Greek physician Hippocrates gives a clear description of kyphosis (curvature of the spine that causes the top of the back to appear more rounded than normal**)** through accurate observations, proclaiming that the result of disease can occur above or below the diaphragm, and it is associated with hard tubercles in the lungs, and abscesses in the lumbar region [7]. Based on previous findings, which includes the visual appearance, radiology, and a limited number of microscopic and histological investigations, Donoghue concluded that TB definitely occurred in ancient populations but it was comparatively rare. The earliest cases recognized were from Neolithic times, with the hypothesis that TB was associated with animal domestication and that human TB originated from *M. bovis* became widely accepted [8–10]. Gómez review clearly indicates that many papers were published about paleopathology of TB, but most of them offer gross descriptions and have no safe chronology [11]. Hence, this brief history of TB only touches on what is TB and how it was realized as a human pathogen.

1.3 Transmission of Tuberculosis

TB is usually spread from person-to-person through the air by droplet nuclei (approximately 5 microns) that are produced when a person with pulmonary or laryngeal tuberculosis coughs, sneezes, talks or sings [12]. Droplet nuclei may also be produced by aerosol-producing investigations such as sputum induction, bronchoscopy and through manipulation of lesions, processing of tissue or secretions in the laboratory [13]. The three factors that determine the likelihood of transmission of MTB are: (i) number of organisms expelled into the air, (ii) concentration of organisms in the air (determined by the volume of the space and its ventilation), (iii) and the length of time an exposed person breathes the contaminated air. Transmission generally occurs indoors, in dark, poorly ventilated spaces where droplet nuclei stay airborne for a long time. Direct sunlight quickly kills tubercle bacilli, but they can survive

in the dark for several hours. This explains why the ancient treatment for tuberculosis was to travel to warmer climate; preferably warmer and drier like Egypt [14]. Close contact and prolonged exposure increases the risk of transmission. Once infected, the progression to active disease is dependent on the immune status of the individual. In those with normal immunity, 90% will not progress and only 10% will develop active disease. The risk is highest in the first two years after infection, when half the cases will occur. Those most at risk include children who are below 5 years of age and the elderly. People with suppressed immunity are more likely to develop active TB than those with normal immunity; 50-60% of HIV positive people infected with TB will go on to develop active disease [1]. The annual risk of TB in an HIV positive person is 10% compared to a lifetime risk of 10% in a healthy individual. Immunosuppressive conditions such as silicosis, diabetes mellitus, and prolonged use of corticosteroids and other immunosuppressive drugs, also increase the risk of progression to active TB. On the other developed studies, it has been realized that TB is a major occupational hazard for healthcare workers worldwide [15]. The transmission risk to healthcare workers is elevated when patients have unrecognized TB or are receiving inappropriate treatment [16]. However, many other factors influence the risk of transmission and progression to active disease, including healthcare setting, occupational category, individual susceptibility or immune status, and the adequacy of TB infection control measures.

1.4 Diagnostic methods for tuberculosis

One of the diagnostic tests that have emerged following the WHO recommendations issued in December 2010 is Xpert MTB/RIF. It has been quickly adopted by countries as an effective tool for the rapid detection of TB and drug resistance at lower levels of the health system. LED microscopy, culture (liquid and solid), phenotypic drug susceptibility testing (DST) and molecular microscopy probe line assay are also endorsed by WHO. Five of the diagnostic methods for TB are summarized hereafter: tuberculin skin test is the simple test to use. Sputum smear microscopy is one of the techniques that has been used for centuries, while Xpert/MTB/RIF test being endorsed as a new rapid, automated nucleic acid and amplification test. The LAM and Quantiferon (QFT)-TB assay are enzyme-linked immunosorbent assays. There are many diagnostic methods for TB and the five summarized were not chosen on the basis whether these diagnostic methods have better efficiency than the other methods. However, this was to give an overview about what is common with these diagnostic methods and why there is still a need to find new diagnostic methods for TB.

1.4.1 Tuberculin skin test

The tuberculin skin test is mainly used for diagnosis of latent TB infection. In this test (Figure 1), tuberculin (a protein extract from tubercle bacillus cultures) is injected (0.1 mL) into the skin on the arm and it takes up to 2 days for the occurrence of a reaction between the tuberculin and the immune system to react [17]. This results in an inflamed response which produces a firm red bump at the area of the injection. This firm red bump or positive test shows that the individual has been exposed to the TB bacterium and additional testing is required to confirm the state of the infection. A negative test shows the individual have not been previously exposed to MTB or the immune system had no reaction with the tuberculin protein. In the case of positive skin test, it is not possible to tell how long an individual have been infected with TB but chest X-ray on the lungs is done to determine if the immune system has reacted with MTB which shows white spots on the lungs [18]. Thereafter, if X-ray shows the presence of the MTB, sputum tests are carried out whereby the samples of sputum are tested for proteins and gene markers of *Mycobacterium tuberculosis*. False-negative reactions may also occur in case of recent TB infection, cutaneous anergy (anergy: the inability to react to skin tests because of a weakened immune system), recent live-virus vaccination, and very old TB infection but they are not the limitations.

Figure 1: How to perform the tuberculin skin test

1.4.2 Sputum smear microscopy test

Sputum smear microscopy has been one of the primary method for diagnosis of TB for a century developed by Ziehl-Neelson based on visualization of bacteria through a light microscope [19]. It is a simple, inexpensive and rapid technique which is widely used in areas

with a very high prevalence of TB. The MTB cells are dropped and air-dried on a glass slide followed by acid wash to remove carbol fuchsin. The cells are then stained with methylene blue and viewed under the light microscope. The technique is relatively simple, inexpensive and rapid but it suffers from an optimum sensitivity of 60 % and incapability to differentiate between MTB complex and non-MTB as wells as not identifying smear negative samples [20]. It also has a poor track of record in extra-pulmonary TB and in patients co-infected with HIV and tuberculosis due to the reduced pulmonary bacillary loads in these patients. It has been found that fluorescent microscopy has a better sensitivity than smear microscopy by 10% but additional data on specificity and on the clinical consequences associated with false positive results are needed to guide implementation of this technology in high HIV prevalence settings [21].

1.4.3 Xpert/MTB/RIF test

Xpert MTB/RIF (Figure 2) is a rapid, automated, cartridge-based and highly selective nucleic acid amplification diagnostic test for MTB and mutations on the rpo B gene for rifampicin resistance within 2 hours of collection [22]. The Mycobacterium tuberculosis from sputum samples are used to isolate the relevant DNA material and amplified through polymerize chain reaction and then detected with fluorescent molecular beacons. This diagnostic system was endorsed by the World Health Organisation in 2011. By the end of December 2014, a total of 3 763 GeneXpert instruments comprising 17 883 modules were procured in the public sector in 116 of the 145 countries eligible for concessional pricing. In 2014, 4.8 million test cartridges were procured by eligible countries, up from 550 000 in 2011. Some of these cartridges, 51% (2.4 million) went to South Africa. The system is automated with minimal extensive skills required. The system is based on a microfluidic, PCR chamber and fluorescent detector integrated system. In some developed studies, the diagnostic system have produced sensitivities of 75 % and 98.7 % for sputum smear negative and sputum smear positive respectively which is far superior to previous diagnostic tools [23]. This technique has a significant accuracy values where it detects 67 % of missed smear microscopy patients and 98 % rifampicin susceptible patients [24]. The main disadvantage of XPERT MTB/RIF is the cost per cartridge.

Figure 2: The Cepheid Xpert system and MTB/RIF test cartridge for the molecular detection of MTB

1.4.4 The LAM test

The urinary antigen detection is an immune-based marker particularly for in co-infected patients with TB and HIV, where sputum is rare. The lipoarabinomannan antigen (LAM) is a heart stable glycolipid specific to mycobacteria that is released by metabolically active bacteria, filtered by the kidney and found in the urine of patients with active TB. The Alere Determine TB LAM Ag test (Figure 3) was developed as a point-of-care diagnostic test for diagnosis of TB. It is based on an immune-chromatographic strip that requires only 60 µL of sample (urine) and provides a result within 25 min. The sensitivity of the LAM strip initially ranged from 38 to 51 %, but the recent studies shows that it is now at about 60 % with a specificity above 95 % [25]. This point of care system has also shown to detect up to 50 % of smear-negative and sputum scarce patients. There is a potential for further development and simplification, resulting in a lateral flow test. The lateral flow test is not as sensitive as the Xpert MTB/RIF, but its applications are vast. And the other advantages; the lateral flow test is cheaply available, easy to operate and quick output of results [26].

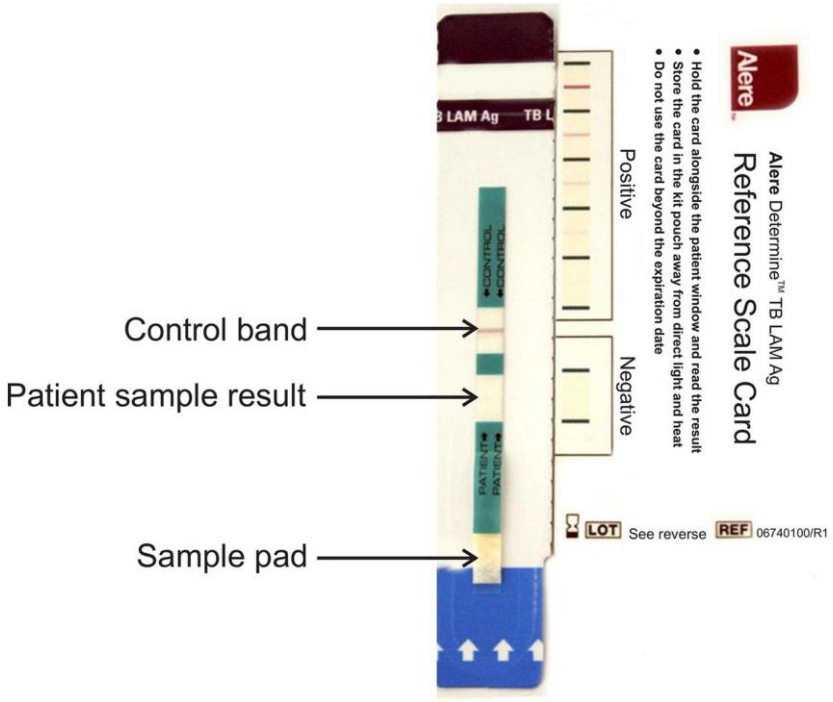

Figure 3: The Alere Determine TB LAM Ag test

1.4.5 Interferon gamma assay test

Quantiferon (QFT)-TB assay test is one of the diagnostic tools that measure interferon gamma released during infection of MTB. Interferon-gamma release assays are immunodiagnostic tests that detect and quantify T-cell induced IFN-γ release into the blood. The release of IFN-γ is stimulated by specific TB antigens, ESAT-6 and CFP-10. The newer version of the test is Quantiferon-TB Gold InTube assay which has a simpler sample preparation and is further enhanced by the addition of the antigen called TB7.7. The mycobacteria are injected into blood samples to stimulate T-cells to produced IFN-γ which is measured via optical density through enzyme-linked immunosorbent assay [19]. The captured IFN-γ are incubated on QFT ELISA plates (already coated with recognition layer) and measured through enzyme-substrate reaction and the absorbance recorded at 450 nm [27]. A major consequence is that the QFT cannot distinguish between latent and active tuberculosis. Below is the table (Table 1) that summarizes the efficiency of the current diagnostic tests for tuberculosis.

1.4.6 Summary of diagnostic methods for tuberculosis

Table 1: Summary of properties of the current diagnostic tests for MTB pathogen

Diagnostic test	Advantage	Drawback	Sensitivity	Reference
Tuberculin Skin Test	Simple, Cheap and readily available	Mycobacterium Specificity; Zero differentiation between latent and active TB		17
Liquid (MGIT) Solid	High sensitive	Long TAT High contamination rates (liquid culture)	87.7%, 89.7%	2
Sputum Smear Microscopy	Rapid, Inexpensive	Low Sensitivity	60%	20
Expert MTB/RIF	High sensitivity, rapid output	Expensive cartridges	69%	23
Alere Determine TB LAM Ag	High specificity	Low Sensitivity, High inter-reader variability	44 – 83 %	26
QuantiFERON-TB Gold-in Tube	Highly Specific for IFN-γ. Expensive ESAT-6 and CFP-10 peptides	Poor distinguish between latent and active TB. High Cost	80 %	19

The drawbacks of these diagnostic tests vary with each diagnostic method, however, all of them suffer from failing to distinguish between latent and active TB except the Expert MTB/RIF which is expensive and need trained personnel. In addition, available diagnostic method are time consuming and expensive to use. Due to these disadvantages, there is a need of simple and cheap methods that can simplify such problems. The LAM and interferon gamma ELISA TB diagnostic tests are a promising start to such developments. Indeed, the ELISA methods to detect TB are cheap and easy to use compared to TB culture methods. Moreover, these methods do not rely on sputum in order to detect the presence of tuberculosis. The immune recognition principle used in ELISA methods can be adopted to develop immunosensors with other

transduction principles to implement the ELISA methods making it rapid and reliable. In the immunosensor design, the sensing element is formed by means of immobilization of antigen or antibody and the binding event is transformed into a measurable signal by the transducer. The following section describes different ways to combine antibody/antigen interactions to develop ELISA tests.

1.5 ELISA protocols

1.5.1 Enzyme-linked immunosorbent assay

The enzyme-linked immunosorbent assay (ELISA) is typically performed to detect the presence and/or amount of a target protein of interest within an experimental sample. ELISA method was invented simultaneously by two research teams [28]. However, ELISA method was instigated largely by the Swiss scientists Engvall, and Perlmann [29]. These two researchers developed the ELISA method in 1971 by modifying the radioimmunoassay (RIA) method. The basic ELISA is distinguished from other antibody-based assays because separation of specific and non-specific interactions occurs via serial specific binding to a solid surface, usually a polystyrene multi-well plate coated with antigens and/or antibodies through a series of incubation and washing steps, the last one being linked or conjugated to an enzyme. The addition of an enzyme substrate-chromogen reagent causes color to develop. This color is directly proportional to the amount of bound sample antibody. The more antibody present in the sample, the stronger the color development in the test wells. When exposed to a substrate, antibody-bound enzyme will cause a color change, thereby indicating the presence of the protein of interest in the sample. There are four types of ELISA assays: direct ELISA, indirect ELISA, competitive ELISA and sandwich ELISA and each method has its own sequence of binding. As outlined previously, ELISA has wide application to development of analytical methods for detection of Mycobacterium antibodies in tuberculosis, rotavirus in feces, enterotoxin of *E. coli* in feces, HIV antibodies in blood and pesticides residues because it can very sensitively and very accurately determine them in samples. It remains the most versatile method among various immunoassays. The direct competitive ELISA (dc-ELISA) and indirect competitive ELISA (ic-ELISA), are generally used for ELISAs intended for the evaluation of neonicotinoid insecticides.

1.5.2 Types of ELISA

1.5.2.1 Direct ELISA

The direct ELISA (Figure 4) uses a primary antibody conjugated with an enzyme that binds directly to the antigen. Direct detection can be performed with antigen that is immobilized directly onto the assay plate. The advantage of a direct ELISA is that only one antibody and fewer steps are utilized, and the cross-reactivity of secondary antibody which results in a nonspecific signal is eliminated. Cross-reactivity occurs when a molecule other than the analyte of interest is bound by the antibody conjugated with the enzyme leading to a false positive result. Interference occurs when other substances in the sample matrix modify the antigen-antibody interaction, preventing an assay from recognizing its designated analyte. However, the primary antibody must be labeled individually, which can be time-consuming and inflexible when performing multiple experiments. In addition, the signal is less amplified in a direct ELISA, which means a lower sensitivity and could be viewed as a disadvantage to some.

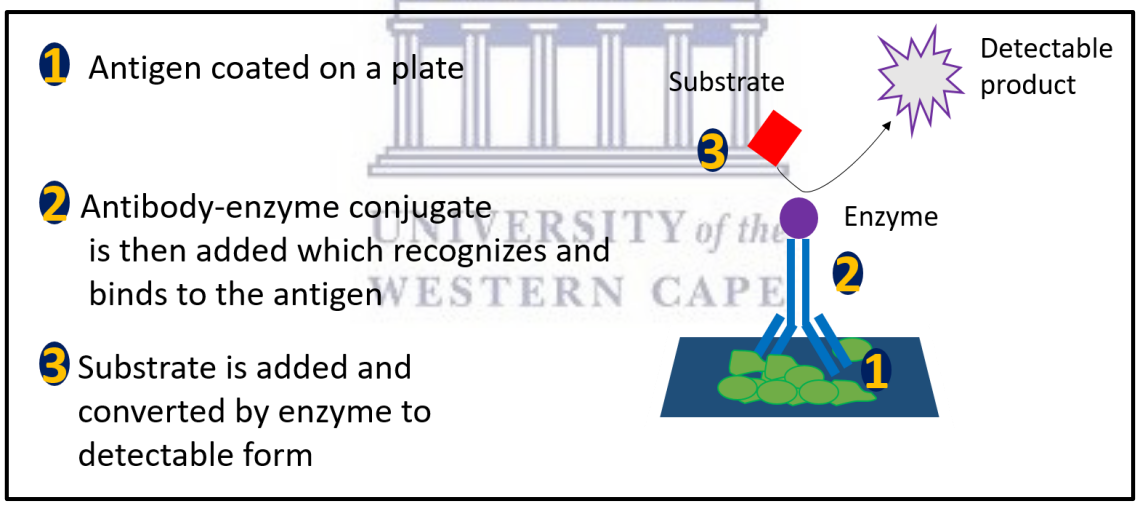

Figure 4: Diagram of the direct ELISA test

1.5.2.2 Indirect ELISA

Indirect ELISA (Figure 5) is a two-step test which involves two successive binding processes, firstly with a primary antibody and then a labeled secondary antibody. In the indirect ELISA test, the target antibody is sandwiched between the antigen coated on the plate and an enzyme-labeled, anti-species globulin conjugate. This format of indirect ELISA is suitable for determining total antibody level in samples.

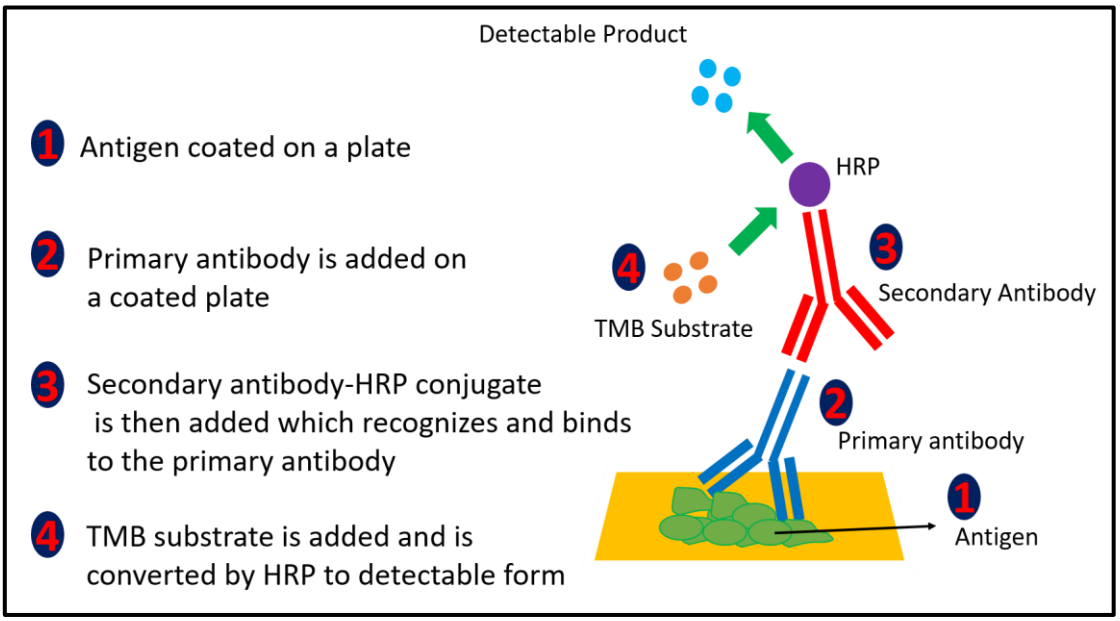

Figure 5: Diagram illustrating the indirect ELISA protocol

1.5.2.3 Sandwich ELISA

The sandwich ELISA (Figure 6) quantifies antigens between two layers of antibodies (i.e. capture and detection antibody). The antigen to be measured must contain at least two antigenic epitope capable of binding to antibody since at least two antibodies act in the sandwich. Either monoclonal or polyclonal antibodies can be used as the capture and detection antibodies in Sandwich ELISA systems. Monoclonal antibodies recognize a single epitope that allows fine detection and quantification of small differences in antigen. A polyclonal is often used as the capture antibody to pull down as much of the antigen as possible.

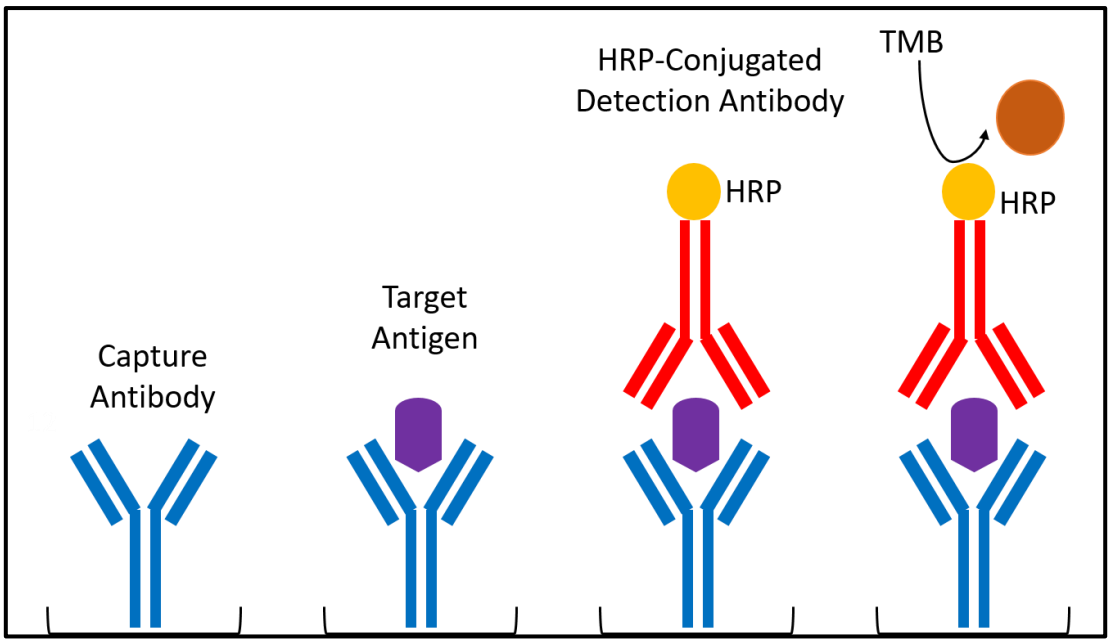

Figure 6: Diagram illustrating the sandwich ELISA protocol

1.5.2.4 Competitive ELISA

The central event of competitive ELISA is a competitive binding process executed by original antigen (sample antigen) and add-in antigen. The procedures of competitive ELISA can be divided into direct and indirect, which are different in some respects compared with Indirect ELISA, Sandwich ELISA, and Direct ELISA.

A. Direct competitive ELISA

The direct competitive ELISA (dc-ELISA) derives from the fact that the format detects an analyte in a sample directly based on competitive antigen-antibody interaction between a target antigen and a derivative antigen of the target covalently conjugated with an enzyme (enzyme-labelled) beforehand. The dc-ELISA uses a format that is immobilized with antibody of a fixed quantity on the surface of each well of a microtiter plate. The antigen and enzyme-labelled antigen are combined competitively with the immobilized antibody in each well. Because the quantities of the immobilized antibody and the enzyme-labelled antigen are constant, the competitive reaction varies depending on the amount of a target antigen in a sample. In that reaction, the concentration range of antigen showing competitive reaction corresponds to the dynamic (or working) range of the dc-ELISA format. After the competitive reaction for

constant time, the unbound components are washed off; then the absorbance is measured by adding a substrate of the labelled enzyme and developing color. The antigen concentration in samples is estimated based on the calibration curve produced by plotting the known concentrations of antigen in the x-axis and the yielded absorbance in the y-axis.

B. Indirect competitive ELISA

Indirect competitive ELISA (ic-ELISA) derives from indirect detection of antibody by capturing a complex of protein-bound antigen and antibody generated by interaction with enzyme-labelled secondary antibody recognized as a signal that is inversely proportional to antigen concentration. Indirect competitive ELISA uses the format that is immobilized with an antigen of the fixed quantity on the surface of each well of microtiter plate. The antigen is combined competitively with the antibody in each well. Because the quantity of the antibody and the coated antigen are constant, the competitive reaction varies depending on the amount of a target antibody in a sample. Like the dc-ELISA format, the concentration range of antibody showing competitive reaction corresponds to the dynamic range of the ic-ELISA format. After the competitive reaction for some time, the unbound components are washed off; then secondary antibody is added. After washing off of the unbound secondary antibody, the absorbance is measured by adding a substrate and developing color. The antibody concentration in samples is estimated based on the calibration curve, which is produced similarly to the dc-ELISA method.

1.5.3 Summary of ELISA

All different types of ELISA use antibodies and depend on the colour change to identify the presence of the substance of interest. The direct ELISA method suffers from having an immobilization method of antigen that is not specific, allowing proteins to stick on the microplate well when serum is used as the source of test and subsequently causes competition between the concentration of the analyte and serum proteins when binding to the well surface. Hence, this lead to a less amplified signal and poor sensitivity. The indirect ELISA method is advantageous to the direct ELISA method since the antibody is specific for the antigen. The chances of obtaining false results are slim as compared to the direct method. The competitive

ELISA possess similar advantages as the indirect ELISA method but are not as simple to use as indirect ELISA method.

1.6 TB antigens commonly used for ELISA

1.6.1 Mycobacterium tuberculosis Ag85B

Antigen 85B *Mycobacterium tuberculosis* (Ag85B) is the most abundant protein exposed by *Mycobacterium tuberculosis*, as well as a potent immune-protective antigen and a leading drug target. The members of Ag85B family are expressed at a stable state ratio of 3:2:1 (Ag85B:Ag85A:Ag85C), while the three genes are unlinked [30]. Antigen 85B can also be called antigen 85-B, 85B, extracellular alpha-antigen, antigen 85 complex B, Ag85B, mycolyl transferase 85B, fibronectin-binding protein B, 30 kDa extracellular protein, fbpB, A85B. Ag85B induces strong T-cell proliferation and IFN-γ secretion in most healthy individuals exposed to *Mycobacterium tuberculosis*, in BCG-vaccinated mice and humans, whereas the antibody against Ag85B are more prevalent in active tuberculosis patients with decreased cellular immune response [31]. The Ag85B major secretory protein of *Mycobacterium tuberculosis* is an important vaccine candidate. The vaccination of guinea pigs with the purified *Mycobacterium tuberculosis* Ag85B induces significant protective immunity against aerosol exposure to *Mycobacterium tuberculosis* bacteria [32]. This was shown in guinea pigs BCG vaccine that overexpression of the Ag85B component induces stronger protective immunity against aerosol challenge than conventional *M. bovis* BCG vaccine. This recombinant BCG vaccine is the first vaccine confirmed to be more potent than conventional BCG vaccine since the recombinant vaccine was developed [33]. The Ag85B antigen has also been used for the application in a competitive ELISA for serodiagnosis of bovine tuberculosis and there was no cross-reactivity found using the indirect ELISA method to detect the mycobacterium [34]. The Ag85B can be used for ascendant preliminary screening antigens for active TB and latent TB patients [35].

1.6.2 ESAT-6

The *Mycobacterium tuberculosis* (MTB) genome consists of 16 regions of differences (RDs). In *Mycobacterium tuberculosis* complex (MTBC), a region of difference is referred to as RD1.

The RD1 plays a key role in the virulence of MTB. Analysis of MTBC molecular biological characteristics have identified several antigens as virulence agents with important role in TB pathogenesis [36]. The protein ESX-1 is the system encoded by *esx* gene family that allows specialized protein secretion, 6-kDa early antigenic target (ESAT-6) and 10-kDa culture filtrate protein (CFP-10) through Mycobacterial cell envelope; ESAT-6 and CFP-10 found in the phagosome. ESAT-6 is a secretory effector inducing membrane lytic of macrophage apoptosis (death of cells) that enables phagosomal escape, cell entry, and intercellular spread, intracellular survival, and a major pathogenic determinant. The *esxA* genes encoding ESAT-6 protein is a member of *esx* genes family, located adjacent to CFP-10-encoding *esxB* gene [37]. ESAT-6 and CFP 10 produce strong immune responses. They are also know to form hetero-dimer complexes that are stable tertiary structures and increased resistance to denaturation via chemical or protease digestion in comparison to the individual proteins. Hence, both ESAT-6 and CFP-10 has significant potential to be used as diagnostic biomarkers for *Mycobacterium tuberculosis.* The only drawback is that they are not bacterium specific and could lead to a false diagnosis

1.6.3 Mycobacterium bovis antigen complex A60

The *Mycobacterium bovis* antigen complex A60 is known to be immunodominant in tuberculosis. A60 is a macromolecule that can be prepared from *M.bovis* and it consists of protein-polysaccharide and lipid [38]. Due to its molecular characteristics, this antigen has high immunogenicity. Diagnostic methods such as ELISA do not necessarily need specimens containing mycobacterium to detect MTB antibodies against A60 antigen. The most of the A60-ELISA kits, A60s are labelled with Horseradish peroxide (HRP) (Figure 8) to catalyze the reaction of 3,3',5,5'- tetramethylbenzidine (TMB) with hydrogen peroxide to form a colored compound (indicating the presence of the antibodies/antigens) and water (Figure 7).

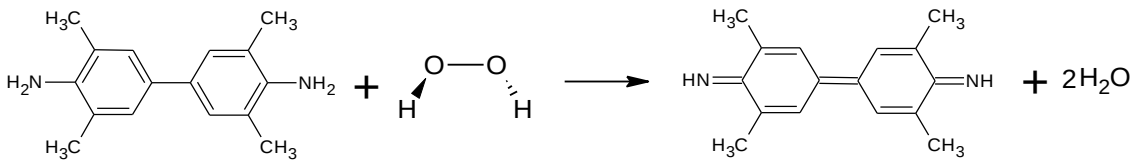

Figure 7: Oxidation of 3,3',5,5'- tetramethylbenzidine

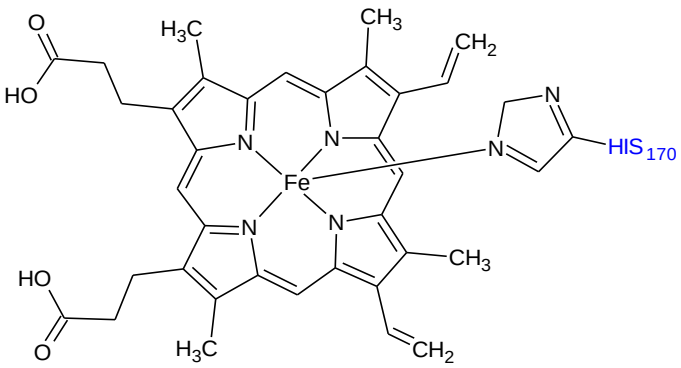

Figure 8: The active site is the heme group of the HRP

1.6.3 Commercial ELISA kits

Table 2 gives a summary of the ELISA kits that are recommended by WHO and commercial available for preliminary screening of tuberculosis. These ELISA kits uses protocols that were discussed in section ***1.5.2***. However, since each ELISA kit use different ELISA method for the detection of tuberculosis, their incubation time and temperatures to perform all the steps vary with each kit and some need the HRP to be conjugated to the detection antibody manually. Each ELISA test has an antigenic composition and indicates what kind of tuberculosis antibodies can be detected with it.

Table 2: The ELISA kits recommended by the world health organizationwork

Name of Test	**Antigenic Composition**	**Antibodies Detected**	**Name of the Manufacturer, Country**
Tuberculosis Specific Antigen	Proprietary	Unknown	Chengdu Pharmaceutical, China
Detect-TB	Proprietary, a cocktail of 3 *M. TB* recombinant proteins and two	IgG	Adaltis – Advanced Laboratory

	synthetic peptide from 5 different proteins		Diagnostics Systems, Italy
Mycobacterium tuberculosis IgG	18-, 36- and 40-kDa recombinant antigens	IgG, IgA, IgM	IBL, Germany
Anda TB-ELISA	A60	IgG, IgM, IgA and IgG plus M	Anda Biologicals, France
AtciveTBDetect	Mtb81, Mtb8, Mtb48, DPEP (MPT32), 38 kDa protein and two additional proprietary antigens	IgG	InBios International, US
Pathozyme TB Complex	Recombinant 38 kDa	IgG	Omega Diagnostics, Scotland
Pathozyme Myco[c]	LAM, Recombinant 38 kDa	IgG, IgA, IgM	Omega Diagnostics, Scotland
Determine TB Glycolipid Assay	Trehalose 6,6'-dimycolate and trehalose Monomycolate, diacyltrehalose, phenolic glycolipid, 2,3,6,6-tetraacyl-trehalose-2-sulfate and 2,3,6-triacyl-trehalose	IgG	Kyowa Medex Co, Ltd, Japan
SEVA	31 kDa, Native glycoprotein antigen from culture filtrate of MTB H37Rv	IgG	Jamnalal Bajaj Tropical Disease Research Centre, Mahatma Gandhi Institute of Medical Sciences, India
TB Enzyme Immunoassay	Kp-90 antigenic compound: LAM, 10, 16, 21, 30, 34, 65, and 95 kDa	IgA, IgA	Kreatech, The Netherlands
Tuberculosis IgG ELISA	Affinity MTB antigens	IgG, IgM	Creative Diagnostics, US

1.7 Electrochemical sensors for TB detection

A vast majority of tuberculosis sensors not based on ELISA tests uses DNA and nanoparticles to ameliorate the targeted detection. The use of electrochemical DNA probes are important because they decrease the time and cost of MTB screening [39]. These electrochemical sensors provide a qualitative analysis and are performed under standard laboratory conditions without affecting the reliability of results [40]. Most of the DNA electrochemical biosensors are based on a sandwich detection strategy [40–43]. In many cases electrochemical impedance spectroscopy (EIS) has emerged as an important tool for DNA sensor analytical response. EIS has the advantage of separating competing electrochemical processes in the frequency domain and therefore, provides a better insight on the interfacial reaction and the mass transport processes in electrochemical systems [40,42,44,45]. However, the range of TB electrochemical sensors is broad and complex, it includes enzymatic, immunosensing and even direct chemical detection of *Mycobacterium tuberculosis*. Electrochemical immunosensors combine the high specificity of traditional immunochemical methods with the low detection limits of modern electrochemical system. The crucial steps for the design of an electrochemical immunosensor are the choice of the basis electrode and immobilization of the immune-agent on the electrode surface. Recently, there have been some developments of TB diagnosis (immunosensors) which are valuable for pre-clinical work prior to conducting large scale clinical observation. These sensitive and simple immunoassay devices have provided an opportunity to gain new insight into detection of MTB by capacitive sensing related to affinity binding or surface plasmon resonance (SPR) immunosensing [46–50].

1.8 First-line anti-TB drugs

First-line agents for treatment of active tuberculosis consist of rifampicin, isoniazid, ethambutol, pyrazinamide and streptomycin. The treatment of tuberculosis involves taking these first-line anti-TB drugs for 6 to 9 months. The first-line anti-TB drugs are discussed below from the newly found drug to the oldest.

1.8.1 Rifampicin

Rifampicin (Figure 9) is bactericidal for *Mycobacterium tuberculosis*, relatively nontoxic and tolerated at a dose of 15 mg/kg per day. It is a rifamycin derivative that was introduced in 1972 as an anti-tuberculosis agent. It is also one of the most effective anti-TB antibiotics and together with isoniazid constitutes the basis of the multidrug treatment regimen for tuberculosis. Rifampicin is active against growing and non-growing bacilli [51]. Rifampicin in *Mycobacterium tuberculosis* targets the β-subunit of the RNA polymerase, while inhibiting the elongation of messenger RNA [52]. The majority of rifampicin-resistant clinical isolates of *Mycobaterium tuberculosis* contain mutations in the *rpoB* gene that codes for the β-subunit of the RNA polymerase. As a result of this, conformational changes occur that decrease the affinity for the drug and results in the high-level of resistance [53].

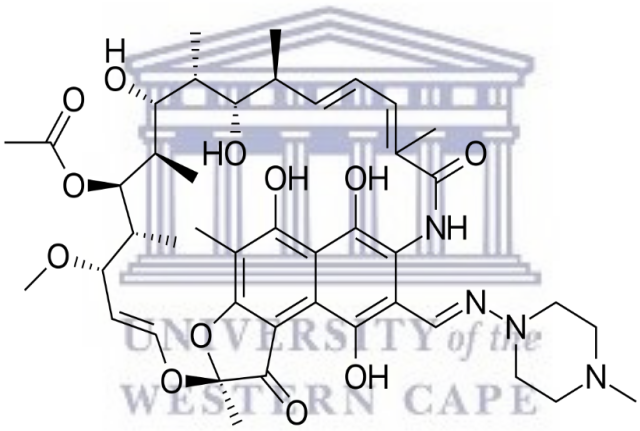

Figure 9: Structure of Rifampicin

1.8.2 Isoniazid

Isoniazid (isonicotinic acid hydrazide) (Figure 10) was introduced in 1952 for the treatment of tuberculosis and it remains, together with rifampicin, as the basis for the treatment of the disease. Unlike rifampicin, isoniazid is only active against metabolically-active replicating bacilli and its usual dosage is 5 mg/kg per day. It is a pro-drug that requires activation by the catalase/peroxidase enzyme KatG, encoded by the *katG* gene, to exert its effect [54]. Isoniazid acts by inhibiting the synthesis of mycolic acids through the NADH-dependent enoyl-acyl carrier protein-reductase, encoded by *inhA* [55]. However, as much as it is simple in its structure,

resistance to this drug has been associated with mutations in several genes, such as *katG*, *inhA*, *ahpC*, *kasA* and NDH.

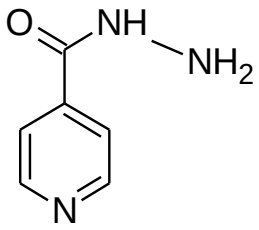

Figure 10: Structure of Isoniazid

1.8.3 Ethambutol

Ethambutol (Figure 11) was first introduced in the treatment of tuberculosis in 1966 and is part of the current first-line regimen to treat the disease. Ethambutol is bacteriostatic against multiplying bacilli interfering with the biosynthesis of arabinogalactan in the cell wall [56]. It also prevents the emergence of drug resistance to other first-line drugs, with a dosage that ranges between 15-25 mg/kg per day. In *Mycobacterium tuberculosis*, the genes *embCAB*, organized as an operon, code for arabinosyl transferase, which is involved in the synthesis of arabinogalactan, producing the accumulation of the intermediate D-arabinofuranosyl-P-decaprenyl [57]. Furthermore, the most important complication of ethambutol therapy is optic neuritis (inflammation that damage the optic nerve) caused by impaired visual acuity, color blindness and restricted visual fields.

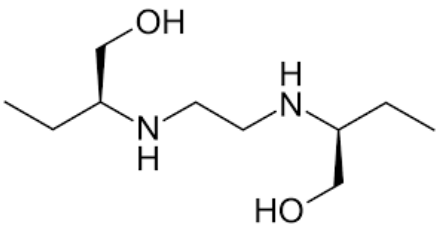

Figure 11: Structure of Ethambutol

1.8.4 Pyrazinamide

Pyrazinamide (Figure 12) was introduced into TB treatment in the early 1950s and constitutes now part of the standard first-line regimen to treat the disease. Pyrazinamide is an analog of nicotinamide and its introduction allowed reducing the length of treatment to six months. It has the characteristic of inhibiting semi-dormant bacilli residing in acidic environments such as found in the tuberculosis lesions [51]. It has a dosage of 30 mg/kg per day that produce little toxicity in adults and are well tolerated in children. Pyrazinamide is also a pro-drug that needs to be converted to its active form, pyrazinoic acid, by the enzyme pyrazinamidase/nicotinamidase coded by the *pncA* gene [58,59].

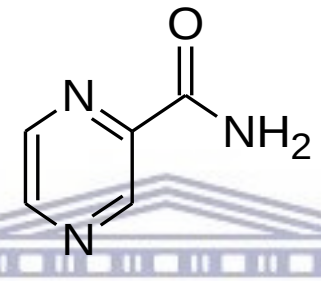

Figure 12: Structure of Pyrazinamide

1.8.5 Streptomycin

Streptomycin (Figure 13) was introduced for the treatment of tuberculosis in 1948. It was originally isolated from the soil microorganism Streptomyces griseus. Streptomycin was the first antibiotic to be successfully used against tuberculosis. Unfortunately, as soon as it was prescribed, resistance to it emerged, a result of being administered as monotherapy [60]. Streptomycin is an aminocyclitol glycoside active against actively growing bacilli and its mode of action is by inhibiting the initiation of the translation in the protein synthesis [61]. More specifically, streptomycin acts at the level of the 30S subunit of the ribosome at the ribosomal protein S12 and the 16S rRNA coded by the genes *rpsL* and *rrs*, respectively [62].

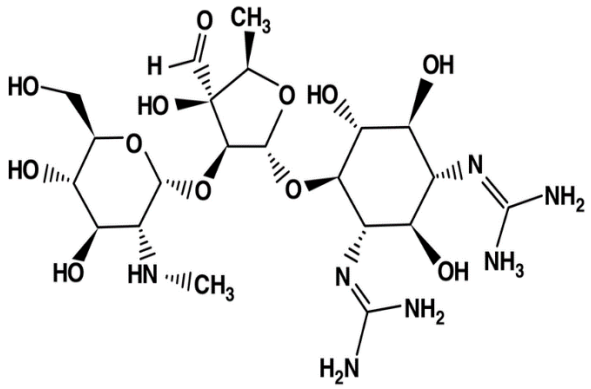

Figure 13: Structure of Streptomycin

Table 3 summarize the properties of the anti-TB drugs, their site of action, the media they are active in and the type of bacilli they target in the individual diagnose with tuberculosis. The table begins with first discovered anti-TB drug and end with recently found. Under targeted bacilli it is evident that the two recently found first-line anti-TB drugs their properties were improved in order to target all bacterial populations.

Table 3: Summary of TB drugs properties

Drug	pH	Drug Property	Target Bacilli	Site of Action
Streptomycin	Alkaline medium	Bactericidal with low potency	Rapidly growing bacilli	Extracellular
Isoniazid	Alkaline and acid media	Bactericidal after 24h. High potency: kills>90% bacilli in first few days of treatment	Rapid and intermediate growing bacilli	Intracellular and extracellular
Pyrazinamide	Acid medium	Bactericidal with a low potency. Achieves sterilizing action within 2-3 months	Slow growing bacilli	Intracellular bacilli only

Rifampicin	Alkaline medium	Bactericidal with 1 hour. High potency and most effective sterilizing agent	All populations including dormant bacilli	Intracellular and extracellular
Ethambutol	Alkaline and acidic media	Bacteriostatic. Low potency. Minimising the emergence of drug resistance	All bacterial populations	Intracellular and extracellular

1.9 Drug resistance

A major concern with treatment of tuberculosis is drug resistance and moreover multidrug resistance. Many different definitions for multidrug-resistant (MDR), extensively drug-resistant (XDR) and pan-drug-resistant (PDR) bacteria are being used in the medical literature to characterize the different patterns of resistance found in healthcare-associated and antimicrobial-resistant bacterial. In simple terms, drug-resistance is the ability of microbes, such as bacteria, viruses, parasites, or fungi, to grow in the presence of a chemical (drug) that would normally kill them or limit their growth.

1.9.1 Drug-resistant tuberculosis

Drug-resistant tuberculosis (DR-TB) is when the bacteria that cause TB can develop resistance to the antimicrobial drugs used to cure the disease, while multidrug-resistant TB (MDR-TB) is when TB bacteria do not respond to at least isoniazid and rifampicin, the 2 most powerful first-line anti-TB drugs. People with TB are cured under strictly followed, drug regimen (6 month) that is provided to patients with support and supervision [63,64]. However, inappropriate and incorrect use of antimicrobial drugs or premature treatment interruption can also cause drug-resistance, which can then be transmitted, especially in crowded settings such as, public transport (taxis, buses etc.), prisons and hospitals [65]. Hence, drug-resistance remains a man-made phenomenon. It is becoming increasingly difficult to treat MDR-TB. Treatment options are limited, expensive and recommended medicines are not always available especially to those TB prevalence and not well-developed countries. Moreover, patients experience many adverse effects from the drugs as they have different metabolic systems. In some cases, severe drug-

resistant TB may develop [66]. This is referred as an extensively drug-resistant TB (XDR-TB), which is a form of multidrug-resistant TB with additional resistance to any fluoroquinolone (second line anti-TB drugs) and to at least one of the injectable second-line drugs: kanamycin, capreomycin or amikacin [67]. In South Africa, a higher number of male than female multidrug-resistant tuberculosis (MDR-TB) cases have been reported, however data from a total of 81 794 TB patients with known sex (95% of all patients) indicates that female TB cases have a 1.2 times higher odds of bearing MDR-TB strains than male TB cases [68]. In 2016, an estimated 490 000 people developed MDR-TB. This number is likely to increase since methods of controlling the spread of MRD-TB are not yet well established.

1.9.2 Drug metabolism

Drug-resistance is always linked with a resistant bacteria and poor biotransformation. Biotransformation is the process that can be defined as the use of biological systems to produce chemical changes on compounds that are not their natural substrates. To defend the body against xenobiotic substances, an array of metabolic reactions (biotransformation) is undergone. Due to the metabolic reactions, the molecular structure of the drug is commonly changed to be more hydrophilic and the substances can be readily eliminated from the body. Biotransformation reactions are divided into two categories known as phase I and phase II reaction and each phase have their own enzymes responsible for metabolic reactions. There are five first-line anti-TB drugs and each drug's enzyme responsible for their metabolism has been studied. Recent studies involves understanding the mechanisms of the drug resistance of *M. tuberculosis* and the relevant molecular mechanisms involved that can improve the available techniques for rapid drug resistance detection [69]. This gives a better knowledge about the mechanisms of action for anti-TB drugs and the development of drug resistance which allows identifying new drug targets and better ways of detecting drug resistance. Electrochemical sensors of TB drug-resistance provide the foundation for the development of cost-effective, accurate and sensitive alternatives for molecular diagnostics of multidrug-resistance and extensively drug-resistance.

1.9.3 Factors associated and promoting drug-resistant tuberculosis

Nosocomial outbreaks of MDR-TB associated with HIV infection have been documented where HIV positive patients being treated in hospitals for drug-susceptible tuberculosis have been re-infected with MDR strains. Studies have shown that patients with active, untreated MDR-TB can infect large numbers of HIV positive individuals, leading to significant outbreaks of MDR-TB with high case-fatality rates. XDR tuberculosis has been reported in 105 countries and is estimated to cause about 10% of cases of MDR-TB [2] and this has increased to 117 countries. Although XDR tuberculosis is being increasingly reported, especially in urban areas in TB-endemic countries such as Africa and India, the absence of validated standards for drug-susceptibility testing (DST) remains a major challenge to diagnosis [3]. Since international travel is becoming more common, the possibility of acquiring TB during travel and importation into low-prevalence settings is increasing. Moreover, active TB is a prominent disease in travelers, although definitive attribution of infection to the travel event is made difficult by the wide range of latency periods. Drug-resistant is not only caused by the above-mentioned factors but poor management of patients and prescription errors also contribute to drug-resistant;

Patient management and prescription errors:

- Poor relationships between patients and healthcare personnel due to the uncaring staff attitudes, showing little empathy for patients, being paternalistic and failing to adopt a problem-solving approach to help resolve issues all contribute to poor adherence.
- Inadequate counseling of patients resulting in low knowledge levels, poor understanding of what is expected of them and of the importance of completing treatment and monitoring the response to treatment also contribute to poor adherence to first-line regimens.
- Ineffective systems, including lack of support for directly observed therapy and unsupervised patients; poor record keeping, follow-up of patients and referral.
- Staffing issues including frequent staff changes, poor staff morale, lack of regular support and supervision and low accountability of staff for programme outcomes.
- Insufficient contact tracing and follow-up of MDR cases also contributes to the spread of MDR-TB.

Dramowski study also indicates that these are not only factors that contributes to the spread of drug-resistant (DR), XDR-TB, and MDR-TB but stigma, fed by a combination of fear and

denial, aggravates delays in diagnosis and treatment and sustains an unspoken culture of 'don't disclose the TB status' [15]. When healthcare workers contract TB, they frequently seek treatment secretly. They dread public disclosure of their TB diagnosis, fearing a backlash from colleagues, who themselves are afraid of contracting TB. Among TB patients, it has been shown that disclosure is more likely to occur when the patient is assured that they will not be stigmatized [70]. HIV is the elephant in the room when discussing stigma and TB in healthcare workers. In Sub-Saharan Africa, TB and HIV are inexorably linked in the minds of many people. If a healthcare worker discloses that they have TB, the reaction of many colleagues is to wonder, or even openly discuss, if that individual could be co-infected with HIV. The psychological effort involved in concealing illness to avoid valid fears of further discrimination can be detrimental [71] Therefore, almost, as a standard rule, they do not disclose their TB/HIV status, even though they are at an even greater risk of TB and could potentially reduce this risk with the use of antiretroviral, additional infection control measures, and alternative work placements [72]. Career implications of a TB diagnosis also play a role in discouraging disclosure and driving stigma. Healthcare work in developing countries is challenging, with generally low salaries and poor working conditions [73]. Many healthcare workers are at the mercy of the public sector and can be fired or re-assigned if they complain about working conditions. This prevents healthcare workers from disclosing their TB diagnoses and advocating for safer working conditions, thus fuelling the vicious cycles of misinformation, discrimination, and unchecked TB transmission in health facilities. Migrant healthcare workers in high-income countries may also be reluctant to disclose a TB diagnosis in the face of stigma and their limited entitlement to sickness pay/social welfare due to restrictions on their immigration status [74]. Nevertheless, the stigma of "don't disclose the TB/HIV status" is not only the factor that have a great contribution to MDR-TB and XDR-TB as compared to patient who are infected with HIV/AIDS. Studies indicating that HIV infection has encouraged the spread of MDR-TB have generated worldwide attention [70,74,75]. MDR-TB among previously untreated patients is mostly related to HIV infection [76]. Patients severely immunosuppressed by HIV infection have a lower response rate and higher fatality rate for MDR-TB treatment than HIV negative cases [77]. Moreover, patients with HIV and drug-resistant TB have a higher risk of adverse drug reactions and drug toxicity, thus requiring increased monitoring by healthcare providers. It is recommended that TB/HIV programmes are well established before adopting drug-resistant TB/HIV interventions [78,79]. The WHO has reported that MDR-TB and XDR-TB, in particular, are recognized as emergent risks in healthcare settings for people living with HIV in areas where there is a high prevalence. It is essential that healthcare and congregate settings have a

plan and implement administrative, environmental and personal infection control and protection measures to reduce the transmission of TB [80].

1.9.4 Factors affecting biotransformation of drugs

There are two main factors that affect the biotransformation of drugs; enzyme induction and enzyme inhibition. Enzyme induction is the process by which exposure to certain substrates results in accelerated biotransformation with a corresponding reduction in unmetabolized drug [81]. Most drugs can exhibit decreased efficacy due to rapid metabolism, but drugs with active metabolites can display increased drug effect and/or toxicity due to enzyme induction [82]. Enzyme inhibition occurs when two or more drugs sharing metabolism via the same isozyme compete for the same enzyme receptor. The more potent inhibitor will predominate, resulting in decreased metabolism of the competing drug. For most drugs this can lead to increased serum levels of the unmetabolized entity, leading to a greater potential toxicity. Disease states affecting metabolism are hepatic disease, which causes decreased blood flow to the liver [83]. A decreased biotransformation occurs in new-borns due to underdevelopment of hepatic microsomal components, while in elderly, a decrease in hepatic blood flow, enzyme activity, and liver mass result in reduced metabolic activity. Thus, cytochrome P450 monooxygenase system is more affected by aging than any other metabolic pathway. The reduced metabolic activity of P450 can contribute to what is called drug-resistance [84].

1.9.5 Cytochrome P450 enzymes

Cytochrome P450 enzymes (CYPs) take part in the most crucial role in drug metabolism, and there are six or more different P450 isozymes – CYP1A2, CYP2C19, CYP2C9, CYP2D6, CYP3A4 and CPY2E1 that have been identified [85]. They comprise a superfamily of heme proteins (proto-hemes), which have a major role in phase 1 metabolic clearance of numerous xenobiotics in the liver. This proto-heme found in the active centre of CYPs is activated through transfer reactions. NADPH and NADH reagent rating enzyme systems are generally used to supply electrons to CYP. The general catalytic cycle of P450 (Figure 15) indicates how the NADPH influences the electron transfer between the CYP enzyme and substrate. The cycle begins with P450 iron in the ferric state (Figure 14). In step (a), the substrate binds to the oxidized enzyme near the distal region of the heme. This step may or may not cause change in

the iron spin state. It also may or may not facilitate step (b), depending on the P450; step (a) is shown before (b) because it is faster, even when the kinetics of step (b) are independent of whether substrate is bound. The electrons are provided to the enzyme P450 NADPH via the accessory flavoprotein NADPH-P450 reductase. Molecular oxygen then binds to the ferrous P450 followed by transfer of a second electron and activation of oxygen [step (c) and (d)]. The addition of a proton [step (e)] is followed by O–O bond cleavage, releasing H_2O [step (f)] with an addition of a proton. An electron-deficient FeO^+ formal complex is left behind. This complex the abstracts an electron from the substrate to produce a substrate radical [step (g)] and the second atom of oxygen is transferred to the incipient substrate radical [step (h)]. Finally, the product is released with the heme iron returned to the ferric state [step (i)] [84–88]. In addition, in artificial systems, an oxygen surrogate (R'O or R'OOH) can be used to convert the ferric iron to one of the high-valent iron-oxygen complexes [(step (j)].

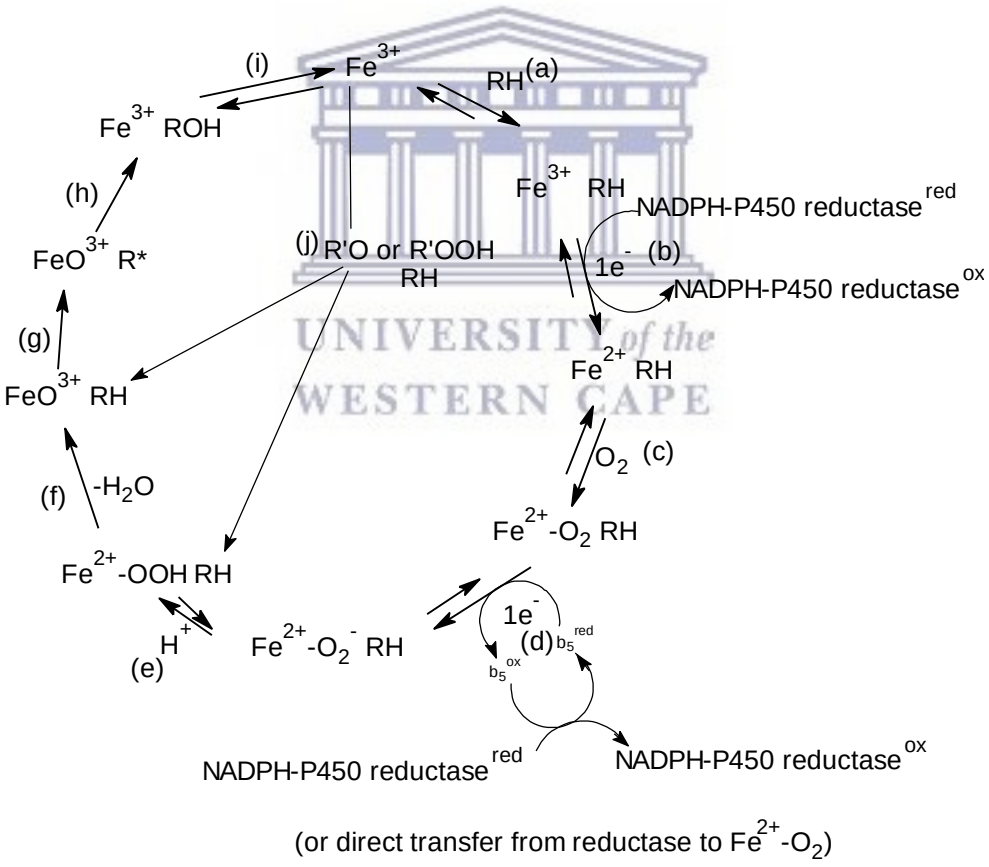

Figure 14: The generalized P450 catalytic cycle where Fe is iron atom I P450 heme, RH = substrate, ROH = product, ox and red indicate the reduced and oxidized (1-electron) states of the reductase involved in the electron transfers [84]

In recent studies it appears that the NADH is more stable and cheaper than NADPH, hence it was assumed that it would be more effective if NADH is used in cell-free bioreduction of systems [89]. However, Scheller established an ultimate approach of direct electron supply from redox electrode to the redox-active group of the P450s [90]. Therefore, for xenobiotics or drugs risk assessment, the suggestion of measuring the substrates specificity and concentration in conjunction with distribution of CYP isozyme and polymorphic enzymes based on biosensors was highly accepted as it would be of high clinical relevance [91]. The use of electrochemistry allows investigating the electrochemical properties of redox enzymes and their mechanism by observing the direct electron transfer in real time [92]. The knowledge of the mechanism of electron transfer in proteins is based on the Marcus theory. Replacing the conventional electron supply system with electrodes has become a promising approach to develop inexpensive and rapid assays. Many laboratory scaled assays have been developed that determines such components. The study of Ajayi and co-workers have also demonstrated that there is a need for a fast and reliable method for the determination of a patient's metabolic profile for TB drugs; in which they developed a nanobiosensor for the determination of the biotransformation of rifampicin. The nanobiosensor comprised of the gold electrode, polymer, nanoparticles and CYP2E1 enzyme [93,94]. The gold electrode was used as the source of electrons. Cytochrome P450s are known to be responsible for or promote biotransformation of many drugs via oxidation. In their proposed mechanism, under anaerobic conditions (presence of oxygen), there were able to detect rifampicin and the presence of oxygen promoted the enzyme interaction with rifampicin. In humans, traces of anti-TB drugs can be detected in urine and they can also be found in environmental water since the residual drugs are resistant to conventional water treatment strategies employed by sewage treatment plants and unmetabolized drugs in water can create resistant bacteria. Therefore, to prevent multidrug-resistance occurrence and monitor metabolism of drugs in patients with multidrug-resistant, the detection of anti-tuberculosis drugs is fundamental.

1.9.6 Optical properties of cytochrome P450

The ferric resting state optical absorption spectra of the heme are sensitive to the spin state of the heme iron reflected in the characteristic positions of Soret band in UV absorption spectra; 415 – 417 nm for low spin P450s and 390 – 394 nm for the high-spin state. Substrate binding to cytochromes P450 is often monitored by the concomitant transition from low spin to high

spin using optical absorption difference spectra [95]. Since all cytochromes P450 have the same heme prosthetic group, their optical absorption spectra vary only by minor extent in the different isozymes. The redox state of the heme iron and oxidation/reduction processes can be monitored by the changes in Soret region [96]. The position of Soret band maximum for the ferrous protein with no ligands to the heme iron (5-coordinated high spin Fe^{2+}) is 408 – 410 nm, while binding of ligands results in splitting and red shifting of the longer wavelength peak to 420 – 425 nm (dioxygen), 430 – 435 nm (NO) or 445 – 450 nm (CO). The oxy-ferrous complex of P450 usually exists at 417 – 418 nm [97].

1.9.7 CYP450 sensors based on direct electron transfer

The study of Fantuzzi [92] shows that the electrochemistry of CYP2E1 on glassy carbon electrodes (GCEs) have a formal potential of -90 mV versus NHE, indicating that CYP2E1 was adsorbed on the electrode surface. While on the modified electrode (with didodecylammonium bromide) the cyclic voltammetry showed two waves with a formal potential of -85 mV versus NHE. On the modified gold electrode the electrochemical response had a formal potential of 191 mV versus NHE. On another study by Mak and co-workers, the electro-catalytic response of CYP2E1 on the self-assembled monolayer of dithio-bismaleimidoethane (DTME) gold electrode functionalized with MUT261/MUT268 was studied and the formal potentials were all in the region of -243 mV versus 3M Ag/AgCl [98]. Hence it seems possible to perform direct electron transfer between the enzyme and an electrode to avoid the use of NADH or NADPH. However, for the cytochrome P450 enzymes at bare electrodes, the electron transfer is achieved at a low rate between the enzyme and the electrode. Fast heterogeneous electron transfer has been realized when glassy carbon electrodes (GCE) are modified. In addition, the modification of GCE with compounds that facilitate electron transfer and using different medium (electrolyte) may cause shift of the redox potentials of CYP P450 enzymes. A list of CYP P450 biosensors based on GCE-mediated electron transfer is presented on Table 4 below.

Table 4: The list of CYP used for biosensors (GCE as a working electrode) and their parameters obtained using different electrochemical techniques.

Electrode	**Electrolyte**	**CYP Species**	**Formal potential $E^{'}$(mV)**	**Technique**	**Reference**
GCE/P450/DDAB/SG	PBS	$P450_{cam}$	-356	CV	99
GCE/P450/DDAB/SG	ACN	$P450_{cam}$	-301	CV	99
GCE/DDAB	PBS	CYP2E1	-334	CV, chronoamperometry	92
GCE/PDDA	PBS	CYP2E1	-334	CV, chronoamperometry	92
Clay-GCE		CPY101	-368	CV	90
Polyaniline doped GCE	PBS	CYP2D6	-120	CV, amperometry	87
GC Disc	HEPES	CYP2E1 CYP102	-500	Staircase CV	101
GCE/CH/AuNP		CYP2B6	-454	CV, HPLC. ESI-MS	87
GCE/clay	PBS	CYP2B4	-292.5	CV, amperometry	91

GCE: glassy carbon electrode, DDAB: didodecyldimethylammonium bromide, SG: sol-gel, PDDA: poly(diallyldimethylammonium chloride), CH: Chitosan, AuNP: gold nanoparticles, PBS: phosphate buffer, HEPES: 4-(2-hydroxyethyl)-1-piperazineethanesulfonic acid buffer, ESI-MS: electrospray ionization-mass spectrometry, HPLC: high-performance liquid chromatography, ACN: acetonitrile.

The GCE/ $P450_{cam}$/DDAB/SG biosensor shows that when different electrolytes are used there is redox potential shift. Hence, the biosensor have different formal potentials when PBS and CH_3CN: H_2O (90%: 10%) were used as electrolytes [99,100]. While on the other biosensors (GCE/DDAB and GCE/PDDA) using GCE as a working electrode, the CYP2E1 enzyme is immobilized on different electrode surfaces but the redox parameters (formal potential) are the same [92]. Other groups have also obtained the redox potential of CYP P450 enzymes that have large redox potentials [101,102]. This can be due to the different materials used for modification of electrodes, where the modified surface can cause a slight alteration to heme environment as to

make it less stable, thus shifting the formal potential to more positive. A positive shift of the redox potential may indicate a low to high spin-state conversion that has been ascribed to strong interaction of CYP with surfaces [87]. Poulos and Jung studies indicated that the positive shifts of the redox potentials are generally observed when water is exclude from the heme pocket as in the case of camphor binding [87].

1.9.8 Nanoparticles in heme-based sensor and biosensors

The CYP 450 enzymes and haemoglobin enzymes all consists of heme-proteins. Since the heme is deeply embed in the centre of these various enzymes, the electron transportation or exchange between the electrode and heme-based biomolecules is regarded as poor when the electrochemistry of these species is studied as previously discussed. Nanomaterials are regarded as semi-conductors materials that ameliorate the conductivity of "not so" conductive materials. They have been used in polymer-based biosensors where they improve the surface area for better electron transfer between the sensor and the analyte. They have also been used to enhance the direct electrochemical and electrocatalytic behaviour of immobilized cytochrome P450. For an example the interaction between cytochrome P450-2B6 (CYP2B6) and zirconium dioxide nanoparticles was investigated by Li et al [103]. When CYP2B6 was cast directly on the bared electrode surface (GCE), the GCE/CYP2B6 showed the response of CYP2B6, but the response was smaller than that of GCE/ Pt-PLL/ZrO_2/CYP. It was evident that adsorption of CYP2B6 on ZrO_2 nanoparticles played an important role in facilitating the electron exchange between the electroactive centre of CYP2B6 and GCE. The formal potential of CYP2B6 in the Pt-PLL/ZrO_2 film was -449 ± 0.4 mV versus SCE at pH 7.4. The electrocalytic behaviour of the same enzyme towards common drugs in the absence of NADPH-cytochrome P450 reductase as electron donor was also studied. In an aerobic solution, direct and reversible electron transfer between the electroactive heme centre of CYP2B6 and the GCE/chitosan-AuNPs film electrode was observed with a formal potential -454 ± 0.6 mV versus SCE at pH 7.4. In the study of direct electrochemistry of haemoglobin immobilized on carbon-coated iron nanoparticles (CIN) for amperometric detection of hydrogen peroxide, no redox peaks were observed at the bare GCE, GCE/chitosan, GCE/chitosan-CIN and GCE/chitosan-CIN/Hb. However, the GCE/chitosan-CIN/Hb gave a couple of stable and well-defined redox peaks -30 mV and -410 mV (E', -220 mV vs Hg_2Cl_2), which was the characteristic of the heme redox couple of the protein [104]. They indicated that the response of

GCE/chitosan-CIN/Hb attributed to the redox of the electroactive centres of the immobilized Hb. In the nvestigation of haemoglobin/gold nanoparticle (GNP/Hb) heterolayer on micro-gap electrode for electrochemical biosensor application, the redox peaks of GNP/Hb showed signal- enhanced redox peak because the GNP facilitated the electron transfer between Hb and H_2O_2 with a formal potential of 206 mV (vs Ag/AgCl) [105]. The CYP2E1 enzyme immobilization at a modified gold electrode (Au/PANSA/PVP-AgNP) was also undertaken to develop of a novel nanobiosensor system for the determination of ethambutol [94]. The cyclic voltammetry shows a clear redox peak currents pair at +790 mV (oxidation) and +150 mV with a formal potential at +450 mV (vs Ag/AgCl). The PANSA/PVP-AgNP nanocomposite platform served as a suitable environment for the enzyme attachment promoting the rapid catalytic conversion of ethambutol to ethambutol aldehyde facilitated by the electron transfer of electrons between the electrode surface and the enzyme active site. Therefore, silver nanoparticles played an important role in facilitating the electron exchange between the electroactive centre of the enzyme and the electrode.

1.10 Problem statement

Tuberculosis infection control requires implementation of core interventions and strengthening of health systems. Control of TB infections is hampered by the ability of bacteria to survive in a latent state in infected individuals hence it has the potential for reactivation. In addition to controlling TB there is also the problem of multidrug-resistant tuberculosis which is a growing public concern and clinical problem. Drug-resistant increases the complexity and cost of therapy. High rates of drug-resistance of TB are mostly found in foreign-born individuals and those who are facing poverty particularly those with a history of previous TB infection and co-infected with TB and HIV. There is a need for new tools and methods towards rapid detection and monitoring during treatment of this disease (TB and MDR-TB). The recommended tests for tuberculosis disease and other diseases that results from tuberculosis vary in terms of the price and some are available in the healthcare facilities depending on the infrastructure. Some of these diagnostic tests of tuberculosis when monitoring the disease and treatment of the disease have a good or poor sensitivity. Diagnostic methods of tuberculosis such as molecular tests uses Genexpert (GXP) instrument and the test is called Xpert MTB/RIF, however it cannot be used for monitoring treatment since it does not distinguish between live and dead bacilli, its use is therefore limited for diagnosis. Using Xpert MTB/RIF test, only a small proportion of

rifampicin resistance detected may not be correlated with physiological resistance. This also includes the line probe assay tests. Some of these diagnostic tests methods they take up to 3-4 weeks for positive results and 1-2 weeks is also needed for drug susceptibility tests (DST). These effective but time-consuming methods also have a contribution to patients being resistant to certain anti-TB drugs; i.e., by the time a patient is introduced to the correct regimes, if their immunity is already being compromised (during the waiting period) up to a stage where the drugs that should be improving their immunity are no longer bactericidal and bacteriostatic (sterilising) at an efficient rate against the active bacilli. Therefore, the patient chances of becoming resistant to the treatment are elevated. In resource-poor countries, laboratories are single room and understaffed with poorly maintained microscopes and some of these laboratories lack consistent sources of electricity and clean water. This may be seldom in low burden TB countries where they have managed to have a good track record of the previous cases and have adequate resources to have good, if not perfect turnaround time for the results. Whereas in high burden TB countries there is high possibility of the treatment not being efficient at a good rate, due to the above-mentioned reasons and the fact that the 1-2 weeks waiting period might be prolonged to a month or more due to the limited resources of making these tests to be done at an expected period. On the other hand, low-quality sanitation is also a 'thorn' in having a high number of patients that are resistant to the anti-TB drugs since pollutants can contribute to creating resistant bacteria. Therefore, it is crucial to have a system implemented that can address issues such as improved health care in terms of cheaply available point of care diagnostic systems that can detect and monitor tuberculosis, drug-resistance and its progression. Point of care systems which are cheaply available reduces the cost of tuberculosis and multidrug-resistant tuberculosis detection of poorer individuals. The immunosensor proposed in this study provides a simple platform for future exploitation of rapid and accurate determination of tuberculosis present in infected individuals. The immunosenosor will combine the high specific antibody-antigen complexes with polymer thin films. While the biosensor provides a simple platform for determination of residual TB-drugs present in aqueous systems.

1.11 Historical Summary

The WHO report of 2015 shows the significant impact of tuberculosis on sub-Saharan Africa, and more importantly in co-infected patients with TB and MDR-TB. A high prevalence for

drug-resistance and multi-drug resistance is also evident. The main contribution to these statistics is the inadequate economic affordability of the more expensive diagnostic tools and poor bacterial-friendly clinical hospitals due to the lack of good infrastructure. The current TB diagnostic methods that are used and applied in improving different ways of detecting tuberculosis disease indicates that some of these methods have limitations and they are expensive. And some of these diagnostic tools suffer insensitivity and intensive laboratory requirements. The more sensitive diagnostic tools such as the XpertMRTB/RIF test, are expensive to implement in poorer regions such as sub-Saharan Africa. The sputum smear microscopy is the primary method for the diagnosis of tuberculosis and relatively simple tool to use, the incapability to differentiate between MTB complex and non-MTB has been overtaken by a recently implemented diagnostic test Xpert/MTB/RIF due to sensitivity and accuracy in detecting MTB and rifampicin-resistance. On the other hand ELISA based methods (which does not require sputum for tests) such as LAM test are proving to be a good and cheap diagnostic test for TB. Its ability to detect TB in co-infected patients with TB and HIV is one of the factors that promote this test to be a promising diagnostic method that can elucidate many problems that other diagnostic methods are not capable of doing. However, the current research based on either electrochemical or optical detection of TB and drug-resistant TB tools requires more intensive laboratory trials to be applicable for cheaper, readily-available and highly sensitive and specific for point-of-care systems. The electrochemical sensor for detection of TB and drug-resistance have shown how some of these cheaper and readily-available tools can be developed. In this study, CYP2E1, a heme-protein-based enzyme is used for the development of biosensors and silver nanoparticles will be expected to contribute its properties by facilitating the electron exchange between the electrode and CYP2E1 when detecting anti-TB drug ethambutol and rifampicin. On the other hand, it appears that under-developed infrastructures may cause to have poor health facilities [15,106–108]. And when health facilities are not well operating, the availability of adequate and good quality diagnostic TB methods can be of poor standard. Therefore, the immunosenosor will be developed to detect *Mycobacterium tuberculosis*. The project framework gives a detailed description for development of *Mycobacterium tuberculosis* immunosensor and enzymatic biosensor.

1.12 Research project framework

There are two parts in this study. The first part is related to the tuberculosis disease and how it can be detected by new methods. While the second part is related to drug-resistant tuberculosis and how the anti-TB drugs can be detected in aqueous media. The first part is the immunosensor pathway for the detection of tuberculosis and the second part is the development of biosensor strategy. For the detection of tuberculosis, electrochemical immunosensor pathway was selected to benefit from its advantages of combining/adopting the high specificity of traditional immunochemical methods (ELISA immunoassays) with the low detection limits, and by considering the that fact there is no requirement of using sputum (such as blood/serum) to detect tuberculosis when using this test. In the second part, an enzymatic biosensor was decided using cytochrome P450 as the enzyme. In both strategies (immunosensor and biosensor), the first step was to modify glassy carbon electrode (GCE) with a polymer in order to immobilize the antigen (development of immunosensor) and the enzyme (development of biosensor).

1.13 Polymers used for the immobilization of biomolecules

Polyamic acid and polypyrrole have characteristics that allow the design of electron transfer pathways between the immobilized biomolecule and the electrode surface. Hence they will be used to modify electrodes for immobilization of antigen and enzyme.

1.13.1 Polyamic acid

1.13.1.1 Properties of polyamic acid

Polyamic acid (PAA) is a precursor of polyimides with cation complexing properties. The complexing power of PAA is believed to be significantly higher than that of imide form, implying the ability of the carboxylic acid groups to produce polyfunctional behavior. In a few studies, it was suggested that PAA could open up the possibility of creating monodisperse, nanoscale particles of noble metals to create a high density of anchor groups for the directed immobilization of biomolecules. Hence, PAA membranes were used in the study of Noah et al for sensing and site-directed immobilization of proteins, which resulted in a significant

improvement in the detection sensitivity [109]. The polymer can be synthesized into two forms, solid and liquid, depending on the solvent(s) used for the synthesis. For instance, when tetrahydrofuran (THF) is used as solvent, the resulting PAA can be prepared as a viscous liquid. When acetonitrile (ACN) is used as solvent, the PAA derivative is obtained in a powdered form, from the same starting material as the synthesis of the liquid PAA (Figure 15).

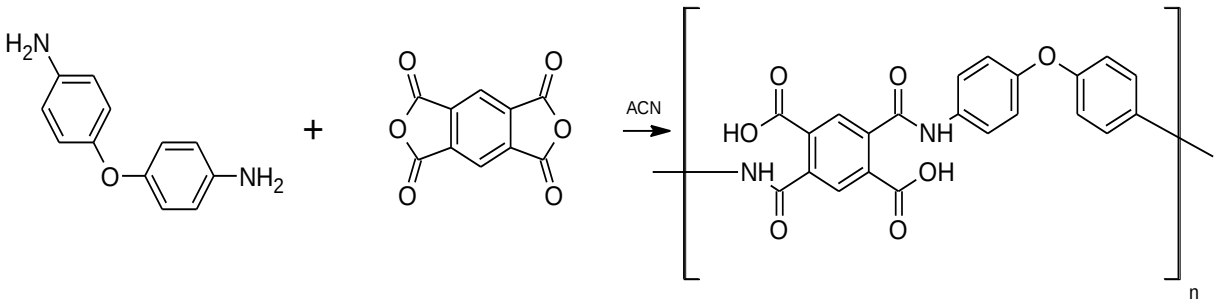

Figure 15: The Chemical Synthesis of Polyamic Acid from 4,4-oxydianiline (ODA) and 1,2,4,5-benzenetetracarboxylic anhydride (PMDA) using acetonitrile (ACN) as a solvent

The powdered polymer is assumed to have good stability over the liquid one since the liquid PAA easily dry up when exposed to air and its liquid form cannot be retained even when it is dissolved in any of the solvents that it dissolves into. Andreescu and co-workers have reported the synthesis, optimization, and characterization of the first PAA-metal nanoparticle composites as electrode materials [110]. It was said in their study that the uniqueness of their approach lied in the preparation of metal nanoparticles within electrodeposited PAA film at low temperature and the ability to prevent the cyclization process. In conclusion to their study, it was suggested that the presence of free carboxylic groups in the PAA and PAA-metal electrode may allow the utilization of this material as immobilization matrices in immunoassays, chromatographic stationary phases, catalysts, biosensor devices and conductivity-enhanced electrode materials. The free carboxylic moieties exposed to the surface of these polymers could be chemically modified to achieve a highly-density anchoring of biomolecules [110]. In few and some recent studies, polyamic acid has been used as a platform for biosensors and immunosensors. In some studies, it has been utilized as a composite or copolymer in developing these platforms. A detailed brief discussion that is relevant to our study is discussed; how polyamic acid has been utilized in different studies, for sensor/biosensors and immunosensors due to the properties it possess.

1.13.1.2 Polyamic acid in sensor and biosensors

In most of the biosensor-based studies that PAA have been utilized as part of the platforms, it is evidently indicated that PAA is a potential candidate for biosensors due to the carboxylic and amide groups available in the polymer which can be used for appropriate covalent attachment of biomolecules. PAA is soluble in both organic and aqueous solvents and binds specifically to biomolecules through its pendant carboxyl groups that are in close proximity to the transducer surface [111]. The carboxylic acid groups in the PAA structure are part of a rigid section of the polymer with a mild degree of rotation about the ether linkages that allow for locked-in orientation during immobilization. These locked-in functional groups in the side chains facilitate in-situ surface reactions for optimization of sensor properties. These characteristics allow the design of electron transfer pathways between the immobilized biomolecule and the electrode surface. In one of the studies where Noah and co-workers were investigating the feasibility of modifying the carboxylic groups available in PAA for site-directed immobilization of biomolecules and as template of electrochemical sensors, they demonstrated that the carboxylic end of the PAA can be modified using EDC/NHS chemistry and subsequently used to immobilize biomolecules on a sensor surface [109]. A simple and sensitive non-enzymatic sensor for the detection of hydrogen peroxide has also been developed using screen-printed electrodes modified with PAA, whereby the electrodeposition method on glassy carbon and drop casting method on screen-printed electrode was used. The drop casting method showed a high sensitivity (899 µA/mM.cm^{-2}) and detection limit of 4 µM of the modified sensors for the detection of hydrogen peroxide. The hydrogen peroxide was screened in urine samples and the PAA-modified screen-printed sensor proved to be an efficient transducer for hydrogen peroxide detection in urine samples. Again, the presence of carboxylic group in PAA, the polymer represents an attractive matrix for chemical immobilization of enzymes such as peroxidase, tyrosinase in developing enzyme biosensors based on detection of hydrogen peroxide [112]. Polyamic acid has also been prepared as a composite film with polypyrrole. The thin films were synthesized by electrochemical method from a solution containing a controlled molar ratio of chemically synthesized polyamic acid and pyrrole monomer [113]. The composition for constituting the novel composites was investigated and supporting evidence for the copolymerization was obtained from spectroscopy, voltammetry, and microscopy. The novel composites produced in this study was specifically prepared for sensing applications, where volatile organic compounds were detected successfully. Hence PAA platform is adapted for immobilization/attachment of tuberculosis antigens and CYP2E1

enzyme on the electrode in this study. In addition, PAA has an excellent biocompatibility. The immunosensor and biosensor will be constructed with electroactive layer of electrodeposited PAA on glassy carbon electrode. The Ag85B antigen and CYP2E1 enzyme will be immobilized on PAA-modified GCE where the carboxylic acid groups from PAA will be expected to bind to amine groups on the corresponding antigen and enzyme.

1.13.2 Polypyrrole

Polypyrrole (PPy) offers tremendous technological potential such as fabrication of molecular electronic devices, electrodes for solid-state batteries, solid electrolytes for capacitors, electromagnetic interference shielding materials, and sensors. Electrochemical polymerization on a metal electrode results in good quality film, while chemical polymerization yields fine conducting powders. Polypyrrole polymerized either electrochemically or chemically (Figure 16) and is known to be insoluble and infusible due to the strong inter and intra-molecular interactions and copolymerization [114]. Ion exchange behaviour during the charging and discharging process of conducting PPy has been widely studied in recent years. The ability of PPy to switch between oxidized and reduced states leading to its conducting and insulating properties has also gained great interest [115]. By employing chemical synthesis routes the PPy is mainly produced in the bulk solution and the transfer of the PPy to a suitable electrode surface is limited.

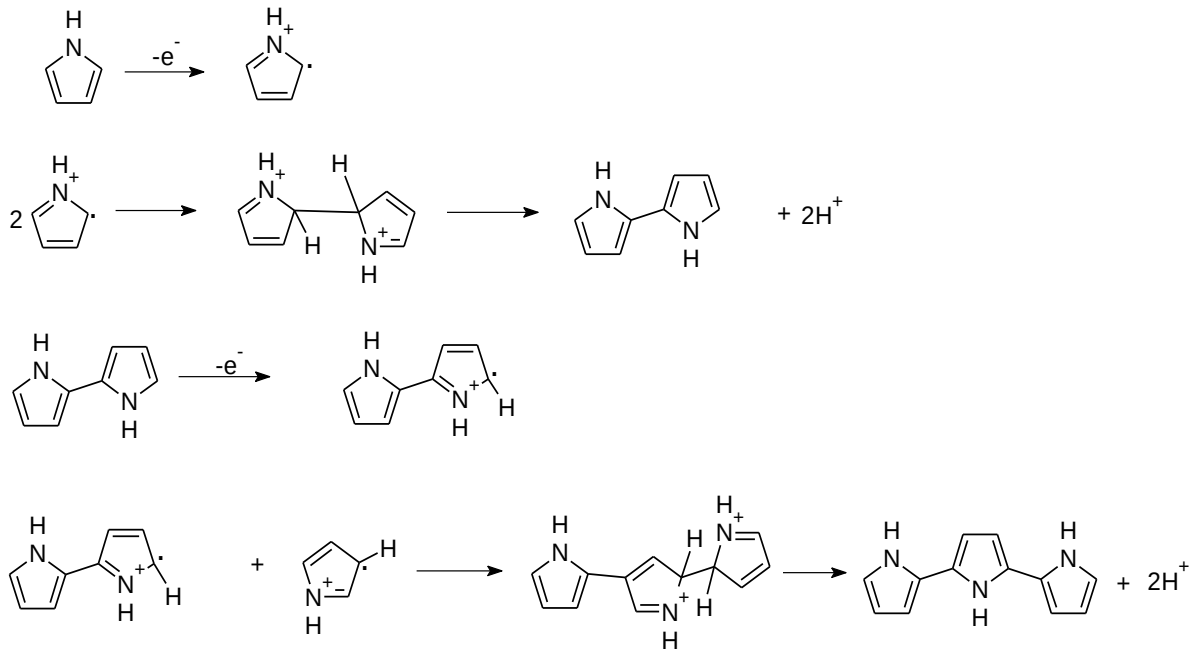

Figure 16: The synthesis of polypyrrole from pyrrole monomer

In the oxidation form, the cationic product contains a staggered, conjugated π-electron network that can be balanced with dopant ions such as $H_2PO_4^-$ ClO^-_4, dodecylbenzenesulfonate (DBS^-), which provide different electrochemical and mechanical properties to the polymer. During the polymerization process cations from electrolyte are expected to exhibit electrostatic repulsion forces with radical cations of pyrrole monomers. This repulsion forces largely depend on the charge of cations. Polypyrrole is insoluble in most common solvents and adherence of PPy to the electrode surface during sensor preparation, is also problematic in the absence of suitable dopants that improves its properties. These disadvantages however may be avoided, if electrochemical polymerization is applied. Thickness and morphology of the film are easily controlled by type of solvent, electrolyte concentration and type of electrode material, current density, applied potential, polymerization time and temperature. The optimization of these parameters in order to obtain nanostructured and reasonably stable PPy in air and in aqueous media opens the way for entrapment and/or doping of polypyrrole by various biomaterials such as small organic molecules, DNA, proteins and even living cells. PPy may also be synthesized in the overoxidized state and entrapped molecules may be removed to produce molecularly imprinted polymer electrodes. Electropolymerization also allows the deposition of films independent of the electrochemical cell geometry and this is particularly useful in the design biosensor systems.

1.14 Presentation of the platforms prepared and used in this study

1.14.1 Part I: Mycobacterium tuberculosis mmunosensor strategy

In this study, we adopted the indirect ELISA method for detecting *Mycobacterium tuberculosis and* subsequently adopt the indirect ELISA protocol into developing the immunosensor for *Mycobactrium tuberculosis*. Figure 17 is the schematic illustration of how the *Mycobacterium tuberculosis* immunosensor will be developed.

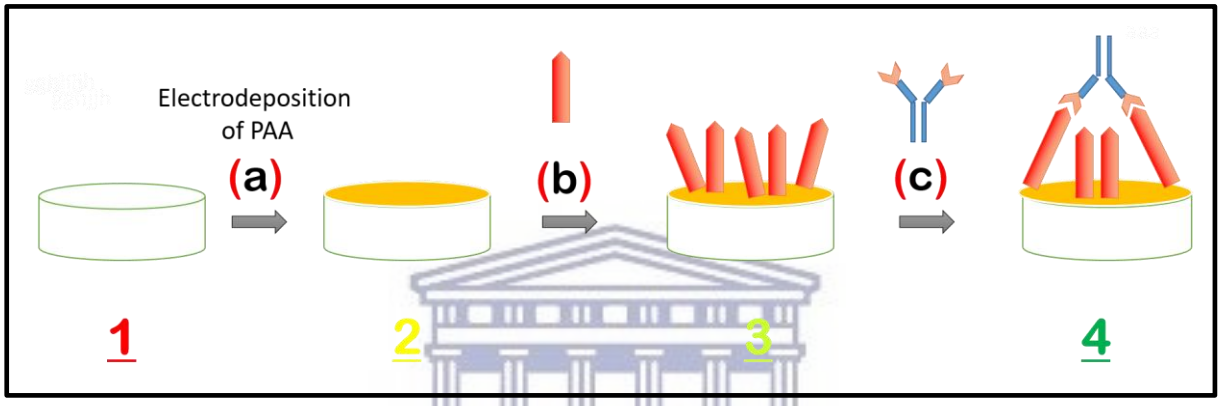

Figure 17: Schematic illustration of the stepwise immunosensor development process

1 Glassy Carbon Electrode (GCE)

(a) Deposition of polyamic acid (PAA)

2 Deposited polyamic acid (GCE/PAA)

(b) Recombinant *Mycobacterium tuberculosis* Ag85B protein (antigen) immobilization

3 Immobilized antigen on modified electrode (GCE/PAA/Ag)

(c) Anti-Mycobacterium tuberculosis Ag85B antibody incubation

4 *Mycobacterium tuberculosis* Ag8B Immunosensor (where electrochemical signals will be produced)

1.14.2 Part II: CYP2E1-based biosensor strategy

Cytochrome P450 play a crucial role in drug metabolism, especially in phase 1 metabolic clearance of numerous xenobiotics in the liver. NADPH regent rating enzymes are generally known to be used to supply electrons to CYP enzymes. However, replacing these enzymes (NADPHs) with electrodes have become a promising approach to develop inexpensive and rapid assays since these enzymes are expensive. Figure 18 is the schematic illustration of how the enzymatic biosensor will be developed.

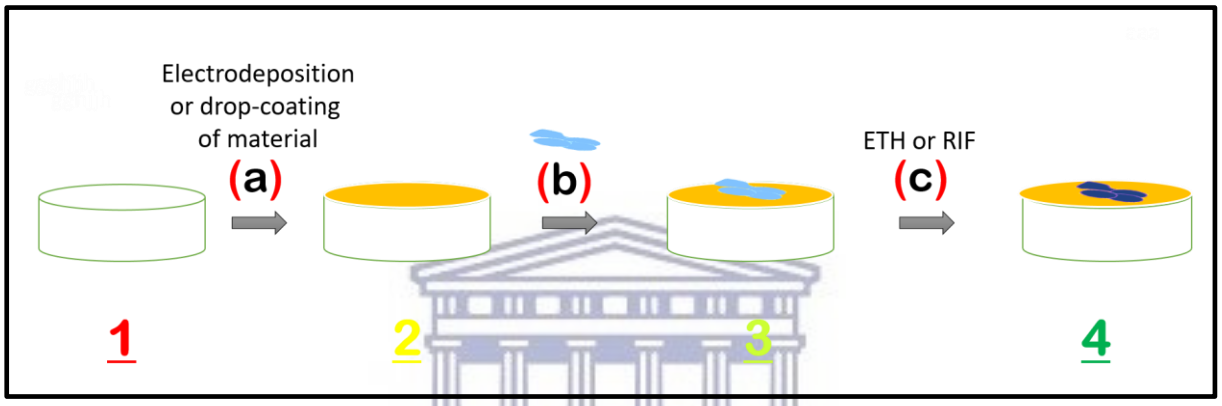

Figure 18: Schematic illustration of the stepwise biosensor development process

1 Glassy Carbon Electrode (GCE)

(a) Deposition of polyamic acid or polypyrrole alone or with silver nanoparticles

2 Modified electrode (GCE/PAA, GCE/PPy, GCE/PAA/AgNPs or GCE/PPy/AgNPs)

(b) Cytochrome P450-2E1 (CYP2E1) enzyme immobilization

3 Immobilized CYP2E1 enzyme on modified electrodes

(c) Adding different concentration of ethambutol/rifampicin

4 Detection of ethambutol/rifampicin with GCE/PAA/AgNPs/CYP2E1 and/or GCE/PPy/AgNPs/CYP2E1 biosensors

1.14.3 Aims and Objectives

Aim 1: Synthesis and characterization of 4,4-oxydianiline (ODA) copolymerization with benzene-1,2,4,5-tetracarboxylic dianhydride (PMDA) using the well-established synthesis by Daniel Andreescu et al. 2005 for the development a conductive polymer and the modification of the polymer with nanoparticles and enzymes. We have demonstrated previously [113] that in situ copolymerization may be effectively used to synthesize polymer nanocomposites with very good electrochemical reactivity. The expertise developed to date in working with amine-imide polymer will be exploited in the design of novel immunosensors and biosensors for detection tuberculosis and monitoring of first-line anti-TB drugs concentrations.

Objective 1: Modification of electrodes to be used as electrochemical transducer in sensor design with polyamic acid may be done by electrodeposition or drop-coating, while polypyrrole can be easily synthesized from pyrrole monomer by means of electropolymerization. The challenge in this work package would be to generate well defined, co-deposited thin films with favorable electrochemical response.

Objective 2: Characterization of the polyamic acid and polypyrrole thin films using the following characterization techniques: Scanning electron microscope (SEM) will be used to provide detailed information of the morphology of polyamic acid thin films and polyamic acid composite. FTIR will be used to observe the shift in vibrations and new bands in newly developed polymer. Electrochemical methods such as cyclic voltammetry will be used to study the electrochemical behavior of the thin films.

Objective 3: The modification of the polyamic acid and polypyrrole thin films with a biological recognition element such as enzyme which can bind their targets with affinities and specificities that can be comparable to those of antibodies to improve the sensitivity and selectivity of the developed biosensor. The modified polymer and nanocomposite will then be characterized using different electrochemical methods such as electrochemical impedance spectroscopy (EIS), square wave voltammetry (SWV) and cyclic voltammetry (CV) to study the effect of the enzyme into the electrochemical behavior (conductivity, diffusivity etc.) of the developed biosensor. The morphology of the modified thin films will also be studied using the selected scanning electron microscope (SEM) and atomic force microscopy (AFM).

Aim 2: To demonstrate the concept capability of the biosensors for the selective detection of chosen first-line anti-TB drugs: ethambutol and rifampicin. Evaluation of concentration-

dependent reactivity (calibration curves) may be followed electrochemical techniques (square wave/differential pulse voltammetry) and morphology evaluation (scanning electron microscopy, atomic force microscopy). All these techniques provide complementary information which will be employed in the mapping of these drugs in acidic and alkaline/basic media.

Objective 1: Construct calibration curves using electrochemical techniques (cyclic/square wave/differential pulse voltammetry). Compare sensitivity and selectivity of the developed biosensors to the other previously developed sensors which are used to detect *Mycobacterium tuberculosis* and anti-TB drugs.

Objective 2: Evaluate the sensitivity and selectivity of the biosensors in detecting ethambutol and rifampicin concentrations in a cocktail or mixture form. Evaluate cross-reactivity with the intention of optimizing resolution, evaluate interfering species which may suppress to enhance detection of the analyte.

1.15 References

1. Esmail, H., Barry, C. E., Young, D. B. & Wilkinson, R. J. The ongoing challenge of latent tuberculosis. *Philos. Trans. R. Soc. B Biol. Sci.* **369,** 20130437–20130437 (2014).

2. Who. Use of high burden country lists for TB by WHO in the post-2015 era. *WHO Press* 19 (2015).

3. Salazar-Austin, N. *et al.* Extensively drug-resistant tuberculosis in a young child after travel to India. *Lancet Infect. Dis.* **15,** 1485–1491 (2015).

4. Fogel, N. Tuberculosis: A disease without boundaries. *Tuberculosis* **95,** 527–531 (2015).

5. Rothschild, B. M. *et al.* Mycobacterium tuberculosis Complex DNA from an Extinct Bison Dated 17,000 Years before the Present. *Clin. Infect. Dis.* **33,** 305–11 (2001).

6. Lugton, I. W. Mucosa-associated lymphoid tissues as sites for uptake, carriage and excretion of tubercle bacilli and other pathogenic mycobacteria. *Immunol. Cell Biol.* **77,** 364–372 (1999).

7. Donoghue, H. D. Insights gained from palaeomicrobiology into ancient and modern tuberculosis. *Clin. Microbiol. Infect.* **17,** 821–829 (2011).

8. Manchester, K. Tuberculosis and Leprosy in Antiquity: an Interpretation. *Med. Hist.* **28,** 162–173 (1984).

9. Canci, A., Mlnozzl, S. & Borgognlnl, S. M. New Evidence of Tuberculous Spondylitis from Neolithic Liguria (Italy). *Int. J. Osteoarchaeol.* **6,** 497–501 (1996).

10. Daniel, T. M. The history of tuberculosis. *Respir. Med.* **100,** 1862–1870 (2006).

11. Gómez I Prat, J. & Mendonça De Souza, S. M. F. Prehistoric Tuberculosis in America: Adding Comments to a Literature Review. *Mem. Inst. Oswaldo Cruz* **98,** 151–159 (2003).

12. Karim, K. Tuberculosis and infection control. *Br. J. Nurs.* **20,** 1128, 1130–3 (1999).

13. Bass, J. R., Farer, L. S., P.C., H., Jacobs, R. F. & Snider Jr, D. E. American Thoracic Society. Diagnostic standards and classification of tuberculosis. *Am Rev Respir Dis* **142,** 725–735 (1990).

14. Herzog, H. History of tuberculosis. *Respiration* **65,** 5–15 (1998).

15. Von Delft, A. *et al.* Why healthcare workers are sick of TB. *Int. J. Infect. Dis.* **32,** 147–151 (2015).

16. Belo, C. & Naidoo, S. Prevalence and risk factors for latent tuberculosis infection among healthcare workers in Nampula Central Hospital, Mozambique. *BMC Infect. Dis.* **17,** 408 (2017).

17. Dacso, C. C. Skin Testing for Tuberculosis. *Clin. Methods Hist. Phys. Lab. Exam.* (1990). at <http://www.ncbi.nlm.nih.gov/pubmed/21250210>

18. U.S. Department of Health and Human Sevices. Self-Study Modules 3: Targeted Testing and Latent Tuberculosis Infection and T uberculosis Disease. *Tuberculosis* (2008).

19. Metcalfe, J. Z. *et al.* Test variability of the QuantiFERON-TB gold in-tube assay in clinical practice. *Am. J. Respir. Crit. Care Med.* **187,** 206–211 (2013).

20. Ryu, Y. J. Diagnosis of pulmonary tuberculosis: Recent advances and diagnostic algorithms. *Tuberc. Respir. Dis. (Seoul).* **78,** 64–71 (2015).

21. Joice, R. *et al.* NIH Public Access. **6,** 1–16 (2014).

22. Theron, G. *et al.* Xpert MTB/RIF Results in Patients With Previous Tuberculosis: Can We Distinguish True From False Positive Results? *Clin. Infect. Dis.* **62,** (2016).

23. Lawn, S. D. *et al.* Advances in tuberculosis diagnostics: the Xpert MTB/RIF assay and future prospects for a point-of-care test. *Lancet Infect. Dis.* **13,** 349–361 (2013).

24. Theron, G. *et al.* Feasibility, accuracy, and clinical effect of point-of-care Xpert MTB/RIF testing for tuberculosis in primary-care settings in Africa: A multicentre, randomised, controlled trial. *Lancet* **383,** (2014).

25. Peter, J. G. *et al.* Diagnostic accuracy of a urine lipoarabinomannan strip-test for TB detection in HIV-infected hospitalised patients. *Eur. Respir. J.* **40,** 1211–1220 (2012).

26. Lawn, S. D. *et al.* Determine TB-LAM lateral flow urine antigen assay for HIV-associated tuberculosis: Recommendations on the design and reporting of clinical studies. *BMC Infect. Dis.* **13,** (2013).

27. Cellestis QIAGEN. QuantiFERON-TB Quick Guide Assay. (2011).

28. Baid, A. ELISA- A Mini Review. *Res. Rev. J. Pharm. Anal.* **5,** 1–8 (2016).

29. Voller, a, Bartlett, a & Bidwell, D. E. Enzyme immunoassays with special reference to ELISA techniques. *J. Clin. Pathol.* **31,** 507–520 (1978).

30. Tsara, V., Serasli, E. & Christaki, P. Problems in diagnosis and treatment of tuberculosis infection. *Hippokratia* **13,** 20–22 (2009).

31. Cardoso, F. L. L. *et al.* T-Cell Responses to the. *Society* **70,** 6707–6714 (2002).

32. Anderson, D. H., Harth, G., Horwitz, M. a. & Eisenberg, D. An interfacial mechanism and a class of inhibitors inferred from two crystal structures of the Mycobacterium tuberculosis 30 kda major secretory protein (antigen 85B), a mycolyl transferase11Edited by I. A. Wilson. *J. Mol. Biol.* **307,** 671–681 (2001).

33. Zheng, Y. *et al.* Applications of bacillus Calmette-Guerin and recombinant bacillus Calmette-Guerin in vaccine development and tumor immunotherapy. *Expert Rev. Vaccines* **14,** 1255–75 (2015).

34. Xu, Z. *et al.* Generation of Monoclonal Antibodies against Ag85A Antigen of Mycobacterium tuberculosis and Application in a Competitive ELISA for Serodiagnosis of Bovine Tuberculosis. *Front. Vet. Sci.* **4,** 107 (2017).

35. Zhang, C. *et al.* Mycobacterium tuberculosis Secreted Proteins As Potential Biomarkers for the Diagnosis of Active Tuberculosis and Latent Tuberculosis Infection. *J. Clin. Lab. Anal.* **29,** 375–382 (2015).

36. Boritsch, E. C. *et al.* A glimpse into the past and predictions for the future: The molecular evolution of the tuberculosis agent. *Mol. Microbiol.* **93,** 835–852 (2014).

37. Mertaniasih, N. M. *et al.* Sequence Analysis of the Gene Region Encoding ESAT-6, Ag85B, and Ag85C Proteins from Clinical Isolates of Mycobacterium tuberculosis. *Procedia Chem.* **18,** 225–230 (2016).

38. Coetsier, C., Baelden, M. C., Coene, M. & Cocito, C. Immunological analysis of the components of the antigen complex A60 of Mycobacterium bovis BCG. *Clin Diagn Lab Immunol* **1,** 139–144 (1994).

39. Wang, J. *et al.* Sequence-specific electrochemical biosensing of M-tuberculosis DNA. *Anal. Chim. Acta* **337,** 41–48 (1997).

40. Thiruppathiraja, C., Kamatchiammal, S., Adaikkappan, P., Santhosh, D. J. & Alagar, M. Specific detection of Mycobacterium sp. genomic DNA using dual labeled gold nanoparticle based electrochemical biosensor. *Anal. Biochem.* **417,** 73–79 (2011).

41. Torres-Chavolla, E. & Alocilja, E. C. Nanoparticle based DNA biosensor for tuberculosis detection using thermophilic helicase-dependent isothermal amplification. *Biosens. Bioelectron.* **26,** 4614–4618 (2011).

42. Yu, X., Chai, Y., Jiang, J. & Cui, H. Sensitive ECL sensor for sequence-specific DNA from Mycobacterium tuberculosis based on N-(aminobutyl)-N-ethylisoluminol functionalized gold nanoparticles labeling. *J. Photochem. Photobiol. A Chem.* **241,** 45–51 (2012).

43. He, F., Xiong, Y., Liu, J., Tong, F. & Yan, D. Construction of Au-IDE/CFP10-ESAT6 aptamer/DNA-AuNPs MSPQC for rapid detection of Mycobacterium tuberculosis. *Biosens. Bioelectron.* **77,** 799–804 (2016).

44. Prabhakar, N., Singh, H. & Malhotra, B. D. Nucleic acid immobilized polypyrrole-polyvinylsulphonate film for Mycobacterium tuberculosis detection. *Electrochem. commun.* **10,** 821–826 (2008).

45. Matsishin, M., Rachkov, a., Errachid, a., Dzyadevych, S. & Soldatkin, a. Development of impedimetric DNA biosensor for selective detection and discrimination of oligonucleotide sequences of the rpoB gene of Mycobacterium tuberculosis. *Sensors Actuators, B Chem.* **222,** 1152–1158 (2015).

46. Díaz-González, M., González-García, M. B. & Costa-García, A. Immunosensor for Mycobacterium tuberculosis on screen-printed carbon electrodes. *Biosens. Bioelectron.* **20,** 2035–2043 (2005).

47. Canovi, M. *et al.* A new surface plasmon resonance-based immunoassay for rapid, reproducible and sensitive quantification of pentraxin-3 in human plasma. *Sensors (Switzerland)* **14,** 10864–10875 (2014).

48. Hong, S. C. *et al.* Ultrasensitive immunosensing of tuberculosis CFP-10 based on SPR spectroscopy. *Sensors Actuators, B Chem.* **156,** 271–275 (2011).

49. De Espíndola, A. L. *et al.* An antibiotic protocol to minimize emergence of drug-resistant tuberculosis. *Phys. A Stat. Mech. its Appl.* **400,** 80–92 (2014).

50. Prasad, B. & Singh, S. In vitro and in vivo investigation of metabolic fate of rifampicin using an optimized sample preparation approach and modern tools of liquid chromatography-mass spectrometry. *J. Pharm. Biomed. Anal.* **50,** 475–490 (2009).

51. Mitchison, D. a. The action of antituberculosis drugs in short-course chemotherapy. *Tubercle* **66,** 219–225 (1985).

52. Brown, T. J. Simultaneous identi ® cation and typing of multi- drug-resistant Mycobacterium tuberculosis isolates by analysis of pncA and rpoB. **49,** 651–656 (2000).

53. Telenti, a. *et al.* Detection of rifampicin-resistance mutations in Mycobacterium tuberculosis. *Lancet* **341,** 647–651 (1993).

54. Zhang, Y., Heym, B., Allen, B., Young, D. & Cole, S. The catalase-peroxidase gene and isoniazid resistance of Mycobacterium tuberculosis. *Nature* **358,** 591–593 (1992).

55. Rawat, R., Whitty, a. & Tonge, P. J. The isoniazid-NAD adduct is a slow, tight-binding inhibitor of InhA, the Mycobacterium tuberculosis enoyl reductase: Adduct affinity and drug resistance. *Proc. Natl. Acad. Sci.* **100,** 13881–13886 (2003).

56. Takayama, K. & Kilburn, J. O. Inhibition of synthesis of arabinogalactan by ethambutol in Mycobacterium smegmatis. *Antimicrob. Agents Chemother.* **33,** 1493–1499 (1989).

57. Mikusová, K., Slayden, R. a, Besra, G. S. & Brennan, P. J. Biogenesis of the mycobacterial cell wall and the site of action of ethambutol . Biogenesis of the Mycobacterial Cell Wall and the Site of Action of Ethambutol. *Antimicrob. Agents Chemother.* **39,** 2484–2489 (1995).

58. Butler, W. R. & Kilburn, J. O. Susceptibility of Mycobacterium tuberculosis to pyrazinamide and its relationship to pyrazinamidase activity. *Antimicrob. Agents Chemother.* **24,** 600–601 (1983).

59. Hirano, K., Takahashi, M., Kazumi, Y., Fukasawa, Y. & Abe, C. Mutation in pncA is a major mechanism of pyrazinamide resistance in Mycobacterium tuberculosis. *Tuber. Lung Dis.* **78,** 117–122 (1997).

60. Crofton, J. & Mitchison, D. Streptomycin Resistance in Pulmonary Tuberculosis. *Br. Med. J.* **2,** 1009–1015 (1948).

61. Moazed, D. & Noller, H. F. Interaction of antibiotics with functional sites in 16S ribosomal RNA. *Nature* **327,** 389–94 (1987).

62. Finken, M., Kirschner, P., Meier, A., Wrede, A. & Böttger, E. C. Molecular basis of streptomycin resistance in Mycobacterium tuberculosis: alterations of the ribosomal protein S12 gene and point mutations within a functional 16S ribosomal RNA pseudoknot. *Mol. Microbiol.* **9,** 1239–1246 (1993).

63. Lemos, A. C. M. & Matos, E. D. Multidrug-resistant tuberculosis. *Brazilian J. Infect. Dis.* **17,** 239–246 (2013).

64. Sotgiu, G. & Migliori, G. B. Facing multi-drug resistant tuberculosis. *Pulm. Pharmacol. Ther.* **32,** 144–148 (2015).

65. Bradford, W. Z. & Daley, C. L. Multiple drug-resistant tuberculosis. *Infect. Dis. Clin. North Am.* **12,** 157–172 (1998).

66. Hoagland, D. T., Liu, J., Lee, R. B. & Lee, R. E. New agents for the treatment of drug-resistant Mycobacterium tuberculosis. *Adv. Drug Deliv. Rev.* **102,** 55–72 (2016).

67. Gandhi, N. R. *et al.* Multidrug-resistant and extensively drug-resistant tuberculosis: a threat to global control of tuberculosis. *Lancet* **375,** 1830–1843 (2010).

68. Report, G. & Surveillanceresponse, O. N. 9789241599191_Eng. (2010).

69. Palomino, J. & Martin, A. Drug Resistance Mechanisms in Mycobacterium tuberculosis. *Antibiotics* **3,** 317–340 (2014).

70. Courtwright, A. & Turner, A. N. Tuberculosis and Stigmatization: Pathways and Interventions. *Public Health Rep.* **125,** 34–42 (2010).

71. Corrigan, P. How stigma interferes with mental health care. *Am. Psychol.* **59,** 614–625 (2004).

72. Gupta, S. *et al.* Cost-effectiveness of the Three I's for HIV/TB and ART to prevent TB among people living with HIV. *Int. J. Tuberc. Lung Dis.* **18,** 1159–1165 (2014).

73. Obermeyer, C. M. & Osborn, M. The utilization of testing and counseling for HIV: A review of the social and behavioral evidence. *Am. J. Public Health* **97,** 1762–1774 (2007).

74. Gandhi, N. R. *et al.* Extensively drug-resistant tuberculosis as a cause of death in patients co-infected with tuberculosis and HIV in a rural area of South Africa. *Lancet* **368,** 1575–1580 (2006).

75. Smith, N. H. *et al.* Ecotypes of the Mycobacterium tuberculosis complex. *J. Theor. Biol.* **239,** 220–225 (2006).

76. Solis, L. *et al.* Evaluation of a lens-free imager to facilitate tuberculosis diagnostics in MODS. *Tuberculosis* **97,** 26–32 (2016).

77. Choi, J., Park, S. J. & Jee, J. G. Analogues of ethionamide, a drug used for multidrug-resistant tuberculosis, exhibit potent inhibition of tyrosinase. *Eur. J. Med. Chem.* **106,** 157–166 (2015).

78. Chakaya, J., Kirenga, B. & Getahun, H. Long term complications after completion of pulmonary tuberculosis treatment: A quest for a public health approach. *J. Clin. Tuberc. Other Mycobact. Dis.* **3,** 10–12 (2016).

79. Kwan, C. & Ernst, J. D. HIV and tuberculosis: A deadly human syndemic. *Clin. Microbiol. Rev.* **24,** 351–376 (2011).

80. The Tuberculosis Coalition for Technical Asssistance (TBCTA). Implementing the WHO Policy on TB Infection Control in Health-Care Facilities , Congregate Settings and Households. 151 (2009). doi:WHO/HTM/TB/2009.419

81. Zanger, U. M. & Schwab, M. Cytochrome P450 enzymes in drug metabolism: Regulation of gene expression, enzyme activities, and impact of genetic variation. *Pharmacol. Ther.* **138,** 103–141 (2013).

82. Ogu, C. C. & Maxa, J. L. Drug interactions due to cytochrome P450. *Proc. (Bayl. Univ. Med. Cent).* **13,** 421–3 (2000).

83. Meunier, B., de Visser, S. P. & Shaik, S. Mechanism of oxidation reactions catalyzed by cytochrome P450 enzymes. *Chem. Rev.* **104,** 3947–3980 (2004).

84. Guengerich, F. P. Common and Uncommon Cytochrome P450 Reactions Related to Metabolism and Chemical Toxicity. *Chem. Res. Toxicol.* **14,** 611–650 (2001).

85. Baj-Rossi, C., de Micheli, G. & Carrara, S. Electrochemical detection of anti-breast-cancer agents in Human Serum by Cytochrome P450-coated Carbon nanotubes. *Sensors (Switzerland)* **12,** 6520–6537 (2012).

86. Furge, L. L. & Guengerich, F. P. Cytochrome P450 enzymes in drug metabolism and chemical toxicology: An introduction. *Biochem. Mol. Biol. Educ.* **34,** 66–74 (2006).

87. Bistolas, N., Wollenberger, U., Jung, C. & Scheller, F. W. Cytochrome P450 biosensors - A review. *Biosens. Bioelectron.* **20,** 2408–2423 (2005).

88. Ajayi, R. F. *et al.* Chemically amplified cytochrome P450-2E1 drug metabolism nanobiosensor for rifampicin anti-tuberculosis drug. *Electrochim. Acta* **128,** 149–155 (2014).

89. Katzberg, M., Skorupa-Parachin, N., Gorwa-Grauslund, M. F. & Bertau, M. Engineering cofactor preference of ketone reducing biocatalysts: A mutagenesis study on a γ-diketone reductase from the yeast saccharomyces cerevisiae serving as an example. *Int. J. Mol. Sci.* **11,** 1735–1758 (2010).

90. Sadeghi, S. J., Fantuzzi, A. & Gilardi, G. Breakthrough in P450 bioelectrochemistry and future perspectives. *Biochim. Biophys. Acta - Proteins Proteomics* **1814,** 237–248 (2011).

91. Shumyantseva, V. V. *et al.* Direct electron transfer of cytochrome P450 2B4 at electrodes modified with nonionic detergent and colloidal clay nanoparticles. *Anal. Chem.* **76,** 6046–6052 (2004).

92. Fantuzzi, A., Fairhead, M. & Gilardi, G. Direct Electrochemistry of Immobilized Human Cytochrome P450 2E1. *J. Am. Chem. Soc.* **126,** 5040–5041 (2004).

93. Ajayi, R. F. *et al.* Chemically amplified cytochrome P450-2E1 drug metabolism nanobiosensor for rifampicin anti-tuberculosis drug. *Electrochim. Acta* **128,** 149–155 (2014).

94. Ngece, R. F. *et al.* A silver nanoparticle/Poly (8-anilino-1-naphthalene sulphonic acid) bioelectrochemical biosensor system for the analytical determination of ethambutol. *Int. J. Electrochem. Sci.* **6,** 1820–1834 (2011).

95. Davydov, D. R., Botchkareva, A. E., Davydova, N. E. & Halpert, J. R. Resolution of two substrate-binding sites in an engineered cytochrome P450eryF bearing a fluorescent probe. *Biophys. J.* **89,** 418–432 (2005).

96. Hlavica, P. Models and mechanisms of O-O bond activation by cytochrome P450: A critical assessment of the potential role of multiple active intermediates in oxidative catalysis. *Eur. J. Biochem.* **271,** 4335–4360 (2004).

97. Ghosh, K. *et al.* NIH Public Access. **44,** 16729–16736 (2008).

98. Mak, L. H., Sadeghi, S. J., Fantuzzi, A. & Gilardi, G. Control of human cytochrome P450 2E1 electrocatalytic response as a result of unique orientation on gold electrodes. *Anal. Chem.* **82,** 5357–5362 (2010).

99. Iwuoha, E. I. *et al.* Reactivities of organic phase biosensors 3: electrochemical study of cytochrome P450cam immobilized in a methyltriethoxysilane sol-gel. *Electroanal* **12,** 980–986 (2000).

100. Johnson, D. L., Conley, a. J. & Martin, L. L. Direct electrochemistry of human, bovine and porcine cytochrome P450c17. *J. Mol. Endocrinol.* **36,** 349–359 (2006).

101. Gilardi, G. *et al.* Molecular Lego: Design of molecular assemblies of P450 enzymes for nanobiotechnology. *Biosens. Bioelectron.* **17,** 133–145 (2002).

102. Munro, a. W., Noble, M. a., Robledo, L., Daff, S. N. & Chapman, S. K. Determination of the redox properties of human NADPH-cytochrome P450 reductase. *Biochemistry* **40,** 1956–1963 (2001).

103. Li, H., Liu, S., Dai, Z., Bao, J. & Yang, X. Applications of nanomaterials in electrochemical enzyme biosensors. *Sensors* **9,** 8547–8561 (2009).

104. Zhang, H. L., Zou, X. Z., Lai, G. S., Han, D. Y. & Wang, F. Direct electrochemistry of hemoglobin immobilized on carbon-coated iron nanoparticles for amperometric detection of hydrogen peroxide. *Electroanalysis* **19,** 1869–1874 (2007).

105. Lee, T. *et al.* Investigation of hemoglobin/gold nanoparticle heterolayer on micro-gap for electrochemical biosensor application. *Sensors (Switzerland)* **16,** (2016).

106. McNerney, R., Cunningham, J., Hepple, P. & Zumla, A. New tuberculosis diagnostics and rollout. *Int. J. Infect. Dis.* **32,** 81–86 (2015).

107. Wang, S., Inci, F., De Libero, G., Singhal, A. & Demirci, U. Point-of-care assays for tuberculosis: Role of nanotechnology/microfluidics. *Biotechnol. Adv.* **31,** 438–449 (2013).

108. Choudhary, S. & Kusum Devi, V. Potential of nanotechnology as a delivery platform against tuberculosis: Current research review. *J. Control. Release* **202,** 65–75 (2015).

109. Noah, N. M. *et al.* Conducting polyamic acid membranes for sensing and site-directed immobilization of proteins. *Anal. Biochem.* **428,** 54–63 (2012).

110. Andreescu, D., Wanekaya, A. K., Sadik, O. a. & Wang, J. Nanostructured polyamic acid membranes as novel electrode materials. *Langmuir* **21,** 6891–6899 (2005).

111. Du, N. *et al.* Flexible poly(amic acid) conducting polymers: Effect of chemical composition on structural, electrochemical, and mechanical properties. *Langmuir* **26,** 14194–14202 (2010).

112. Zamfir, L. G. *et al.* Non-enzymatic polyamic acid sensors for hydrogen peroxide detection. *Sensors Actuators, B Chem.* **226,** 525–533 (2016).

113. Hess, E. H., Waryo, T., Sadik, O. a., Iwuoha, E. I. & Baker, P. G. L. Constitution of novel polyamic acid/polypyrrole composite films by in-situ electropolymerization. *Electrochim. Acta* **128,** 439–447 (2014).

114. Su, N., Li, H. B., Yuan, S. J., Yi, S. P. & Yin, E. Q. Synthesis and characterization of polypyrrole doped with anionic spherical polyelectrolyte brushes. *Express Polym. Lett.* **6,** 697–705 (2012).

115. Ohtsuka, T. Corrosion protection of steels by conducting polymer coating. *Int. J. Corros.* **2012,** (2012).

Chapter Two

This chapter presents the development of immunosensor platforms by adopting the indirect ELISA method. Firstly, the chapter presents the results and discussion on the synthesis and characterization of polyamic acid by FTIR. Secondly, electrodeposition of PAA on GCE is described and followed by electrochemical characterization of the modified electrode by cyclic voltammetric and square wave voltammetric analysis to evaluate the electrochemical behaviour of polyamic acid. On the other hand, the ELISA was used to detect the tuberculosis IgG antibodies using the indirect ELISA method. Thirdly, the mycobacterium tuberculosis immunosensor platforms preparation and characterization by cyclic and square wave voltammetry is also presented. Finally, the immunosensing performance was evaluated using square wave voltammetry. The development of immunosensor platforms is illustrated in Figure 19.

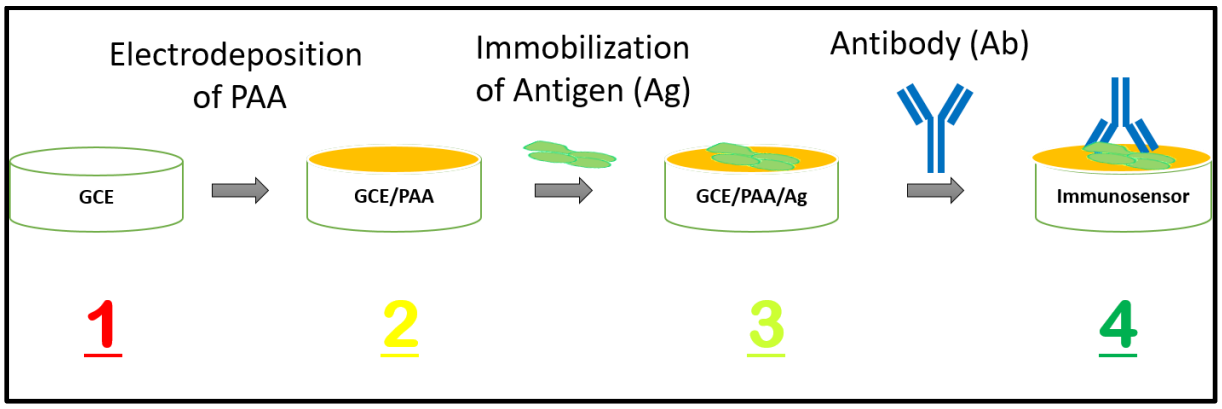

Figure 19: Schematic illustration of the development of the immunosensor

2.1 Polyamic acid synthesis

Polyamic acid (PAA) was synthesized in an organic medium acetonitrile (ACN) using 4,4-oxydianiline (ODA) and 1,2,4,5-benzenetetracarboxylic anhydride (pyromellic dianhydride, PMDA) precursors (Figure 20). The synthesized PAA was then characterized using Fourier transform infrared spectroscopy (FTIR).

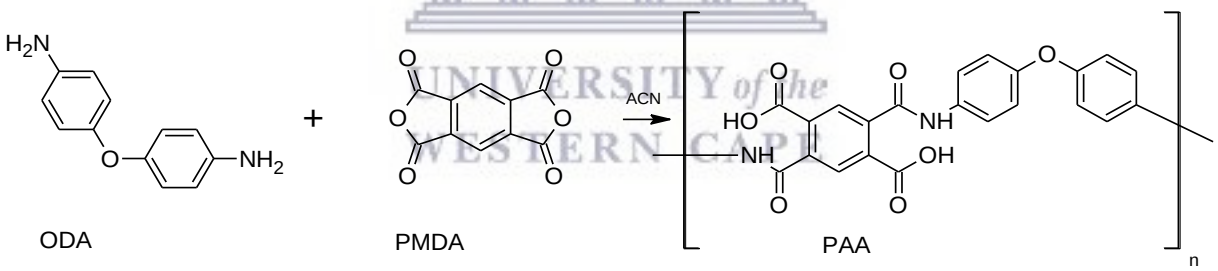

Figure 20: The Chemical Synthesis of Polyamic Acid (PAA) from 4,4-oxydianiline (ODA) and 1,2,4,5-benzenetetracarboxylic anhydride (PMDA) monomers

The FTIR spectrum of solid PAA was recorded as powder (pellet formed using KBr) in a range of 300 and 4500 cm^{-1} (Figure 21). The peak at 1718 cm^{-1} and the absorption bands that occur at 1387 cm^{-1} were assigned to the vibrational modes of the carboxylic acid group, while the bands occurring at 1510 and 1620 cm^{-1} were assigned to the vibrational mode of the amide group. The peak around 1231 cm^{-1} was associated with a stretching vibration of the ether group, while the broad peak at a range of 3500 – 2800 cm^{-1} is associated with the vibrational mode of

the amine and hydroxyl groups. The spectrum presents absorption bands that corresponds to each functional group in the PAA structure [1–3]. Therefore, the FTIR spectrum confirms that the chemical synthesis of PAA was successful. To link the peaks of the functional groups from the polymer, Figure 22 shows the structure of PAA where the functional groups associated with the vibrational modes in the FTIR spectrum are highlighted. The functional groups highlighted in red are carboxylic groups. The amides groups are highlighted in navy while the ether group is highlighted in green.

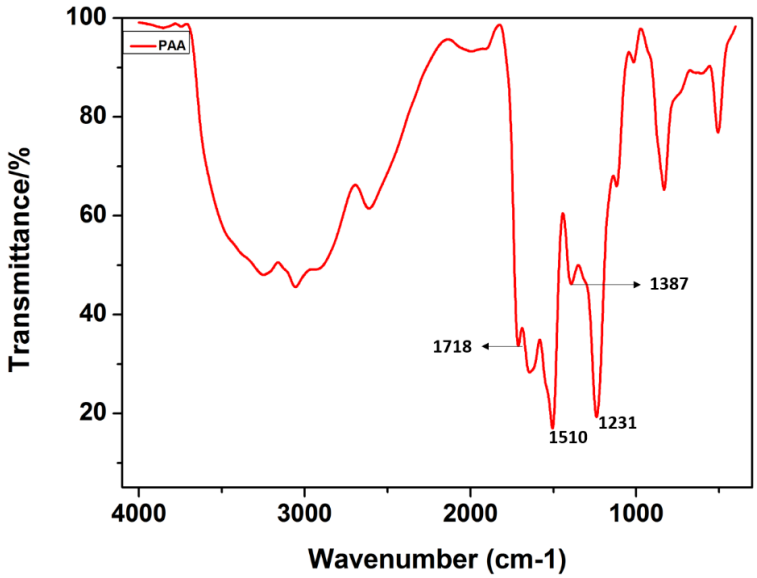

Figure 21: FTIR spectrum of Powdered Polyamic Acid

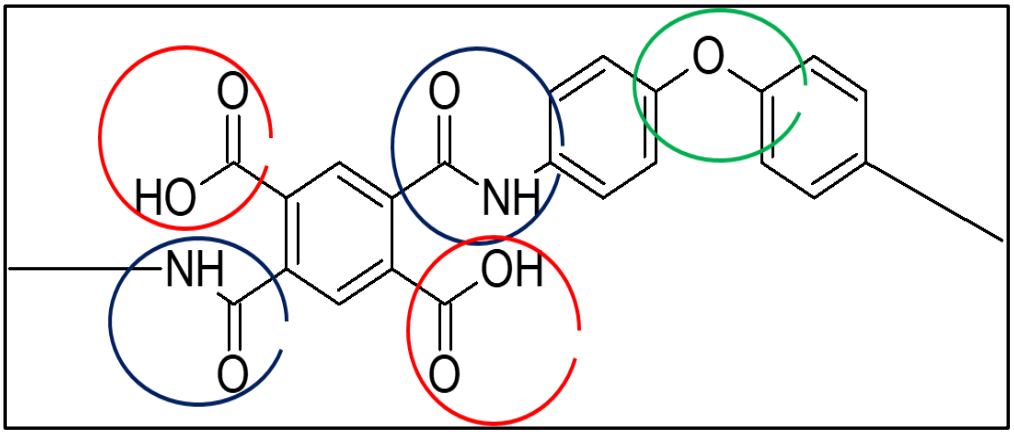

Figure 22: Structure of polyamic acid

2.2 Electrodeposition of PAA

Cyclic voltammetry (CV) is generally used to study the electrochemical properties of an analyte in a solution or to characterize any conducting material that can be attached on the surface of the working electrode such as conducting polymer films, in order to study the reversibility of electron transfer since the oxidation and reduction can be monitored in the form of a current-potential plot/diagram. However, CV can also be used for electrodeposition of materials on the electrodes. The electrodeposition of PAA has been adopted in many studies as a method of modifying/depositing the polymer on the surface of the working electrode. Different working electrodes have been used from different studies such as glassy carbon electrode [3], indium tin oxide electrode [4], gold electrode [5], screen printed carbon/gold electrode [3,5,6]. CV was used to perform the electrodeposition of PAA thin films on glassy carbon electrode (GCE). To achieve the electrodeposition of PAA on GCE, the potential was cycled 5 times from -1.0 to +1.0 V at a scan rate of 50 mV/s as indicated in section ***A.1.3***. The cyclic voltammograms for the electrodeposition of PAA on GCE are shown Figure 23. On the first scan there was an oxidation peak at 540 mV indicating the deposition/adsorption of PAA on the surface of GCE. From the second to the fifth scan two stable oxidation peaks and one reduction peak were observed indicating that PAA was deposited/adsorbed on the surface of GCE. To confirm that PAA was attached on the surface of GCE, the electrodeposited PAA film was further characterized in 0.1 M PBS at different scan rates.

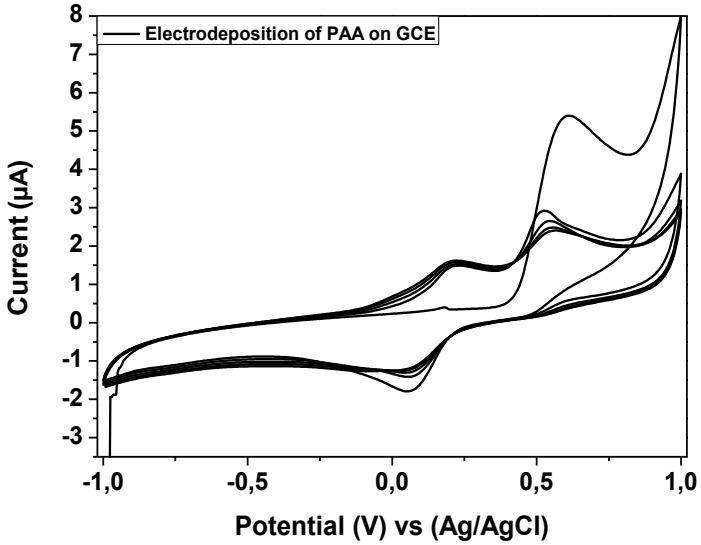

Figure 23: Electrodeposition of PAA on glassy carbon electrode in 0.1 M PBS (pH7.01) at a scan rate of 50 mV/s

2.3 Electrode modified with PAA

The electrochemical behaviour of the GCE/PAA prepared from PAA dissolved in different solvent was evaluated as it is well-known that the amount of polymer film electrodeposited onto an electrode surface is dependent on the composition of the growth medium (solvent, supporting electrolyte, etc.) and other deposition conditions [7].

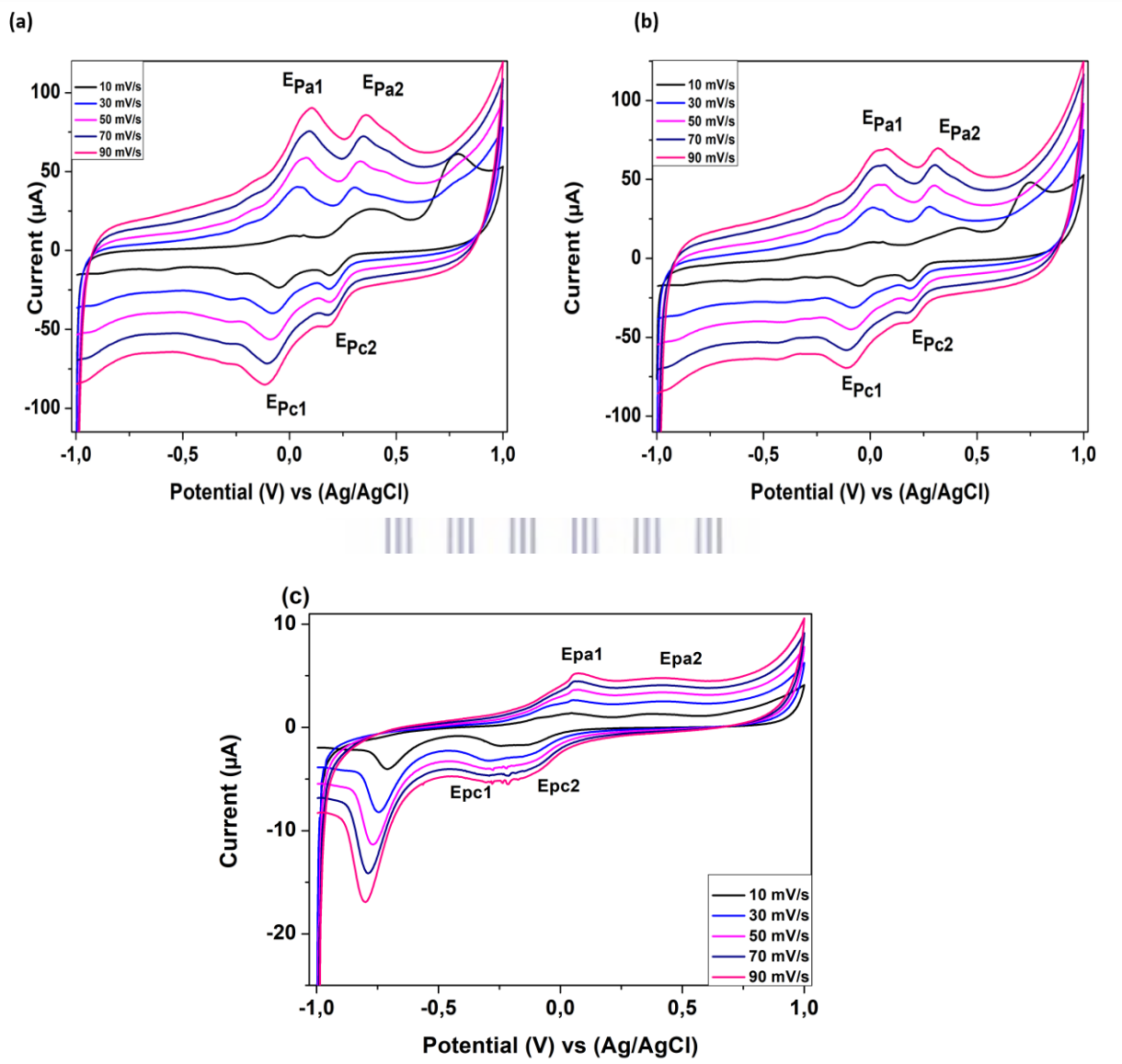

Figure 24: Cyclic voltammograms characterization of GCE/PAA electrodes prepared from PAA dissolved in acetonitrile (a), dimethylformamide (b) and phosphate buffer (c) at different scan rates in 0.1 M PBS (pH7.04) electrolyte

In this study, PAA was firstly dissolved in three different solvents (acetonitrile, dimethylformamide and phosphate buffer solution) and then diluted in phosphate buffer electrolyte for electrodeposition. PBS was also the electrolyte used for the characterization of PAA in all three experiments. The cyclic voltammograms at different scan rates of the three deposits prepared from the three solvents are shown in Figure 24. The same electrochemical signals were observed in terms of the number of oxidation and reduction peaks and it was evident that each solvent had a different impact on the material. When organic solvents DMF and ACN were used to dissolve PAA, the current signal of PAA in each voltammogram at different scan rates was higher than of the PAA dissolved in PBS. Dissolving PAA in organic solvents such as DMF retains the carboxyl group [1]. Different solvents may influence the transport rate of mobile species through a film. Hence, when PAA was dissolved in PBS, the current signal of PAA was low and this may have been caused by the nature of PBS; neutral pH of 7.04. Thus, the redox peaks of PAA were less pronounced in the PBS dissolved-PAA than PAA dissolved in DMF and ACN. This indicated less background current from the polymer and which favours the development of immunosensor whereby it will be easy to identify the new electrochemistry caused by the analyte. Hence, the following experiments of GCE/PAA modified electrodes were all prepared from PAA solution dissolved in PBS. For all three solvents the oxidation and reduction peaks of PAA appeared at different potentials and Table 5 shows the comparison of these oxidation and reduction peaks that were observed from GCE/PAA electrodes that were prepared from PAA dissolved in three different solvents.

Table 5: Redox peaks of PAA dissolved in acetonitrile, dimethyformamideand phosphate buffer solvents

Solvent	E_{pa1} (mV)	E_{pa2} (mV)	E_{pc1} (mV)	E_{pc2} (mV)
Acetonitrile	85	340	-105	194
Dimethyformamide	65	310	-115	180
Phosphate Buffer	80	420	-208	-92

In all solvents the Epa1 peak was due to the removal of one electron from nitrogen atoms at the polyamic acid structure in each repeating unit to yield one stable delocalised radical cation, and the Epa2 was due to one stable quinoid type dication (Figure 25). The reverse scan showed two reduction couples (Epc1 and Epc2). Based on the increasing current at anodic and cathodic

peaks as a function of scan rate for PAA on the GCE electrode, the PAA film was considered being attached on the surface of the GCE.

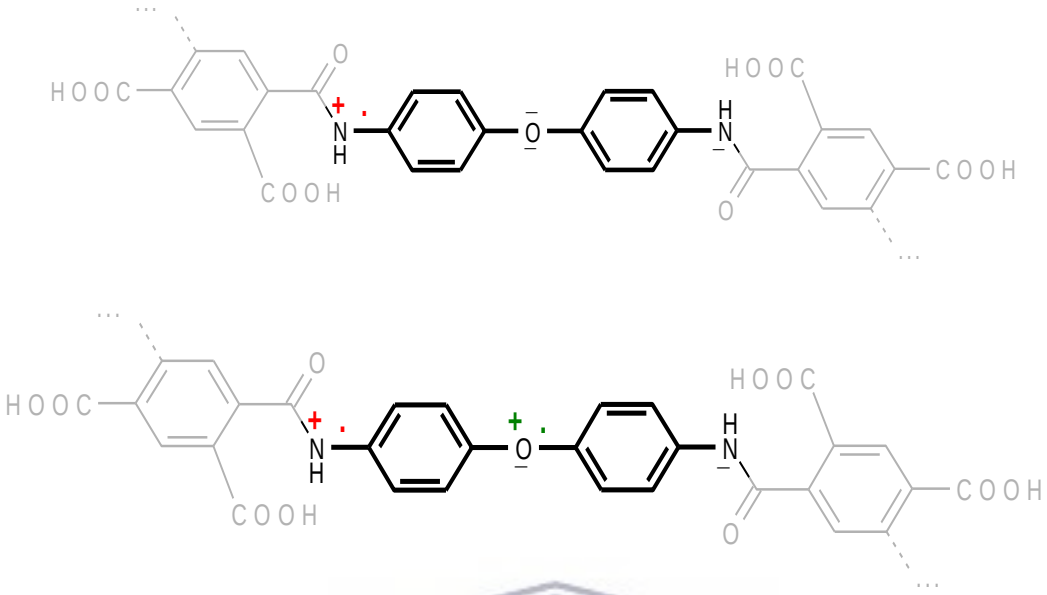

Figure 25: Repeating units of PAA structure of one stable delocalized radical cation and one quinoid-type dication

2.4 ELISA analysis

Indirect ELISA is a two-step ELISA which involves two binding process, firstly being the binding of primary antibody and then a labelled secondary antibody. The labelled secondary antibody in this study was conjugate-HRP antibody. In this ELISA test, the target antibody was sandwiched between the antigen coated on the plate and an enzyme-labelled, anti-Mycobacterium HRP-conjugate. Figure 26 shows the actual steps of how this format of ELISA test was achieved related to indirect ELISA protocol described in section ***A.1.2***. The addition of an enzyme substrate-chromogen reagent (TMB) caused a blue colour to develop (Figure 27). The intensity of the colour was directly proportional to the amount of bound sample antibody. The blue colour turned yellow after stopping the reaction with sulfuric acid (Figure 27). After stopping the reaction, the amount of colour was then measured by means of taking absorbance readings using UV visible multilabel plate reader. Figure 28 shows the UV-visible absorbance spectra of 2 positives and 3 negatives controls. The maximum absorbance of 1.3 and 1.4 was observed at 630 nm for positive controls whereas no peak was observed for the negatives ones.

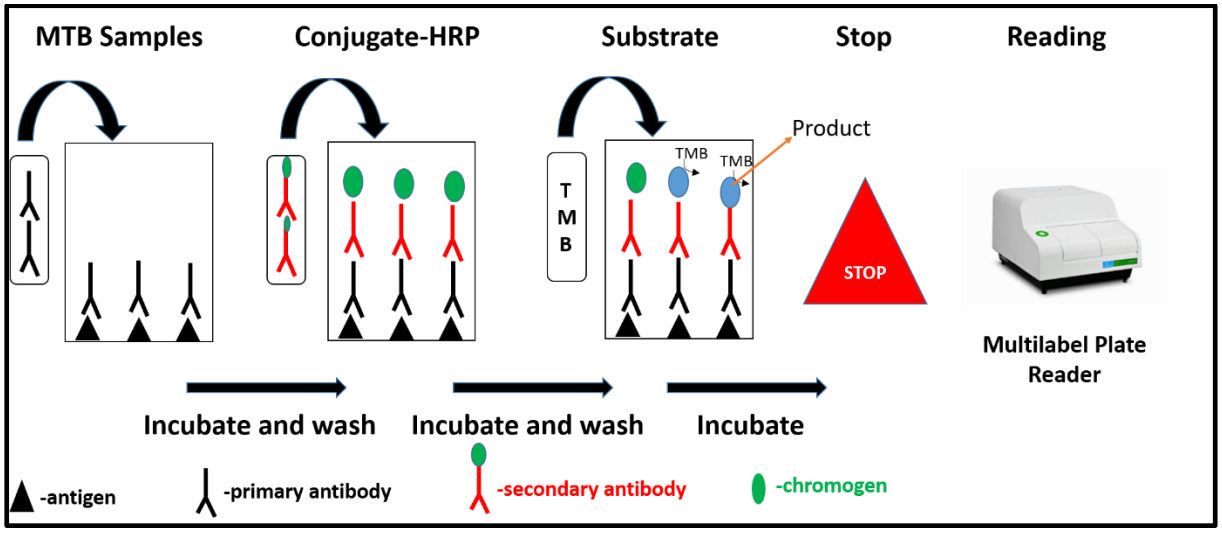

Figure 26: The indirect ELISA scheme test of detecting Mycobacterium tuberculosis IgG antibodies

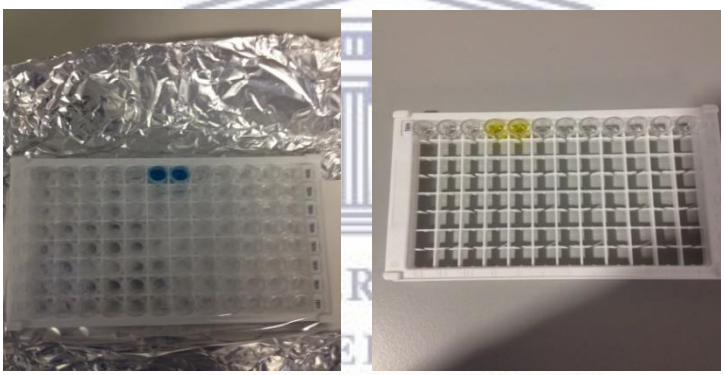

Figure 27: The positive control and MTb IgG positive sample wells that were coloured in blue after the addition of chromogen solution and coloured yellow after the addition of stop solution, sulfuric acid

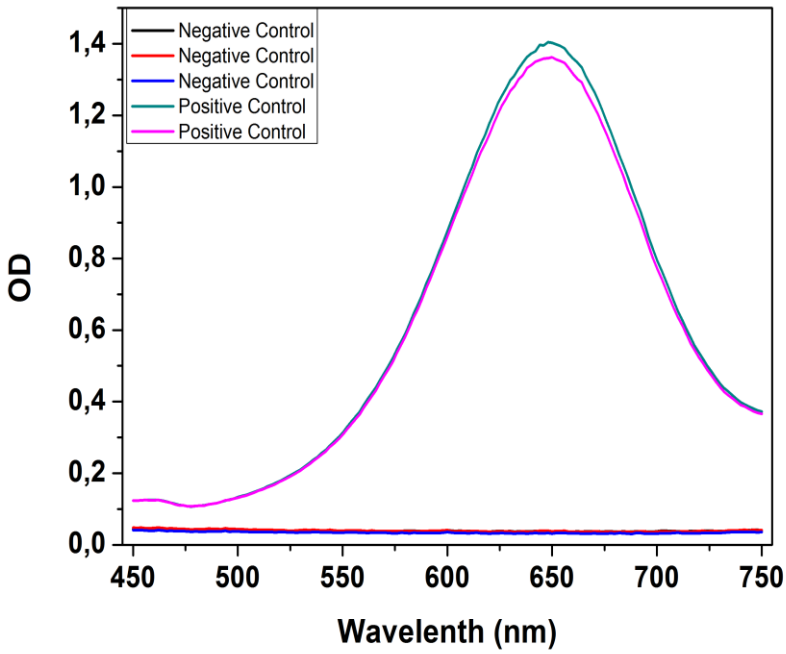

Figure 28: Absorbance spectra of conjugated-HRP anti-IgG antibodies after bind to the IgG antibodies using Indirect-ELISA protocol when the reaction was catalyzed by HRP between TMB and H_2O_2.

From the absorbance spectra of the detected IgG antibodies the following values were extracted:

S = the individual absorbance (OD) of each specimen

C.O. = the Cut-off value

C.O. was calculated to be 0.19, using this equation (C.O.) = *Nc + 0.15 (whereby *Nc is the mean absorbance value for three negative controls). Negative Results S/C.O. <1: samples giving absorbance less than the Cut-off value are negative for this assay, which indicated that no IgG antibodies of *Mycobacterium tuberculosis* were detected with this TB IgG ELISA. Positive Results when S/C.O.≥1: samples giving an absorbance greater than or equal to the Cut-off values were considered reactive, which indicated that IgG antibodies of *Mycobacterium tuberculosis* have been detected using the TB IgG ELISA. Figure 28 provide the absorbance of negative and positive controls. The sensitivity of the TB indirect ELISA was 100 %. The ELISA analysis will not be compared to the immunosensor analysis in terms of limit of detection, sensitivity or specificity as the supplier Creative-Diagnostics indicated that the actual concentrations information of the ELISA kit reagents was not available. The reagents

concentrations were adjusted in accordance with the coated plates when this kit was prepared. The indirect ELISA method of detecting *Mycobacterium tuberculosis* IgG antibodies was adopted for immunosensors development.

2.5 Immunosensor platform preparation

The GCE/PAA modified electrodes were first immersed in an antigen (Ag85B) solution for 24 hours and incubated at 4^0C to obtain GCE/PAA/Ag electrodes, then the obtained electrode was characterized in 0.1 M PBS (pH 7.04) using cyclic voltammetry. Cyclic voltammetry is a convenient technique to demonstrate the changes of electrode behaviour after each deposition/immobilization step on their surface, since the electron transfer between the solution species and the electrode usually occur by tunnelling either through the surface or through the defects in the surface.

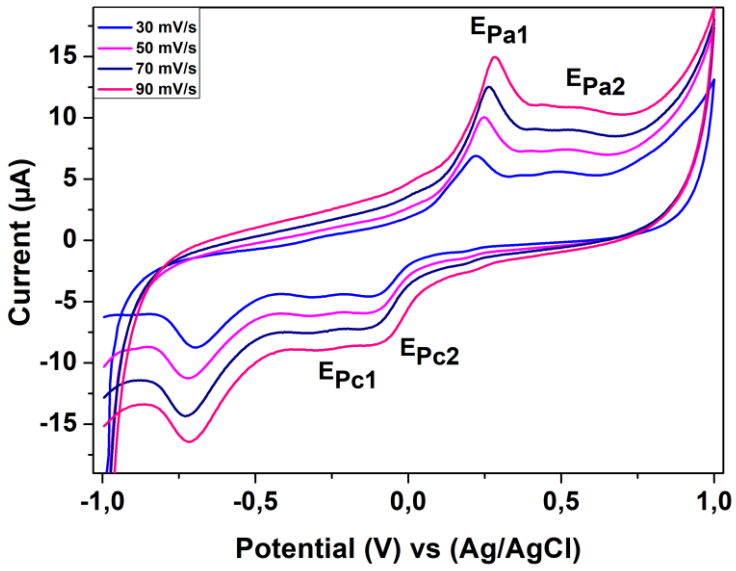

Figure 29: Cyclic voltammograms of GCE/PAA/Ag at different scan rates using 0.1 M PBS (pH 7.04) as an electrolyte

Hence, the GCE/PAA/Ag modified electrode was then characterized by cyclic voltammetry in 0.1 M PBS (pH 7.04) (Figure 29) and the redox peak currents were similarly increasing as the redox peaks of the GCE/PAA electrode. The appearance of oxidation peak potentials were significantly shifted to higher potentials (Ep_{a1}: 215 mV and Ep_{a2}: 500 mV) as compared to the

GCE/PAA (Ep_{a1}: 80 mV and Ep_{a2}: 420 mV) (Figure 29 (c)) potential peaks without the antigen. In the reduction scan, there was no significant shift of peak potentials but the great shift of potential peaks on the oxidation scans indicates that the antigen has been immobilized/adsorbed on the electrode surface, and the number of redox peaks showed that PAA was still on the surface of the electrode.

To further confirm that the Ag85B antigen was immobilized on the modified electrode (GCE/PAA), we compared the characterization of GCE/PAA and GCE/PAA/Ag using square wave voltammetry. As it was observed on cyclic voltammetry characterization of GCE/PAA/Ag, all the peaks were increasing as the scan rate was increased. The Ep_{a1} was not stable in each scan rate (appearing at different potentials), hence we only looked at the reduction sweeps of GCE/PAA/Ag in the square wave voltammetry. The SWV reduction sweep plots of GCE/PAA (red) and GCE/PAA/Ag (black) are shown in Figure 30. GCE/PAA/Ag showed what is typically expected when an antigen is immobilized on the surface of the conducting system. Antigens/antibodies are proteins that consist of amino acids and amino acids are known to be insulators. However, amino acids have physicochemical properties that can promote hydrophilicity or hydrophilicity depending on their size and functional groups. Therefore, due to these properties amino acids are capable of hydrogen bonding and they may promote/hinder electron transfer when they are immobilized on the conductive surfaces such as electrodes modified with polymers. Hence, an increase/decrease in current response can be expected from the electrode modified with antibody/antigen. There was an increase in current at peak (**a**) when there was an Ag85B antigen on the suface of the GCE/PAA electrode, while peak (**b**) was due to the reduction of oxygen. An increse in current at peak (**a**) confirmed that the antigen was attached on the surface of the electrode. The immunosensor perfomance was monitored using the square wave voltammetry at the reduction scan.

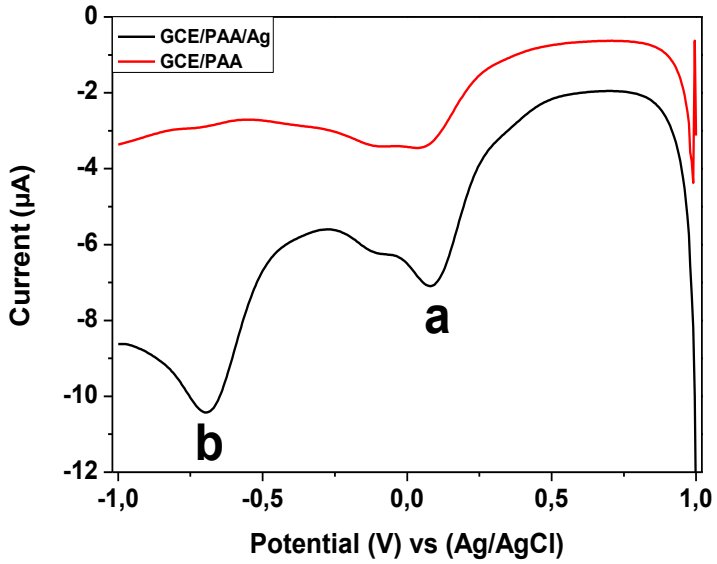

Figure 30: Square wave voltammograms of GCE/PA/Ag (black curve) and GCE/PAA (red curve) at 50 mV/s scan rate using 0.1 M PBS (pH7.01) as an electrolyte

2.6 Immunosensing tests

For the detection of anti-mycobacterium tuberculosis Ag85B antibody (Ab), GCE/PAA/Ag modified electrodes were used to detect Ab at different concentrations in 0.1 M PBS (pH 7.01) in order to form an immune-complex between Ag and Ab. It is well known that formation of an immuno-complex can result in the decrease of the detection signal in electrochemical immunoanalysis due to the adsorption of large biomolecules at the electrode surface that will change the interfacial capacitance. Hence, the influence of the formation of immune-complex on the electron transfer of the platform was investigated using square wave voltammetry. Figure 31 shows the detection of anti-mycobacterium tuberculosis Ag85B antibody (Ab) in different concentrations using square wave voltammetry. After the immunoreaction was achieved on the electrode surface, the electrochemical signal decreased for peak (**a**) and increased for peak (**b**), and the change in current response was determined by each addition of the anti-Ag85B (Ab) concentration. The peak labelled as (**a**), decreased with increasing Ab concentration which showed the formation of an immuno-complex layer inhibiting the electron transfer from the analyte to the electrode [8]. This may be referred as antigen-antibody interaction decreasing the mobility of electron transfer between the electrode surface and analyte.

Therefore, the quantitative detection of Ab was obtained from the change of the reduction peak (**a**) amperometric during the antigen-antibody reaction. Peak (**b**) was due to the reduction of oxygen. The calibration plot for anti-Ag85B detection using the proposed immunosensor is shown in Figure 32. The equation of the calibration curve is Y (µA) = 698.72X (g/mL) – 6.75, *R*= 0.9948. The current change was proportional to Ab concentration in the range of 0.3 to 1.6 mg/mL with a detection limit (LOD) of 0.08 mg/mL and a sensitivity of 698.98 µA/g.mL $^{-1}$.

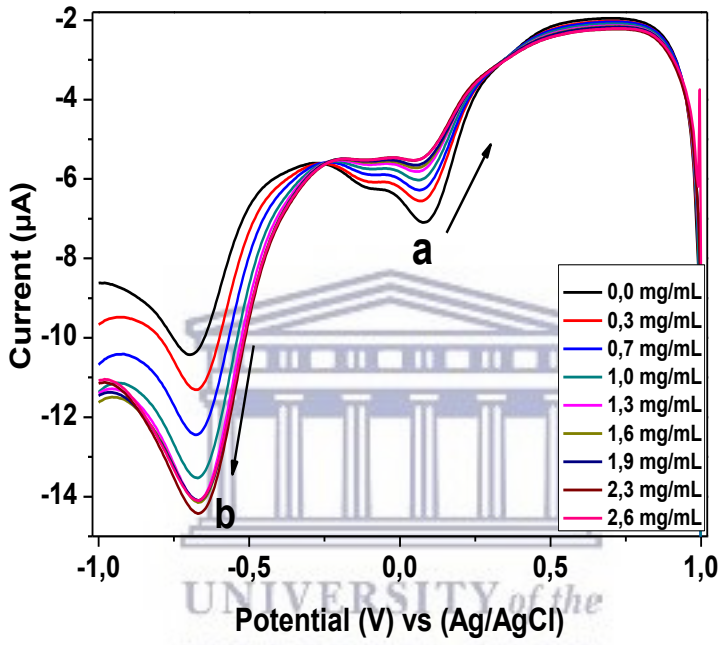

Figure 31: Square wave voltammograms of GCE/PAA/Ag after incubation with different concentrations of Ab at 50 mV/s scan rate using 0.1 M PBS (pH7.01) as an electrolyte

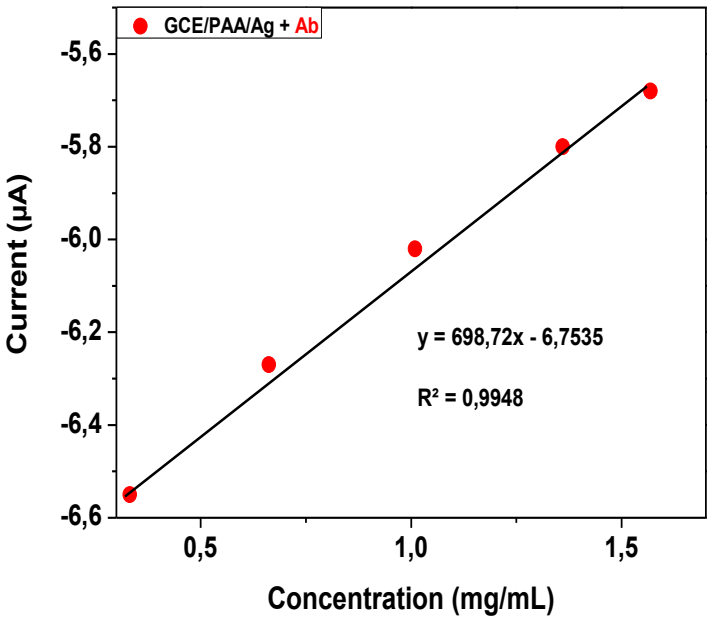

Figure 32: Calibration curves of GCE/PAA/Ag/Ab immunosensor

2.7 Conclusion

The main objective to reduce the spread of tuberculosis is affording diagnostic assays that are capable of detecting biomarkers of tuberculosis with high sensitivity and good turnaround time. There has been a great achievement in providing numerous government hospitals in South Africa with XpertMTB/RIF diagnostic test but this highly sensitive diagnostic test suffers from being incapable to determine latent and extra-pulmonary TB. And some methods take up to 1-2 weeks to obtain results after diagnosis. The indirect ELISA test of detecting Mycobacterium tuberculosis IgG antibodies that was used in this study only takes up to 60 minutes to obtain the results. The indirect ELISA method was adopted for immunosensor development in this work and the label-free immunosensing test takes place within 1 hour as well. Both methods does not need sputum for diagnosis, hence they are easy to use and can be cheaply available. However, there is still a gap between commercially available sensors and the research-based sensors. Research based on measurable output signals as electrochemical for detection and quantification of TB biomarkers requires more intensive experiments to be applicable for cheaper and highly sensitive point of care tools. Thus, the development of *Mycobacterium tuberculosis* immunosensor can contribute to that domain. The deposition of PAA on glassy carbon electrode was achieved by electrodeposition method. The PAA that was dissolved in

PBS showed less background current from the polymer than PAA dissolved in DMF and ACN, which was an advantage for development of immunosensor. The immobilized antigen (Ag) on GCE/PAA platforms was confirmed using cyclic voltammetry and square wave voltammetry. The linear response when detecting the tuberculosis antibodies was in the range of 0.3 to 1.6 mg/mL with a detection limit (LOD) of 0.08 mg/mL and a sensitivity of 698.98 µA/g.mL $^{-1}$. The immunosensor has a good sensitivity. However, comparing the limit of detection and the linear response of this immunosensor with other previously developed immunosensors in Table 6, the efficiency of the other immunosensors was better than the efficiency of the immununosensor for this study. The efficiency of this immunosensor is yet to be improved in order to detect the *Mycobacterium tuberculosis* even at low concentrations, i.e., 10^{-9} g/mL.

Table 6: Comparison of limit of detection TB-antibodies and efficiency of immunosensors

Imunosensor	Linear Range	Limit of detection	Reference
Ag360-based	0.005 µg/mL – 0.1 µg/mL	0.001 µg/mL	9
CFP-based	0.1 µg/mL – 1 µg/mL	0.1 µg/mL	10
IFN-γ-based	0.1 pg/mL – 10 pg/mL	0.2 pg/mL	11
Ag85B-based	0.3 mg/mL – 1.6 mg/mL	0.08 g/mL	This work

2.8 References

1. Andreescu, D., Wanekaya, A. K., Sadik, O. a. & Wang, J. Nanostructured polyamic acid membranes as novel electrode materials. *Langmuir* **21,** 6891–6899 (2005).

2. Du, N. *et al.* Flexible poly(amic acid) conducting polymers: Effect of chemical composition on structural, electrochemical, and mechanical properties. *Langmuir* **26,** 14194–14202 (2010).

3. Zamfir, L. G. *et al.* Non-enzymatic polyamic acid sensors for hydrogen peroxide detection. *Sensors Actuators, B Chem.* **226,** 525–533 (2016).

4. Ngema, X. T., Ward, M., Hamnca, S., Baker, P. G. L. & Iwuoha, E. I. Spectro-Electrochemical of Detection Anthracene at Electrodeposited Polyamic Acid Thin Films. *J. Nano Res.* **44,** 63–78 (2016).

5. Hess, E. H., Waryo, T., Sadik, O. a., Iwuoha, E. I. & Baker, P. G. L. Constitution of novel polyamic acid/polypyrrole composite films by in-situ electropolymerization. *Electrochim. Acta* **128,** 439–447 (2014).

6. Hamnca, S., Ward, M., Ngema, X. T., Iwuoha, E. I. & Baker, P. G. L. Development of Graphenated Polyamic Acid Sensor for Electroanalytical Detection of Anthracene. *J. Nano Res.* **43,** 11–22 (2016).

7. M., M., Z., B., S., J., Lj., T. & N., B. Electrochemical Polymerization of Aniline. *Electropolymerization* (2011). doi:10.5772/28293

8. Wang, R., Feng, J. J., Liu, W. D., Jiang, L. Y. & Wang, A. J. A novel label-free electrochemical immunosensor based on the enhanced catalytic currents of oxygen reduction by AuAg hollow nanocrystals for detecting carbohydrate antigen 199. *Biosens. Bioelectron.* **96,** 152–158 (2017).

9. Díaz-González, M., González-García, M. B. & Costa-García, A. Immunosensor for Mycobacterium tuberculosis on screen-printed carbon electrodes. *Biosens. Bioelectron.* **20,** 2035–2043 (2005).

10. Hong, S. C. *et al.* Ultrasensitive immunosensing of tuberculosis CFP-10 based on SPR spectroscopy. *Sensors Actuators, B Chem.* **156,** 271–275 (2011).

11. Kim, J. H. *et al.* Detection of IFN-?? for latent tuberculosis diagnosis using an anodized aluminum oxide-based capacitive sensor. *Biosens. Bioelectron.* **51,** 366–370 (2014).

Chapter Three

This chapter presents the results and discussion of chemical synthesis, modification and characterization of PAA and PPy thin films. Fourier Transform Infrared spectroscopy was used to study the structure and identify functional groups of PAA. It also presents the synthesis of silver nanoparticles (AgNPs) in which were incorporated into PAA and PPy films. Cyclic Voltammetry, square wave voltammetry and differential pulse voltammetry were used to evaluate the electrochemistry of the AgNPs, PAA thin films, PAA/AgNPs, and GCE/PAA/AgNPs/CYP2E1 biosensor as well as PPy thin films, PPy/AgNPs and GCE/PPy/AgNPs/CYP2E1. The optical properties of polyamic acid PAA solution, AgNPs and PAA/AgNPs composite were evaluated using Ultra-violet visible spectroscopy. The morphology of the PAA and PPy thin films and their composite with nanoparticles was also studied by SEM and AFM

3.1 FTIR study of the second batch of solid PAA

The solid polyamic acid (PAA) was synthesized whereby silver nanoparticles will be incorporated into PAA in order to covalently link AgNPs to the polymer to prevent leakage of any component of the platform and improve the electroactivity of the polyamic acid. Fourier Transform Infrared (FTIR) spectrometer was employed to characterize the structure and functional groups of the second batch PAA. The FTIR spectrum in Figure 33 was the same as the FTIR spectrum of PAA in chapter 2. The second batch of PAA was not mixed with KBr to form a pallet for the analysis in this case. The FTIR analysis was done directly on the synthesized powdered PAA.

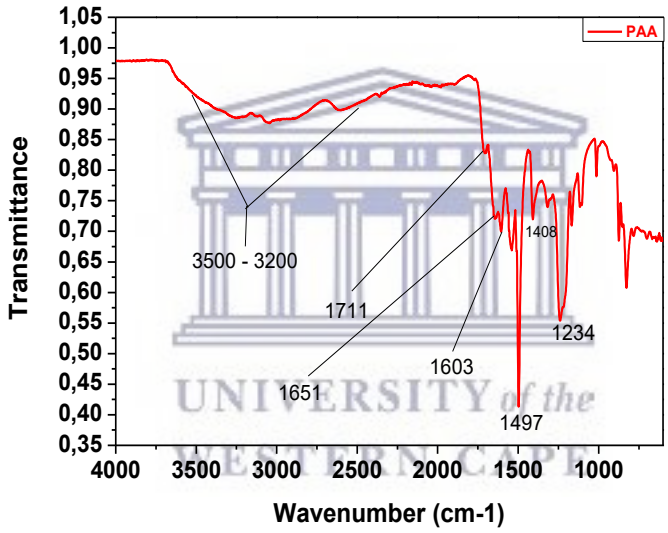

Figure 33: FTIR spectrum of solid PAA

3.2 Ultraviolet visible absorbance analysis of AgNPs, PAA and PAA/AgNPs

Silver nanoparticles were synthesized by chemical reduction method of $AgNO_3$ salt using $NaBH_4$ as indicated in section **A.2.2**. The information about the physical state of the nanoparticles can be obtained by analysing the spectral properties of AgNPs in solution, i.e., water. Hence, the UV-vis absorbance of the silver nanoparticles was measured after the synthesis. Their strong interaction with light occurs because the conduction electrons on the metal surface undergo a collective oscillation when the particles are excited by light at specific wavelengths (Plasmon resonance). As shown in Figure 34, the synthesized AgNPs absorbed

visible light at 403 nm (blue spectrum) when the absorbance measurements were taken at a range of 200 – 800 nm. Figure 34 also shows the UV-vis spectrum of a dissolved PAA solution (5 mg/mL) in PBS. The calculated band gap of 5.08 eV for PAA is typical of materials that are optically transparent. The large band gap was due to the para-quinoid type chromophore that the polymer consist of. This para-quinoid type chromophore from PAA absorbed light at 244 nm (red spectrum) and such short wavelength indicated high energy of transition because these chromophore molecules have only π-π^* transition. In the mixture of AgNPs/PAA (green spectrum), AgNPs absorbed visible light at 403 nm and the PAA broad peak at 244 nm that was observed in the red spectrum was split into a pair of peaks due to the presence of AgNPs.

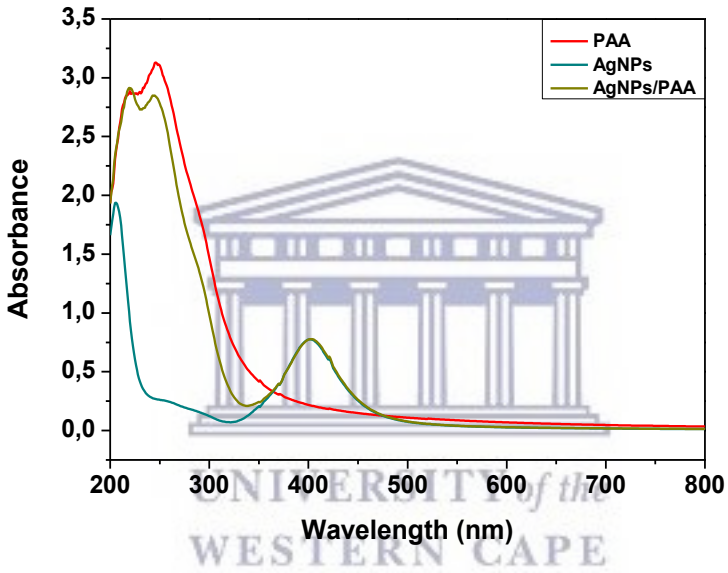

Figure 34: UV-vis spectra of PAA (red), AgNPs (blue) and PAA/AgNPs (green) solution in 0.1M PBS

The DLS size distribution graph of synthesized silver nanoparticles by the reduction of $AgNO_3$ from NaB_4 is shown in Figure 35. The size distribution of the silver nanoparticles was found to be in a range of 3 to 10 nm. Furthermore, the size and the shape of the resultant AgNPs were obtained using TEM between a scale of 100 and 20 nm and the characterization of the AgNPs by TEM was done in a third month after the synthesis. The TEM micrograms (Figure 36) suggests that the measured size of the particles have an average size of 17 nm. The particles were of spherical shape. However, the size measured by TEM analysis was higher than the size measured by DLS. Therefore, the DLS and TEM analysis suggests that the absorption band of

AgNPs at 403 nm (UV-vis) have sizes between 3 – 17 nm and the AgNPs were still stable even after 3 months.

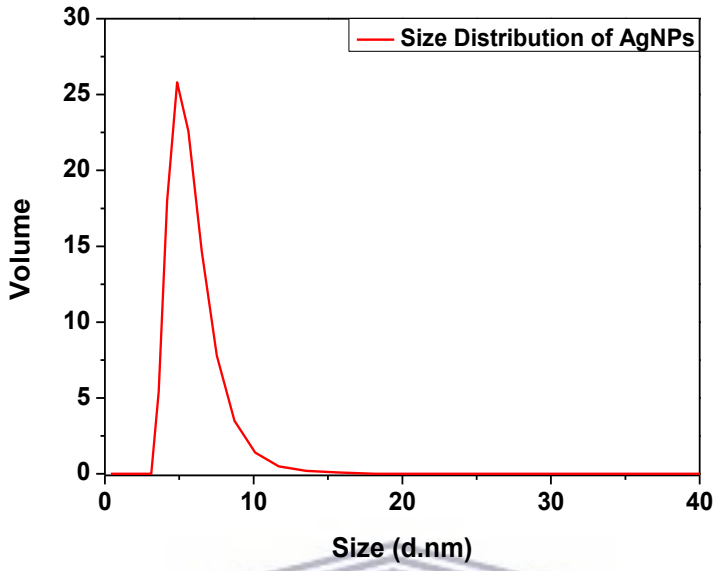

Figure 35: Size distribution of the synthesized silver nanoparticles

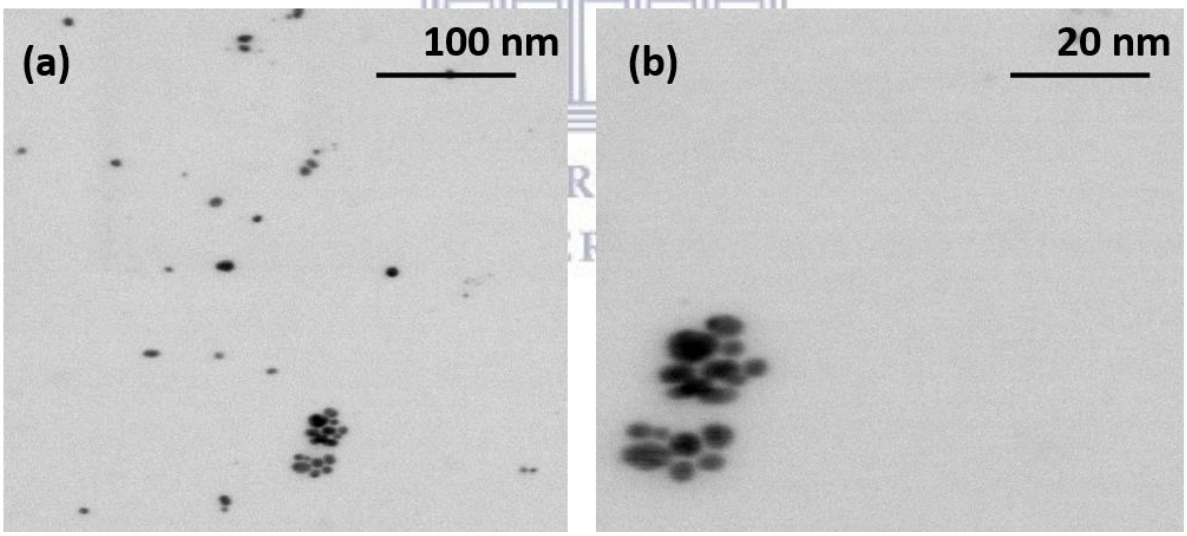

Figure 36: TEM micrograms of spherical silver nanoparticles

3.3 Electrodeposition method

3.3.1 Electrodeposition of AgNPs

The electrodeposition of AgNPs on glassy carbon electrode surface was achieved by cycling the potential 10 times between -1.0 and +1.0 V at a scan rate of 50 mV/s as indicated in section ***A.2.2.2***. Studies have shown that the electrochemical characterization of AgNPs deposited on glassy carbon electrode and gold electrode yields a couple redox peaks; the anodic peak which can be ascribed to the formation of Ag^{+} while the cathodic peak can be attributed to the reduction of Ag^{+} to Ag^{o} in silver precipitate deposited on the electrodes [1–4]. All the electrochemical experiments were performed without degassing the electrolyte (PBS) since the development and application of the biosensor required undegassed electrolyte (with a minimum natural oxygen from PBS).

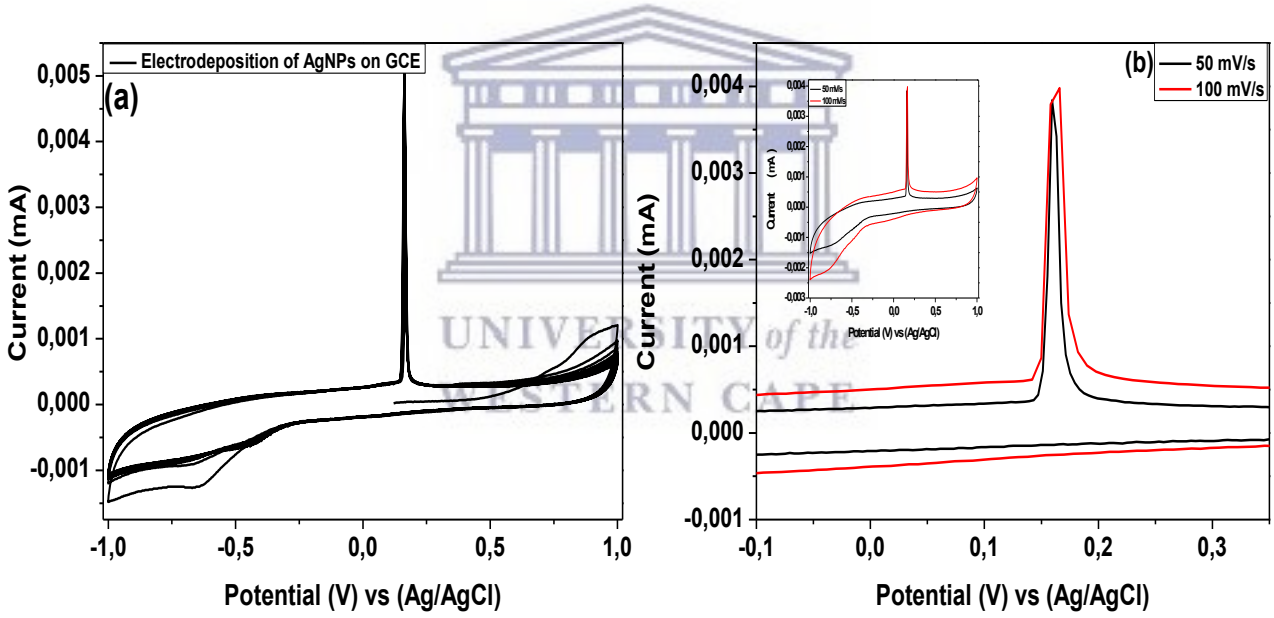

Figure 37: Cyclic voltammograms of the electrodeposition of AgNPs (a) and electrodeposited AgNPs (b) on GCE in 0.1 M PBS at a scan rate of 50 and 100 mV/s

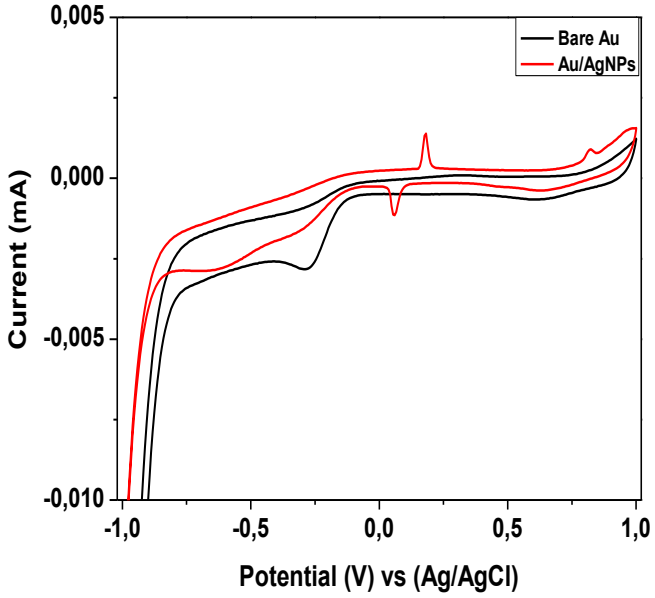

Figure 38: Cyclic voltammogram electrodeposited AgNPs on Au electrode in 0.1 M PBS at a scan rate of 50 mV/s

During the electrodeposition of AgNPs on glassy carbon electrode (GCE) in Figure 37(a), no peak related to the oxidation of AgNPs was observed on the first oxidative sweep starting at 0 V which was consistent with the absence of AgNPs deposited on the electrode in the initial state. However, a sharp oxidation peak at 160 mV of AgNPs was observed on the following oxidative scans which indicated that the AgNPs were adsorbed during the reverse sweep. In addition, no reduction of Ag^{+} to Ag^{o} was observed as some studies have shown. Figure 37(b) shows the cyclic voltammograms of the electrodeposited AgNPs on GCE. The oxidation peak at 160 mV of AgNPs was observed with no reduction of Ag^{+} to Ag^{o} on the reverse scan. The voltammetric study of the influence of various phosphate anions on silver nanoparticle oxidation by Navolotskaya et al also showed the similar electrochemical behaviour of the silver nanoparticles as the AgNPs of this study [5]. Their study suggested that the pH of each phosphate solution yields a different electrochemical behaviour (in terms of potential peak appearance) in different concentrations of electrolytes. However, in this study the electrochemical behaviour of AgNPs on GCE was not studied at different concentrations and pH of PBS. Alternatively, the electrochemistry of silver nanoparticles was investigated on gold (Au) electrode (Figure 38) using the same conditions as the electrodeposition and characterization of AgNPs on GCE. The Ag/Ag^{+} redox couple was observed at 182 mV

(oxidation) and 60 mV (reduction). Therefore, the Ag/Ag^+ redox couple observed from AgNPs on the Au electrode, suggests that the nature of GCE and the experiment conditions of the electrodeposition and characterization of AgNPs on GCE did not favour the reduction of Ag^+ to Ag^o since such redox peak was not observed on GCE.

3.3.2 Electrodeposition of PAA and PAA/AgNPs on GCE

The electrodeposition of PAA on glassy carbon electrode surface was achieved by cycling the potential 5 times between -1.0 and +1.0 V at a scan rate of 50 mV/s as described in chapter 2. The same procedure was also adopted for the electrodeposition of PAA/AgNPs on GCE where silver nanoparticles were expected to improve the electroactivity of polyamic acid film. The cyclic voltammograms for the electrodeposition of PAA and PAA/AgNPs on GCE surfaces are shown in Figure 39. The shapes of cyclic voltammograms are similar in both cases. There was an intense oxidation peak at 0.5 V which correspond to chemical grafting of PAA. On the reverse scan, reduction peaks **Epc1** and **Epc2** as well as the oxidation peaks **Epa1** and **Epa2** of PAA were observed. However, there was no oxidation of silver nanoparticles during electrodeposition of PAA/AgNPs.

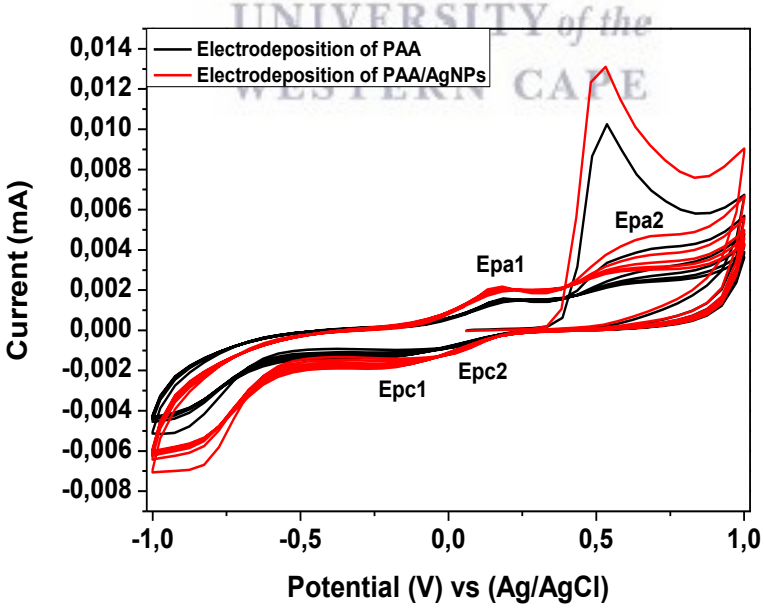

Figure 39: Cyclic voltammograms of the electrodeposition of PAA and PAA/AgNPs in 0.1 M PBS at a scan rate of 50 mV/s

3.3.3.1 Characterization of Electrodeposited PAA and PAA/AgNPs on GCE

The electrodeposited PAA and PAA/AgNPs films were further subjected to characterization by cyclic voltammetry in 0.1 M PBS at different scan rates between 10, 30, 50, 70 mV/s. The electrochemical behaviour of the electrodeposited PAA is well understood and quite noticed with two oxidation peaks (**Epa1**and **Epa2**) that forms two redox couples due to the other two reduction peaks (**Epc1**and **Epc2**). The first peak **Epa1** is the gain of an electron from nitrogen atoms and the second peak **Epa2** is a stable quinoid-type dication from the polymer [6] (Figure 40(a)).

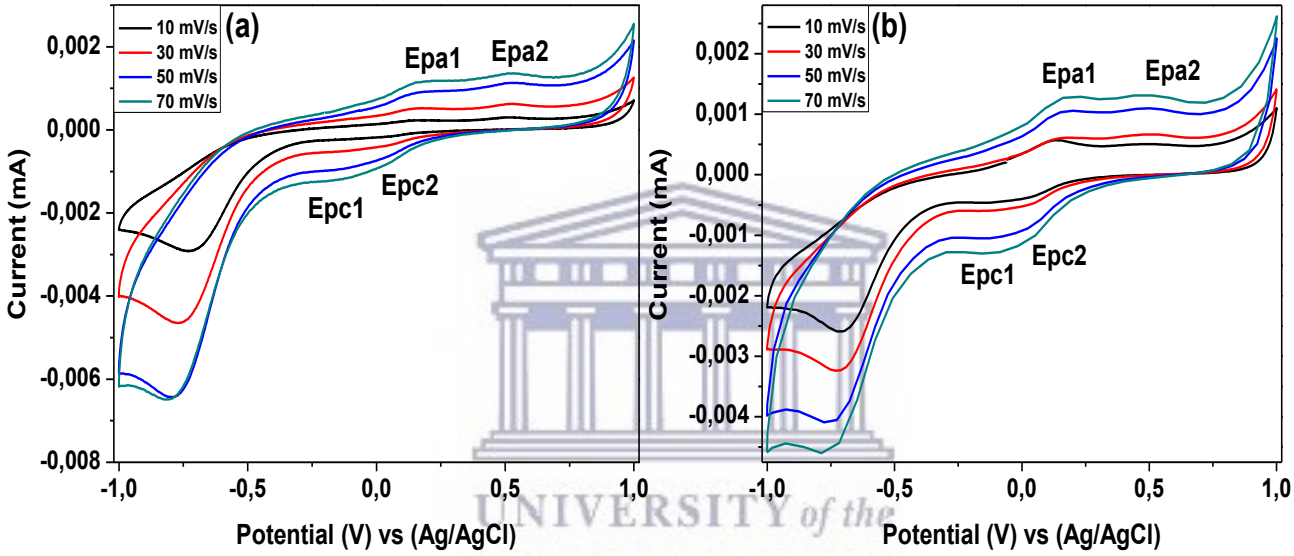

Figure 40: Cyclic voltammograms of the electrodeposited PAA (a) and PAA/AgNPs (b) in 0.1 M PBS at different scan rates

In Figure 40(b), the PAA/AgNPs electrochemical behaviour showed a signal similar to the one of PAA with two oxidation and reduction peaks. Comparing the intensities of the redox peaks of PAA and PAA/AgNPs at a potential around 200 mV (Figure 41), the electroactivity of PAA/AgNPs film was improved by a current of 0.2 µA since the intensity of the redox peak was at 0.9 µA for PAA, while for PAA/AgNPs the current was at 1.1 µA. The electrochemical behaviour of PAA/AgNPs showed a signal-enhanced peak intensities than the peaks of PAA. The redox peaks of the electrodeposited PAA and PAA/AgNPs on GCE were of poor intensities. Hence, the reduction peaks [(**Epc2**) and (**Epc1**)] were not distinguishable as a pair

of peaks. The redox of AgNPs was also not observed when the nanoparticles were incorporated into PAA. The drop coating method was then adopted as a method of modifying GCE.

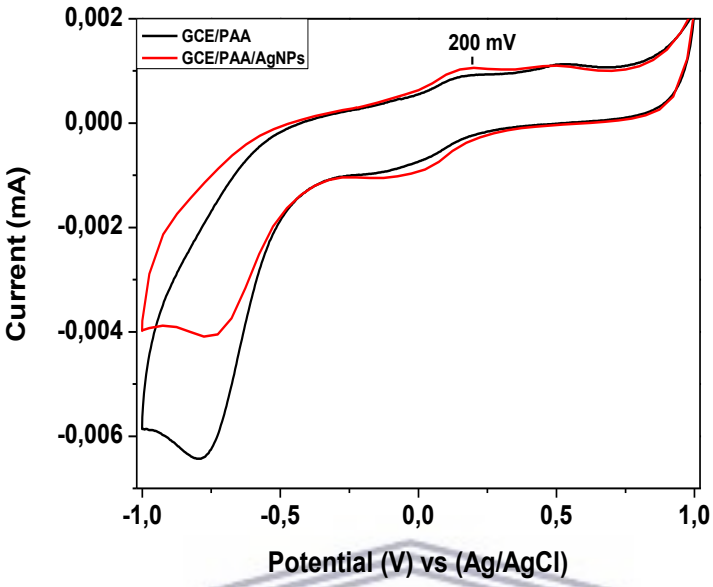

Figure 41: Cyclic voltammograms of the electrodeposited PAA (black) and PAA/AgNPs (red) in 0.1 M PBS at a scan rate of 50 mV/s

3.4 Drop-coating method

3.4.1 Characterization of drop-coated PAA and PAA/AgNPs

After attempting the 'classical' (electrodeposition) method of depositing PAA on the working electrode, drop coating method was explored since it is not only a very fast and simple method but it has proven that it can maintain high sensitivity of the modified sensors for detection of hydrogen peroxide [7]. The preparation and the setup of this experiment were done following the procedure in section ***A.2.2.1*** and ***A.2.2.3***. The first scan of the cyclic voltammogram of the drop coated PAA at 10 mV/s (Figure 42) produced a similar electrochemistry of PAA as the electrodeposition of PAA on GCE using 5 cycles of cyclic voltammetry (Figure 39). The redox of the polyamic acid confirmed that the polymer was adsorbed/attached on the surface of the glassy carbon electrode (chemical grafting) since this behaviour was similar to the electrodeposition of PAA (Figure 39). The first cyclic voltammetric scan at 10 mV/s produced a distinguishable redox peaks (improved intensities) of PAA. Subsequently to the

electrodeposition method not yielding distinguishable redox peaks of PAA, drop-coating method proved to be a suitable procedure of modifying the electrodes. Thus, drop-coating method was used in all the experiments of preparing/modifying glassy carbon electrode with PAA and PAA/AgNPs.

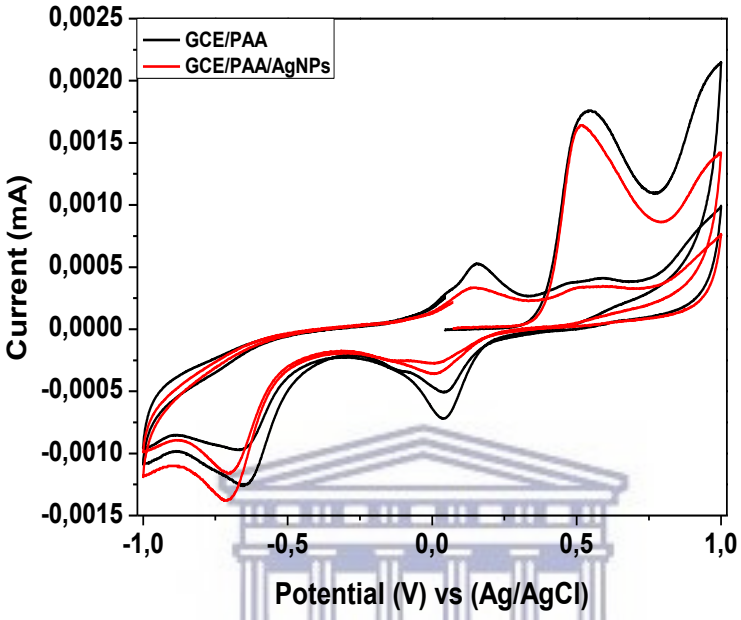

Figure 42: Cyclic voltammograms of the drop-coated PAA (black) and PAA/AgNPs (red) on GCE in 0.1 M PBS at a scan rate of 10 mV/s

The characterization of PAA and PAA/AgNPs was also conducted at different scan rates between 10, 20, 30.., 100 mV/s (Figure 43(a) and Figure 43(b)). The comparison between PAA and PAA/AgNPs cyclic voltammograms at 50 mV/s in Figure 44 clearly showed that the electroactivity of PAA was improved when AgNPs were incorporated in the polymer. The PAA film was considered to have good diffusion controlled electron mobility as showed by the increase in current (mA) as the scan rate was increased. Randles Sevcik plots of current (mA) vs. the square root of the scan rate (mV/s) confirmed a direct proportionality with correlation coefficients of ±0.99 (Figure 45). The same electrochemical behaviour for PAA/AgNPs composite was observed. As observed in the electrodeposited PAA/AgNPs the presence of AgNPs in PAA was also not observed is drop-coated PAA/AgNPs but the redox peak intensities were improved compared to PAA. The effect of the incorporated AgNPs using drop coating method did not seem to yield a better electroactivity of PAA than the electroactivity of

PAA using electrodeposition method since the current of the redox peak **Epa1** of PAA/AgNPs for both methods was at the same current range 1.1 µA. However, the drop-coating method proved to be a better method of depositing PAA and PAA/AgNPs on GCE than electrodeposition method as the redox peaks of the drop coated PAA/AgNPs were clear than of the electrodeposited PAA/AgNPs. As discussed in chapter 2, Figure 43(a) shows the first oxidation peak **Epa1** that was due to the one electron removal from the nitrogen atoms at the PAA structure in each repeating unit to yield one stable delocalized radical cation. The second oxidation peak **Epa2** was due to one quinoid-type dication. There were two reduction peaks **Epc2** and **Epc1** at 20 mV and -192 mV on the reverse scan from 1.0 V to -1.0 V.

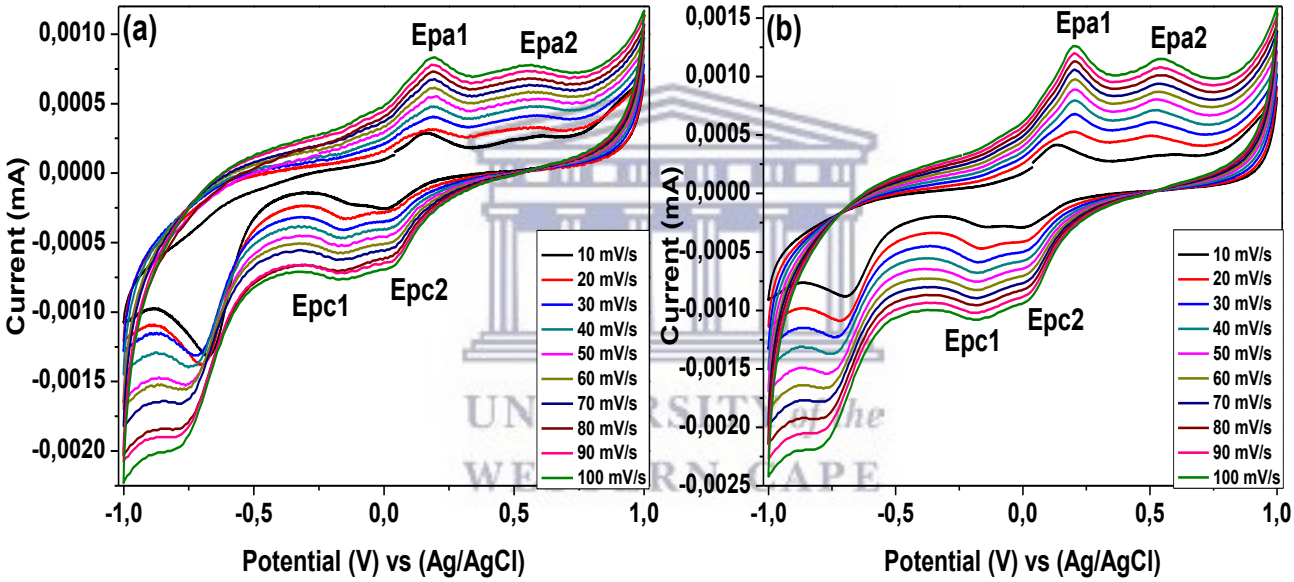

Figure 43: Cyclic voltammograms of the drop-coated PAA (a) PAA/AgNPs on GCE in 0.1 M PBS at different scan rates

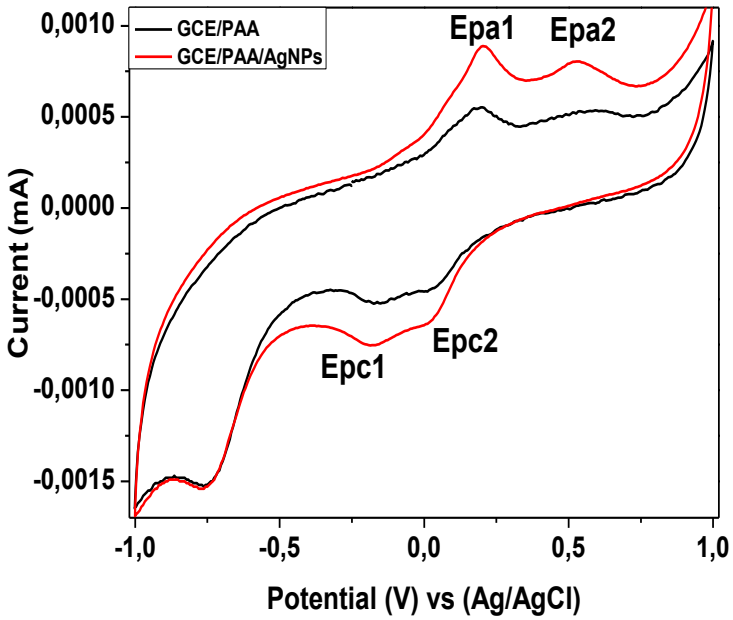

Figure 44: Cyclic voltammograms of the drop-coated PAA (black) and PAA/AgNPs (red) in 0.1 M PBS at a scan rate of 50 mV/s

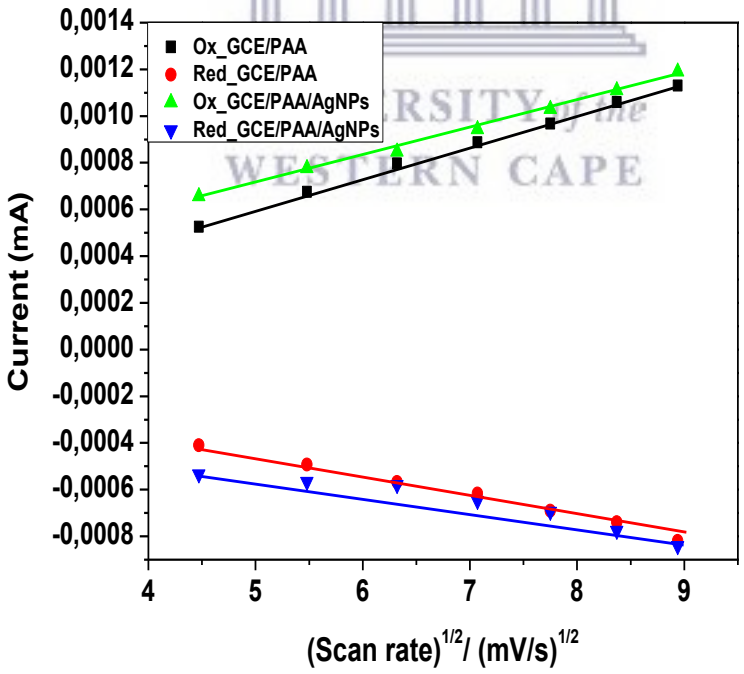

Figure 45: Randle Sevcik plot for the determination of diffusion coefficient of the drop-coated PAA and PAA/AgNPs on GCE

The diffusion coefficient of the electron through the polymer layer was calculated using Randle Sevcik equation:

$$i_p = 2.69x10^5\ n^{3/2}\ A\ C\ D^{1/2}$$

Using peak **Epa1** for both materials, PAA and PAA/AgNPs (Figure 43(a) and Figure 43(b)) to calculate the diffusion coefficient, the electron diffusion coefficient (D_e) was found to be $5.25x10^{-6}$ cm^2/s and $5.09x10^{-6}$ cm^2/s, respectively. The D_e for both materials are in the same range with the previously reported D_e of PAA [6,8,9].

3.5 Summary of polymer composite layers

Two deposition methods for studying the electrochemistry of PAA and PAA/AgNPs on the surface of glassy carbon electrode were used. When the electrodeposition method was used, the resolution of the redox peak intensities of PAA was poor, while in the drop coating method the resolution of these redox peak intensities was improved. The electrochemistry of AgNPs was not observed when the nanoparticles were incorporated in PAA using both methods. Polyamic acid have a background current at a potential range between 160 mV to 500 mV where the redox response of AgNPs was expected. Therefore, due to that strong background current/electrochemistry of PAA between 160 mV to 500 mV, no redox response of AgNPs was observed. However, in the drop coated PAA/AgNPs the incorporation of AgNPs was noticed by a better electroactivity of PAA/AgNPs when compared to the electroactivity of PAA without AgNPs. Therefore, due to the drop coated PAA/AgNPs having an improved electroactivity than the electrodeposited PAA/AgNPS and drop coated PAA and PAA/AgNPs giving distinguishable redox peaks compared to electrodeposited materials, drop coating method was adopted for all the platforms preparation for biosensor development. Furthermore, polypyrrole (PPy) was used to prepare the same platforms since PPy is a classical conductive polymer, that has less background current (redox peaks) in the region where the redox response of silver nanoparticles is expected and also to compare the electroactivity of the two polymers, with and without the silver nanoparticles.

3.6 Voltammetric studies of Ppy modified with AgNPs

3.6.1 Electrodeposition of PPy and PPy/AgNPs

The electropolymerization or electrochemical synthesis of PPy from the monomer pyrrole (Py) was achieved by chronopotentiometry (potential-time) as discussed in section ***A.2.2.4***. The chronopotentiometry curves and the quality of the films are very dependent on the applied current density. Figure 47 shows the electropolymerization process of Py to PPy, while Figure 46 shows the chronopotentiometric plots of electropolymerization of Py to PPy (red curve) and Py/AgNPs to PPy/AgNPs (blue curve) on the surface of glassy carbon electrodes at a current density of 0.071 µA/cm^2. The chronopotentiometric response showed the occurrence of a steady-state electropolymerization process of Py to PPy. The electropolymerization process of Py in the presence of AgNPs was similar to the electropolymerization of Py to PPy. However, the presence of AgNPs caused the electropolymerization process to reach a steady state at 250s while in the absence of AgNPs the steady-state was only reached after 400s. The plateau was reached at 0.7 V for both electropolymerization processes suggesting the homogeneous formation of PPy and PPy/AgNPs films on GCE.

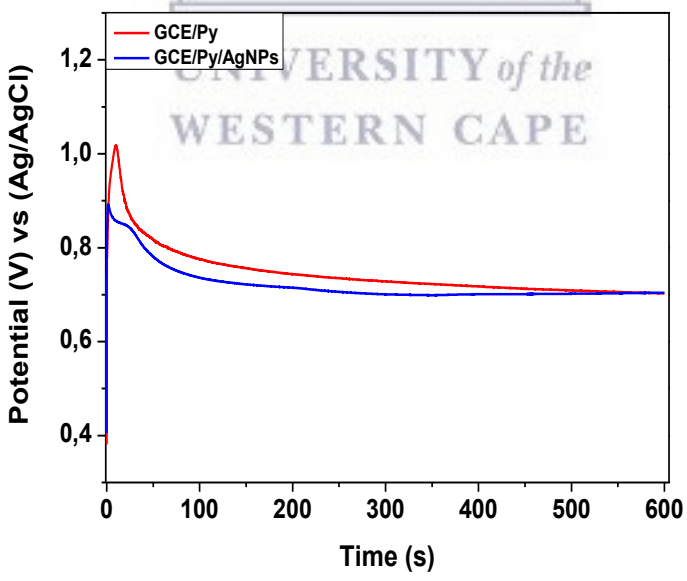

Figure 46: Potential-time curves of the electropolymerization of PPy (red) and PPy/AgNPs (blue) on GCE in 0.1 M PBS at current density of 0.071 µA/cm^2 with a total charge of 43 mC/cm²

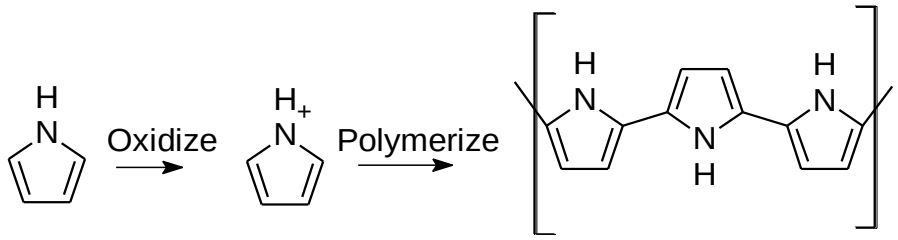

Figure 47: Electropolymerization of Py to PPy

3.6.2 Characterization of PPy and PPy/AgNPs on GCE

The cyclic voltammetry was used to characterize the film of PPy at the glassy carbon electrode. Figure 48 is the characterization of the PPy that was obtained after electropolymerizing Py to PPy using chronopotentiometry (red curve in Figure 44). The cyclic voltammograms of PPy film in Figure 48 exhibited the oxidation peak (p-doping) of polypyrrole that involves two simultaneous processes: (1) the diffusion of the counter-ion into of the polypyrrole film to maintain charge neutrality, and (2) the transfer of electrons from polypyrrole. In the successive scan of different scan rates, the redox peak associated with the oxidation **Epa1** as well as the reduction **Epc1** peaks which is the p-doping and de-doping of PPy, increased as the scan rate was increasing and it was evident that the polymer was successfully attached/deposited on the surface of GCE.

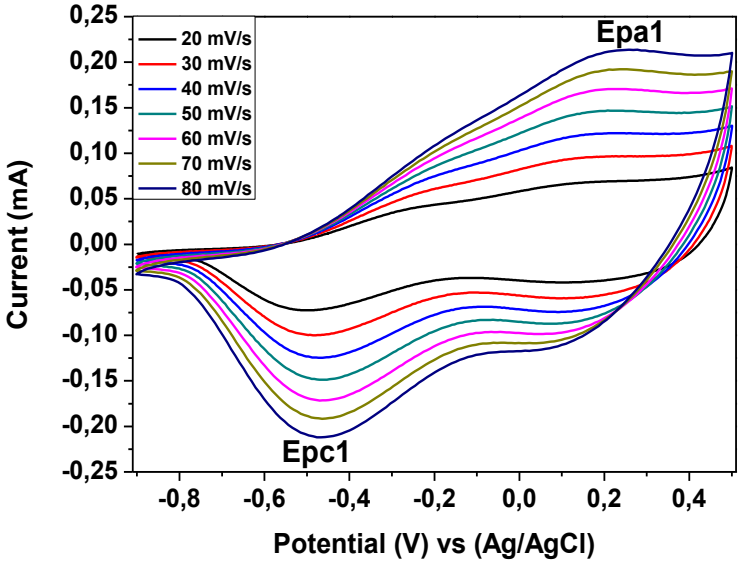

Figure 48: Cyclic voltammograms of electrodeposited PPy on GCE in 0.1 M PBS at different scan rate

Figure 49(a) shows the electrochemical behaviour of PPy/AgNPs on GCE in 0.1 M PBS electrolyte at different scan rates. The oxidation **Epa1** and reduction **Epc1** peaks of polypyrrole were always present while the oxidation peak around -0.5 V was due to the incorporated silver nanoparticles. The growth of the redox peaks **Epa1** and **Epc1** of PPy/AgNPs was similar to the one of the PPy, confirming that PPy/AgNPs was attached on the surface of GCE.

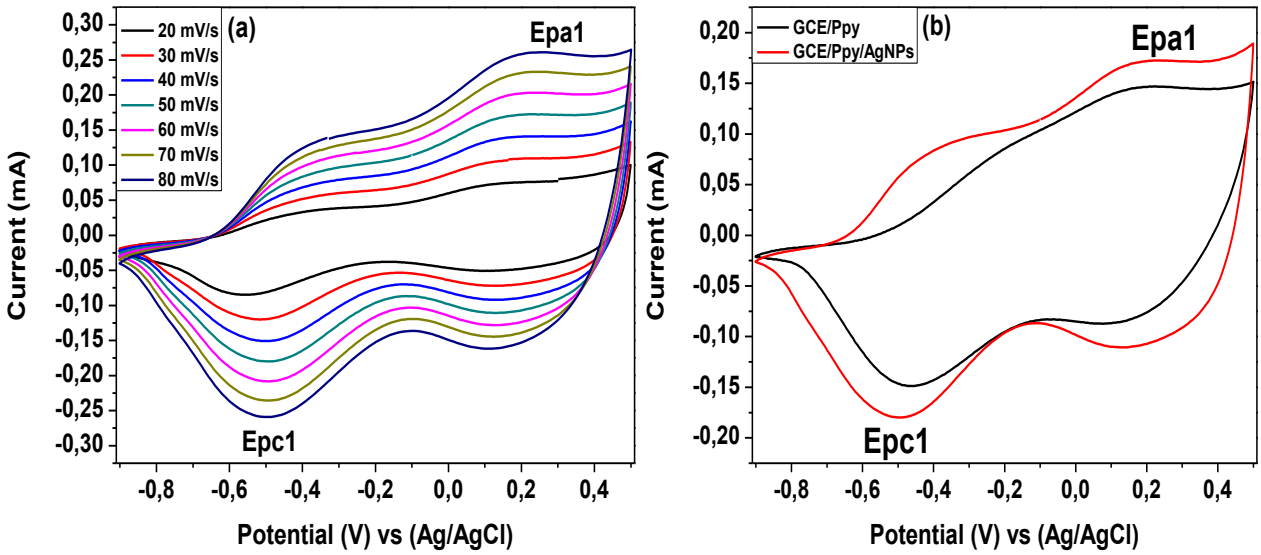

Figure 49: Cyclic voltammograms on GCE in 0.1 M PBS of (a) the electrodeposited PPy/AgNPs at different scan rates and (b) the electrodeposited PPy and PPy/AgNPs at a scan rate of 50 mV/s

Comparing the polymer (PPy) and the composite (PPy/AgNPs) at scan rate of 50 mV/s in Figure 49(b), the PPy/AgNPs showed that the current response (electroactivity) of the polymer was improved when nanoparticles were incorporated. Looking at peak **Epa1** in Figure 49(b), the current of the polymer PPy was at 0.147 mA, while when the silver nanoparticles were incorporated (PPy/AgNPs) the current was at 0.172 mA. This further confirmed the presence of AgNPs in polypyrrole matrix. The Randle Sevcik plot also confirmed that current was increasing as the scan rate was increased on both materials, GCE/PPy and GCE/PPy/AgNPs (Figure 50). The slope (maximum current) of the oxidation peak of GCE/PPy/AgNPs (0,0417x) was higher than the slope of GCE/PPy (0,0326x), confirming that AgNPs improved the electroactivity of PPy. Therefore, the incorporation of nanoparticles in PPy improved the electron transfer of the polymer. However in PAA, the incorporation of silver nanoparticles did not show the same effect. The aim of incorporating silver nanoparticles in a readily conductive polymers (PAA and PPy) was not only targeted to improve the electroactivity, but also to use the nanoparticles properties for biosensors development in order covalently link the nanoparticles to the polymer and/or the enzyme and prevent leakage of any component of the platform. Nanoparticles are known to play a role of contributing their properties by facilitating

the electron exchange between the electrode and heme-protein, i.e., CYP2E1 enzyme. The polymer that has good conductive properties may be expected to yield a biosensor with good sensitivity, however, this does not suggests that the platform with a good conductive polymer will have good electron mobility between the electrode and the enzyme since such aspect may be determined either by the properties of nanoparticles or polymer in each platform. The GCE/PAA, GCE/PAA/AgNPs, GCE/PPy and GCE/PPy/AgNPs platforms were further used for the development of biosensors, whereby the CYP2E1 was immobilized on the surface of these platforms.

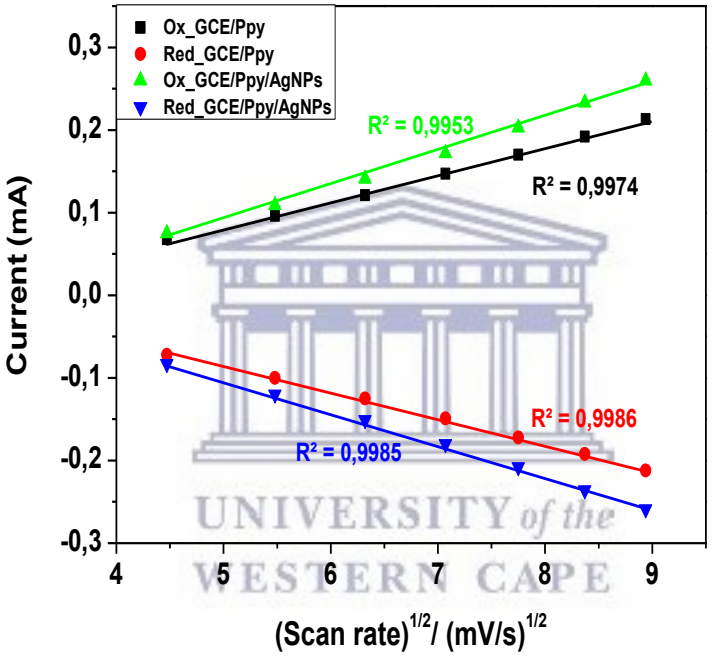

Figure 50: Randle Sevcik plot of the electropolymerized PPy and PPy/AgNPs on GCE

It was also observed that the incorporation of AgNPs to each polymer had a different impact. Comparing two polymers PAA and PPy using Table 7, it was noticed that when silver nanoparticles were incorporated in PAA using electrodeposition method, the potential peaks shifted to the negative potentials. While in the drop-coating method, the incorporation of nanoparticles caused a shift of PAA potential peaks to the positive potentials. The electrochemistry of silver nanoparticles was not observed in terms of oxidation/reduction peaks when there were incorporated into a polymer (polyamic acid and polypyrrole). In polypyrrole,

the presence or the effect of silver nanoparticles was noticed by an increase in current in the redox response of the polymer.

Table 7: Potential peaks of polyamic aacid (drop-coated and electrodeposited) and polypyrrole

Material	Ep_{a1} (mV)	Ep_{a2} (mV)	Ep_{c1} (mV)	Ep_{c2} (mV)
PAA[e]	186	522	-13	-158
PAA/AgNPs[e]	161	511	53	-152
PAA[d]	196	532	24	-169
PAA/AgNPs[d]	202	539	20	-192
Ppy	245	-	-464	-
Ppy/AgNPs	243	-	-498	-

PAA[e], electrodeposited polyamic acid; PAA/AgNPs[e], electrodeposited polyamic acid/silver nanoparticles; PAA[d], drop-coated polyamc acid; PAA/AgNPs[d], drop-coated polyamic acid/silver nanoparticles; Ppy, polypyrrole; Ppy/AgNPs, polypyrrole/silver nanoparticles; Epa = anodic peak potential; Epc = cathodic peak potential.

3.7 Morphological characterization of PAA, PAA/AgNPs, PPy and PPy/AgNPs

3.7.1 Atomic force microscopy analysis

AFM was used to study the surface morphology/topography of the electrodeposited polymer PAA, PPy and the composites of PAA/AgNPs and PPy/AgNPs on the screen printed electrode. The surface features of drop coated PAA and PAA/AgNPs composite samples were also examined by AFM. For drop-coated PAA and PAA/AgNPs a height distribution between -300 to 300 nm was observed (Figure 51(a) and Figure 51(b)). PAA presents a spherical structure slightly lower than 400 nm diameter whereas PAA/AgNPs composite shows bigger structure. The same effect is also observed with the electrodeposited PAA and PAA/AgNPs (Figure 52(a) and Figure 52(b), the size of the grains increases with AgNPs. In addition, grains are much smaller than the spheres of drop-coated PAA and PPA/AgNPs. Figure 53(a) and Figure 53(b) shows the morphology of PPy and PPy/AgNPS at height distribution of -150 to 150 nm, respectively. The PPy and PPy/AgNPs were both observed to have granular surface

morphology. The presence of AgNPs in PPy/AgNPs composite increased the size of the grains in the polymer. The two polymers PAA and PPy have surface features that can be clearly distinguished. Grains of PPy are much smaller than sphere of PAA. The incorporation/presence of silver nanoparticles was clearly observed by increasing/enlarging the size of the spheres (PAA) and grains (PPy).

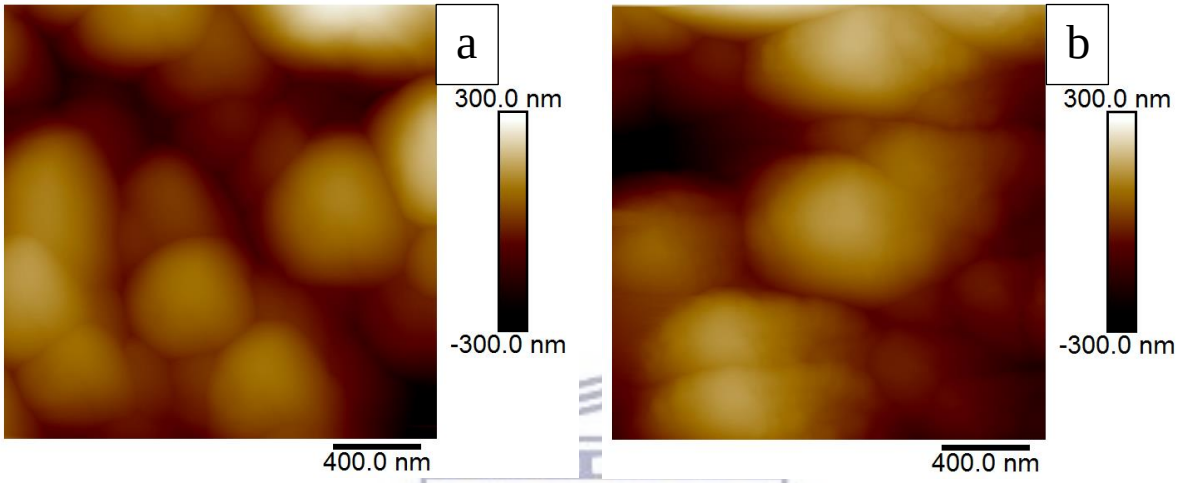

Figure 51: AFM image of drop coated PAA (a) and PAA/AgNPs (b) on screen printed carbon electrode

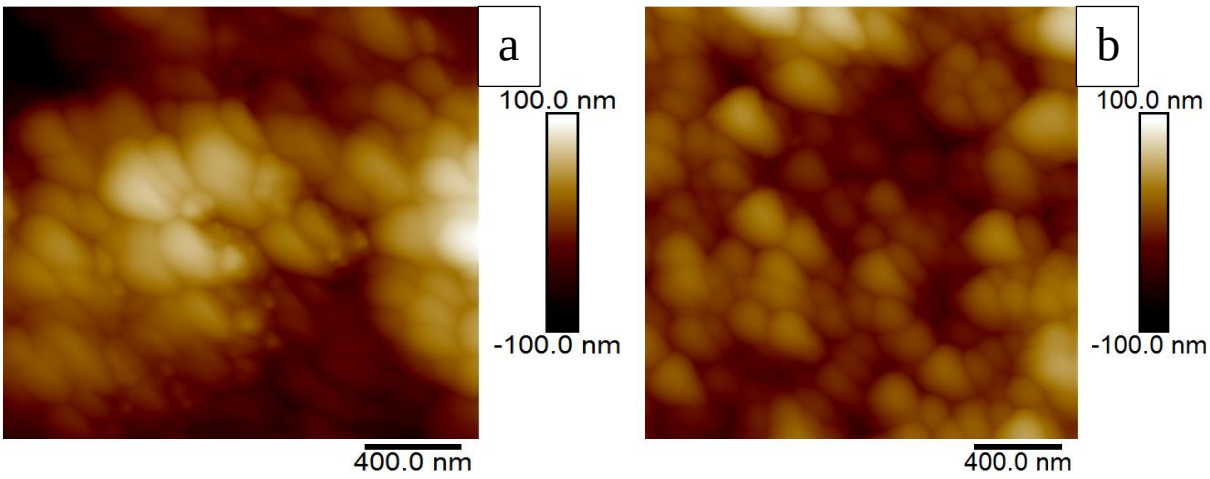

Figure 52: AFM image of electrodeposited PAA (a) and PAA/AgNPs (b) on screen printed carbon electrode

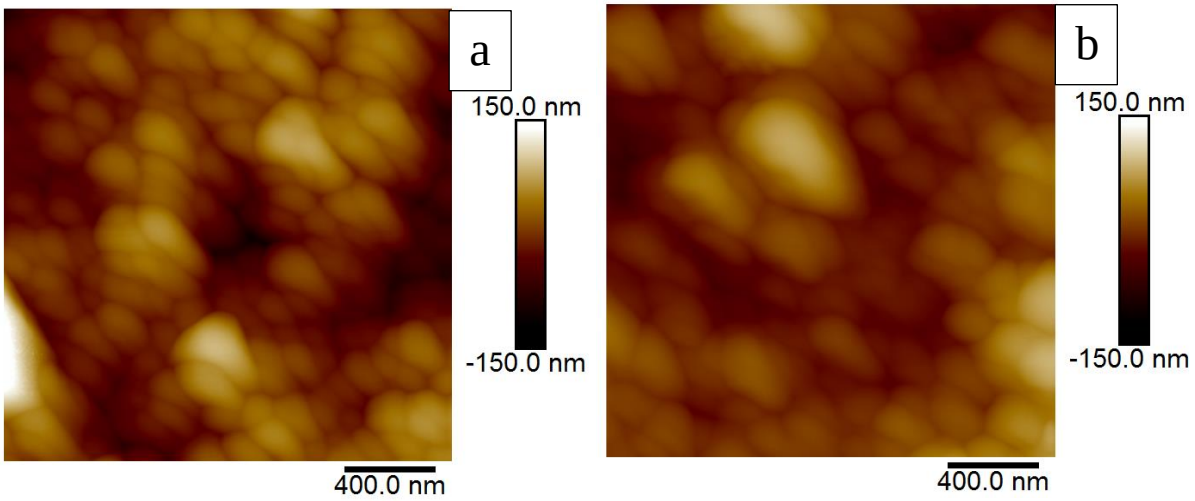

Figure 53: AFM image of electrodeposited PPy (a) and PPy/AgNPs (b) on screen printed carbon electrode

3.7.2 Scanning electron microscopy analysis

The surface morphological characterization of PAA, PPy and the composites of PAA/AgNPs and PPy/AgNPs on the screen printed electrode (SPCE) was also conducted with scanning electrom microscopy (SEM). All the SEM images where taken at a scale of 2 μm with a maginification of 2.5 K (x2500). Figure 54(a) shows a smooth surface for drop coated PAA film on SPCE with some network-like craks formed, these network-like craks may have formed when the PAA film was drying up at room temperature (24^0C). The drop coated PAA/AgNPs composite showed the smooth surface with some sphere-like patches on the top of the film that could be caused by the incorporation of silver nanoparticles (Figure 54(b)). While the surface morphology of polypyrrole appeared to be a thick porous film with small white spots that may have resulted from artefacts such as electron accumulation at edges of grains (Figure 54(c)). The PPy/AgNPs composite showed the same surface morphology as polypyrrole, possessing similar small grains (Figure 54(d)). The electrodeposited PAA and PAA/AgNPs showed a smooth surface, PAA/AgNPs showing no presence of AgNPs (Figure 54(e) and Figure 54(f)).

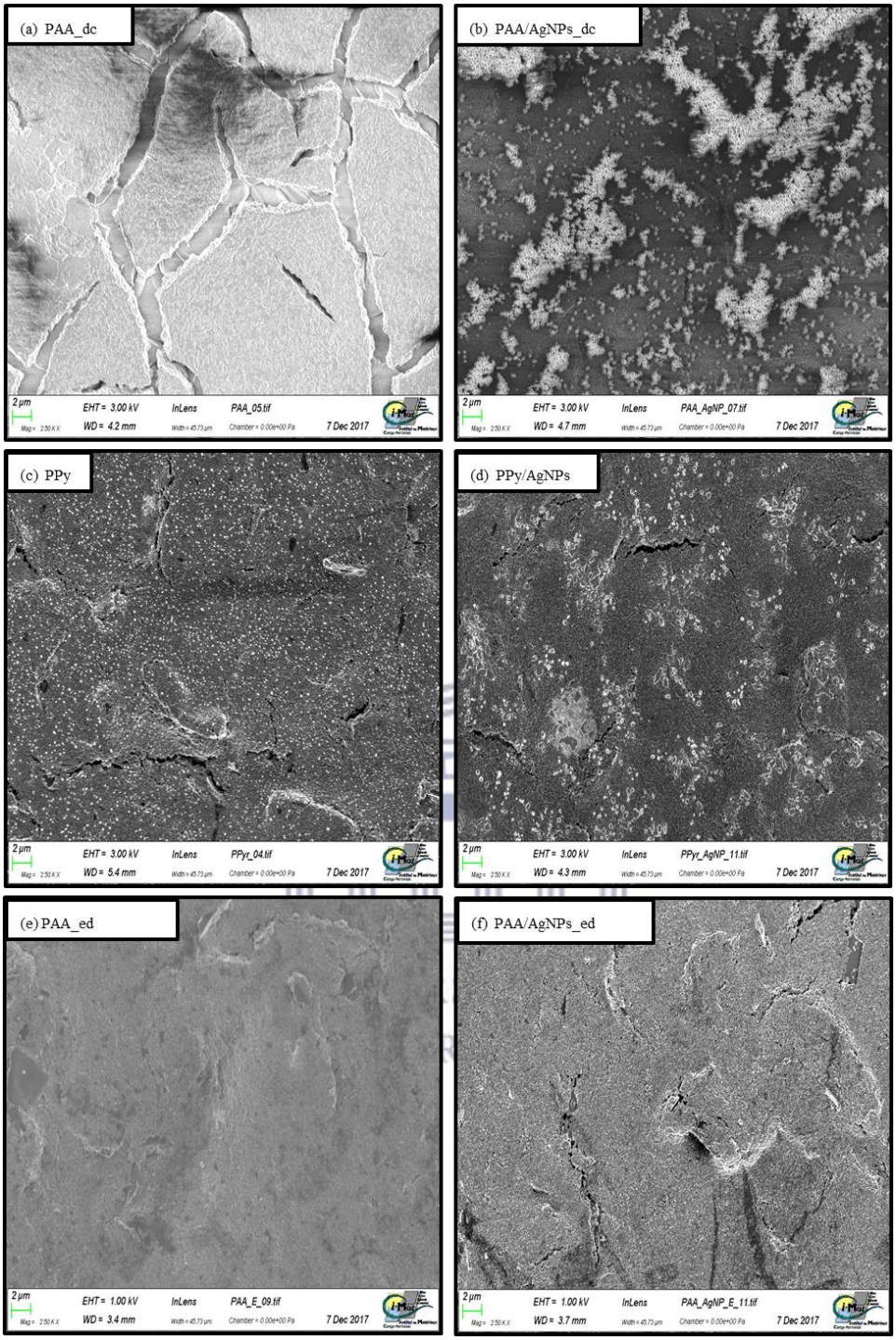

Figure 54 (a): SEM image of drop coated PAA on screen printed carbon electrode. (b): SEM image of drop coated PAA/AgNPs on screen printed carbon electrode. (c): SEM image of electropolymerized PPy on screen printed carbon electrode. (d): SEM image of electropolymerized PPy/AgNPs on screen printed carbon electrode. (e): SEM image of electrodeposited PAA on screen printed carbon electrode. (f): SEM image of electrodeposited PAA/AgNPs on screen printed carbon electrode

From the legend of the SEM images, PAA_dc; drop coated polyamic acid, PAA/AgNPs_dc; drop coated polyamic acid-silver nanoparticles, PAA_ed: electrodeposited polyamic acid, PAA/AgNPs_ed; electrodeposited polyamic acid-silver nanoparticles.

Both analysis (SEM and AFM) were able to indicate indirectly the incorporation/presence of AgNPs on the polymers. In AFM, the presence of AgNPs in PPy and PAA was observed by increasing the grain/sphere size of the polymer, respectively. While in SEM analysis such difference was difficult to notice or observe.

3.8 Conclusion

The four different platforms of GCE/PAA, GCE/PAA/AgNPs, GCE/PPy and GCE/PPy/AgNPs were prepared using electrodeposition, drop coating (GCE/PAA and GCE/PAA/AgNPs), and electropolymerization (GCE/PPy and GCE/PPy/AgNPs) methods. The incorporation of silver nanoparticles in PAA was observed more by the shift of the redox peaks of PAA in the electrochemical behaviour of GCE/PAA/AgNPs. While in the polypyrrole, their incorporation was observed with an increase of current in the electrochemical behavior of GCE/PPy/AgNPs. From the morphology of PAA/AgNPs and PPy/AgNPs on screen printed carbon electrodes, the presence of AgNPs was evident by the formation of sphere-like structure on the surfaces of both polymers, PAA and PPy. This can be correlated with the electrochemical behaviour of GCE/PAA/AgNPs (drop coated) and GCE/PPy/AgNPs, giving proof that the incorporation of AgNPs in polymers was observed.

3.9 References

1. Wang, Q. & Zheng, J. Electrodeposition of silver nanoparticles on a zinc oxide film: Improvement of amperometric sensing sensitivity and stability for hydrogen peroxide determination. *Microchim. Acta* **169,** 361–365 (2010).

2. Mailu, S. N. *et al.* Determination of anthracene on Ag-Au alloy nanoparticles/overoxidized-polypyrrole composite modified glassy carbon electrodes. *Sensors (Switzerland)* **10,** 9449–9465 (2010).

3. Chen, H. *et al.* A hydrogen peroxide sensor based on Ag nanoparticles electrodeposited on natural nano-structure attapulgite modified glassy carbon electrode. *Talanta* **86,** 266–270 (2011).

4. Ngece, R. F. *et al.* A silver nanoparticle/Poly (8-anilino-1-naphthalene sulphonic acid) bioelectrochemical biosensor system for the analytical determination of ethambutol. *Int. J. Electrochem. Sci.* **6,** 1820–1834 (2011).

5. Navolotskaya, D. V., Toh, H. S., Batchelor-McAuley, C. & Compton, R. G. Voltammetric Study of the Influence of Various Phosphate Anions on Silver Nanoparticle Oxidation. *ChemistryOpen* **4,** 595–599 (2015).

6. Noah, N. M. *et al.* Conducting polyamic acid membranes for sensing and site-directed immobilization of proteins. *Anal. Biochem.* **428,** 54–63 (2012).

7. Zamfir, L. G. *et al.* Non-enzymatic polyamic acid sensors for hydrogen peroxide detection. *Sensors Actuators, B Chem.* **226,** 525–533 (2016).

8. Hess, E. H., Waryo, T., Sadik, O. a., Iwuoha, E. I. & Baker, P. G. L. Constitution of novel polyamic acid/polypyrrole composite films by in-situ electropolymerization. *Electrochim. Acta* **128,** 439–447 (2014).

9. Ngema, X. T., Ward, M., Hamnca, S., Baker, P. G. L. & Iwuoha, E. I. Spectro-Electrochemical of Detection Anthracene at Electrodeposited Polyamic Acid Thin Films. *J. Nano Res.* **44,** 63–78 (2016).

Chapter Four

This chapter presents the immobilized CYP2E1 on GCE and modified GCE electrodes in preparation for the construction of biosensors. Electrochemical characterization of the immobilized CYP2E1 and the application of the developed biosensors are also discussed. Cyclic, square wave and differential pulse voltammetry were used to characterize the electrochemical behaviour of CYP2E1 enzyme and the enzyme's response to each analyte (ethambutol and rifampicin) in 0.1 M PBS at pH 7.4. The GCE/PAA/AgNPs/CYP2E1 and GCE/PPy/AgNPs/CYP2E1 biosensors were prepared by drop coating 1µL of CYP2E1 solution. The calibration curves were constructed after the detection of analyte species and the limits of detection were determined.

4.1 Enzyme modified GCE electrode

4.1.1 Cyclic and square wave voltammetric analysis

In order to investigate the electrochemical properties of the CYP2E1 enzyme immobilized on GCE modified electrodes, the CYP2E1 properties on GCE were investigated first. The electrochemistry of CYP enzymes has been investigated in previous studies on glassy carbon electrodes modified with different conducting materials as indicated in Table 4 chapter one. It was important to understand the electrochemistry of CYP2E1 on the bare electrode before immobilizing it on the modified glassy carbon electrode. In Figure 55, the redox behaviour of CYP2E1 on GCE was observed at 57 mV (oxidation peak labelled **a**) and at 28 mV (reduction peak labelled **b**). The pair of redox peaks arose from the redox of the heme Fe centre of CYP2E1 attributed to the Fe^{2+}/Fe^{3+} transition [1]. While the peak at -800 mV arose from the reduction of oxygen. The square wave voltammetry was further used to characterize CYP2E1 on GCE due to its excellent sensitivity and rejection of background currents over cyclic voltammetry. Cyclic voltammetric analysis of CYP2E1 on GCE revealed a redox behaviour of CYP2E1 enzyme at formal potential of 43 mV (Figure 55). While with the square wave voltammetric analysis the formal potential was at 36 mV (Figure 56). The oxidation and reduction peaks of CYP2E1 enzyme on GCE were distinguishable more easily in the square wave voltammograms than in cyclic voltammograms. The square wave voltammetry proving to have better sensitivity over cyclic voltammetry.

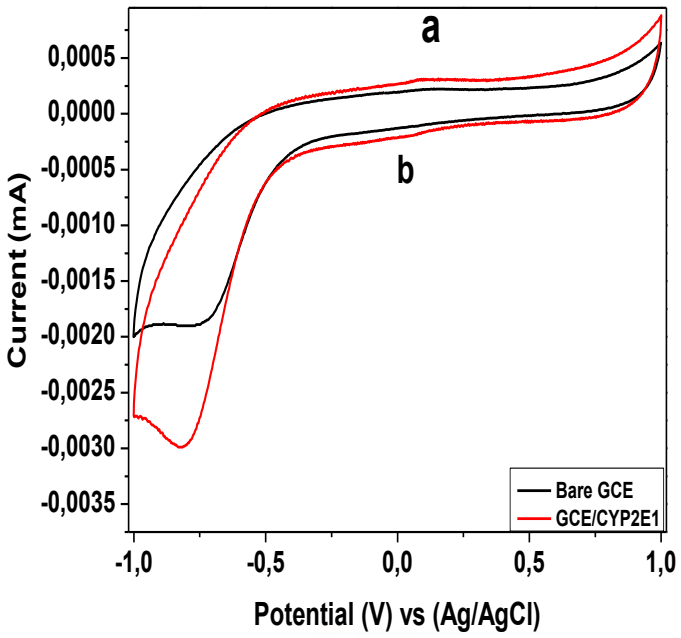

Figure 55: Cyclic voltammograms of the drop-coated CYP2E1 on GCE in 0.1 M PBS at a scan rate of 50 mV/s

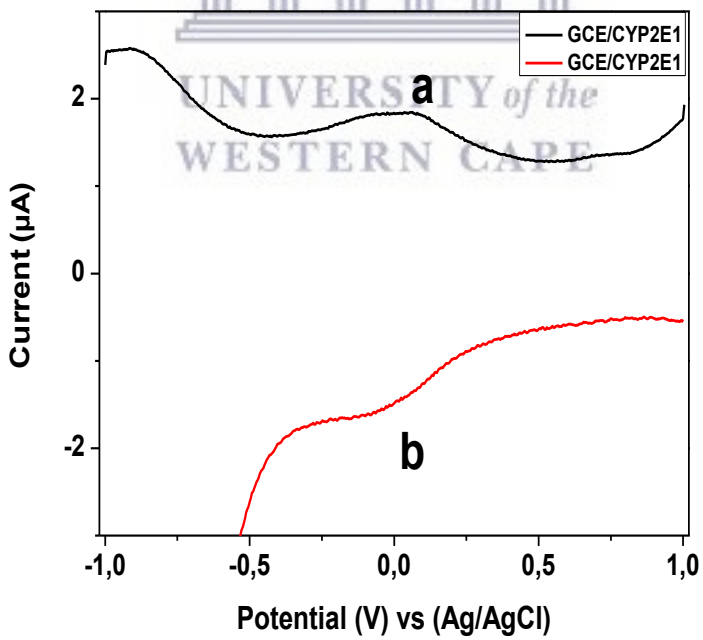

Figure 56: Square wave voltammograms of the drop-coated CYP2E1 on GCE in 0.1 M PBS at a scan rate of 50 mV/s

4.2 Enzyme modified GCE/PAA/AgNPs/CYP2E1 electrode

4.2.1 Cyclic and square save voltammetric analysis

After investigating the electrochemical properties of CYP2E1 on GCE; the electrochemical properties of CYP2E1 on the modified GCE/PAA and GCE/PAA/AgNPs electrodes were also examined and compared to the electrodes without the enzyme as shown in Figure 57 that present the cyclic voltammograms. Compared to the GCE/CYP2E1 electrode, there was no visible electrochemical oxidation and reduction of the enzyme around 57 mV and 28 mV, respectively. This may be due to PAA having a strong background current (oxidation and reduction peaks) at the region where the electrochemical properties of CYP2E1 was expected (from -200 mV to 400 mV for oxidation and 250 mV to -250 mV for reduction). The peak at -800 mV was due to the reduction of oxygen. Regardless of the oxidation and reduction peaks of CYP2E1 enzyme not being observed on the modified electrodes namely: GCE/PAA and GCE/PAA/AgNPs, there was a noticeable growth of the second oxidation peak (**b**) (which is identified as one quinoid-type dication poly(amine-amide)$^{2+}$ from PAA) when the enzyme CYP2E1 was immobilized on both electrodes. This may be regarded as current-peak-enhancement effect on PAA caused by CYP2E1 and CYP2E1 showing no indication of hindering the charge transport across the PAA/AgNPs film. Indeed, it is known that heme proteins exhibit different formal potentials which are attributed to different system configurations and different microenvironments that promotes direct electron transfer [2]. In addition, studies of cytochrome P450 immobilized through physical adsorption onto gold surfaces have demonstrated that hydrophobic interactions can be generated between hydrophobic residues of the protein and hydrophobic surfaces [3]. PAA may have a strong capacitive current at a potential range where the electrochemical behaviour of CYP2E1 was expected and subsequently 'overshadowed' or supressed the redox behaviour of the CYP2E1 enzyme. Nevertheless, it was evident when comparing the cyclic voltammograms of GCE/PAA/CYP2E1, GCE/PAA/AgNPs/CYP2E1 with cyclic voltammogram of GCE/PAA and GCE/PAA/AgNPs at 50 mV/s (Figure 57) that there was electron transfer between CYP2E1 enzyme and the electrodes and that the enzyme was attached on the modified electrodes as confirmed by the current-enhancement in peak (**b**).

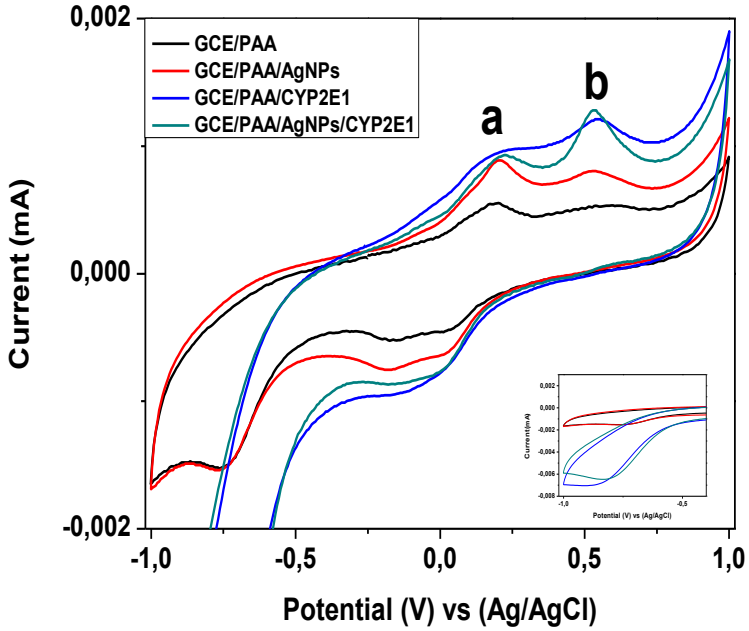

Figure 57: Cyclic voltammograms of GCE/PAA and GCE/PAA/AgNPs electrodes without enzyme (black and red curves respectively) and with CYP2E1 (blue and green curves respectively) in 0.1 M PBS at a scan rate of 50 mV/s

To further confirm these observations, square wave voltammetry was used due its advantages over cyclic voltammetry. Figure 58 shows a comparison of electrodes; GCE/PAA, GCE/CYP2E1, GCE/PAA/AgNPs, GCE/PAA/CYP2E1 and GCE/PAA/AgNPs/CYP2E1. The comparison of the electrodes was made by monitoring the change in peak (**a**) and (**b**). In both GCE/PAA (black curve) and GCE/PAA/AgNPs (blue curve) the intensity of the oxidation peaks [(**a)** and (**b**)] was higher compared to the electrodes modified with CYP2E1 enzyme (GCE/PAA/CYP2E1 and GCE/PAA/AgNPs/CYP2E1). A decrease of intensity of the oxidation peaks from GCE/PAA/CYP2E1 (green curve) indicated that there was the presence of CYP2E1 enzyme on the surface of the electrode. Similar behaviour was observed when CYP2E1 enzyme was immobilized on GCE/PAA/AgNPs surfaces (pink curve), but the current decreased even more in the platform of GCE/PAA/AgNPs suggesting that the system became more complex (slowing the electron transfer between the surface of the electrode and enzyme) when CYP2E1 was immobilized on the surface of the electrode. It should be noted that is acceptable behaviour after enzyme immobilization resultant from the protein surrounding the active sites of enzymes. It is their presence that is responsible for hindering electron flow while

carrying out their desired function. However, the decrease of current in both electrodes (GCE/PAA/CYP2E1 and GCE/PAA/AgNPs/CYP2E1) reduced the background current in favour of having less noise interference from the polymer when these biosensors are applied for the detection of anti-TB drug analyte.

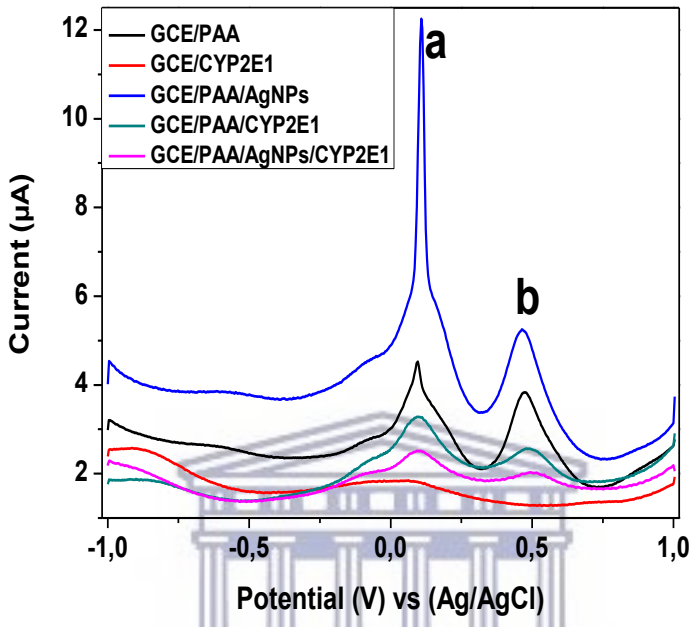

Figure 58: Square wave voltammograms of GCE/PAA (blue) and GCE/PAA/AgNPS (black) and the drop-coated CYP2E1 on GCE (red), GCE/PAA (green) and GCE/PAA/AgNPs (pink) in 0.1 M PBS at a scan rate of 50 mV/s

4.3 Enzyme modified GCE/PPy/AgNPs/CYP2E1 electrode

Polypyrrole (PPy) was used instead of PAA for the development of GCE/PPy/AgNPs/CYP2E1 biosensor. Polypyrrole has been extensively studied and its properties are known. These properties include environmental stability, good redox properties and the ability to give high electrical conductivities. PPy is frequently used in electrocatalytic and affinity sensors and biosensors based on its unique electrical and thermal properties. Thus, PPy was also used in this study in order to compare the efficiency of GCE/PAA/AgNPs/CYP2E1 and GCE/PPy/AgNPs/CY2E1 biosensors.

4.3.1 Cyclic and differential pulse voltammetric analysis

Figure 56 illustrates the cyclic voltammetric response of CYP2E1 enzyme modified electrodes when polypyrrole was used instead of PAA. The voltammetric potentials were scanned from -0.9 to 0.5 V. The enzyme modified electrodes; GCE/PPy/CYP2E1 (Figure 59(a)) and GCE/PPy/AgNPs/CYP2E1 (Figure 59(b)) were compared to GCE/PPy and GCE/PPy/AgNPs, respectively in order to identify any redox change that was caused by the immobilization of CYP2E1 as it was observed on the bare GCE. However, the presence of CYP2E1 on the modified electrodes was only observed by a current (mA) decrease in CV of polypyrrole. In addition, contrary to electrodes modified with PAA, the square wave voltammetry analysis of electrodes modified with PPy yielded voltammograms with high intensities of electrical interference when the enzyme modified electrodes were characterized using this technique (results not shown). Hence another pulse technique was used, which is the differential pulse voltammetry (DPV) and it gave a signal response with less noise than square wave voltammetry. Figure 60 shows the differential pulse voltammetric analysis of the CYP2E1 enzyme modified electrodes where the potentials were scanned reductively from 0.5 to -0.9 V. Compared to cyclic voltammetric analysis, the redox change that was brought by the immobilization of CYP2E1 enzyme to each platform GCE/PPy and GCE/PPy/AgNPs was clearly observed with the differential pulse voltammetric analysis. Comparing the electrodes modified with the enzyme and unmodified, the change was noticed by the negative shift in potentials of the reduction peaks when the CYP2E1 enzyme was immobilized on both electrodes; GCE/PPy/CYP2E1 (blue curve) and GCE/PPy/AgNPs/CYP2E1 (green curve) (Figure 60). This was mainly due to the resistive effect brought by the CYP2E1 enzyme resulting from the presence of protein around the active site which is thus responsible for reducing electron flow. Table 8 below shows the potentials of the CYP2E1 enzyme modified and unmodified electrodes.

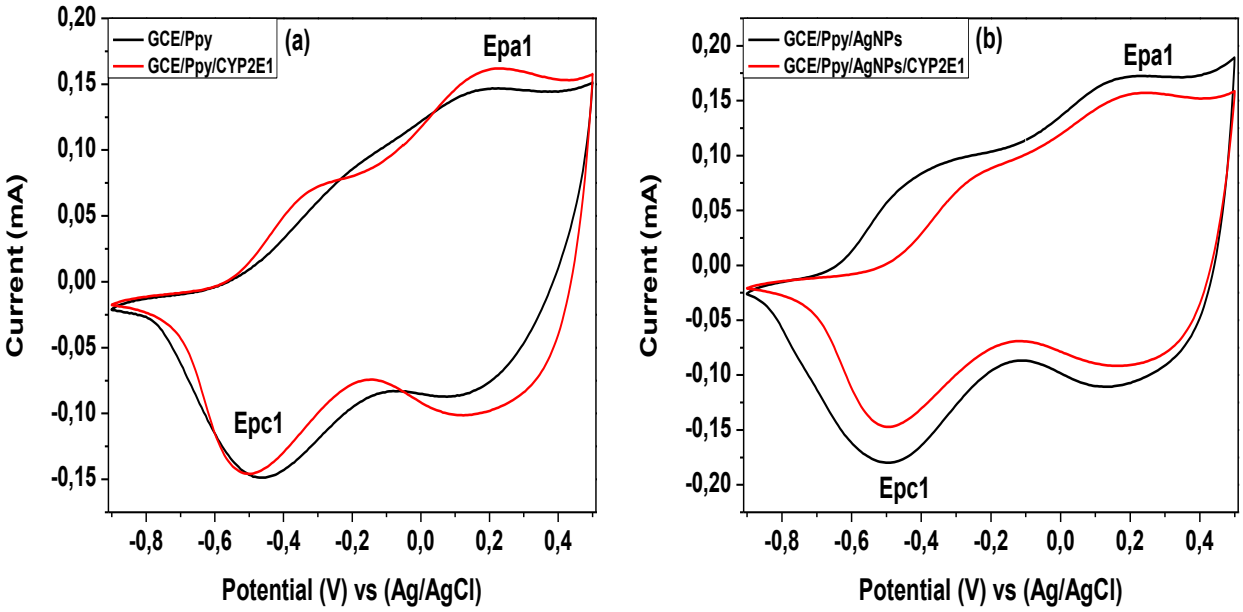

Figure 59: Cyclic voltammograms of the immobilized CYP2E1 on GCE/PPy (a) and GCE/PPy/AgNPs (b) in 0.1 M PBS at a scan rate of 50 mV/s

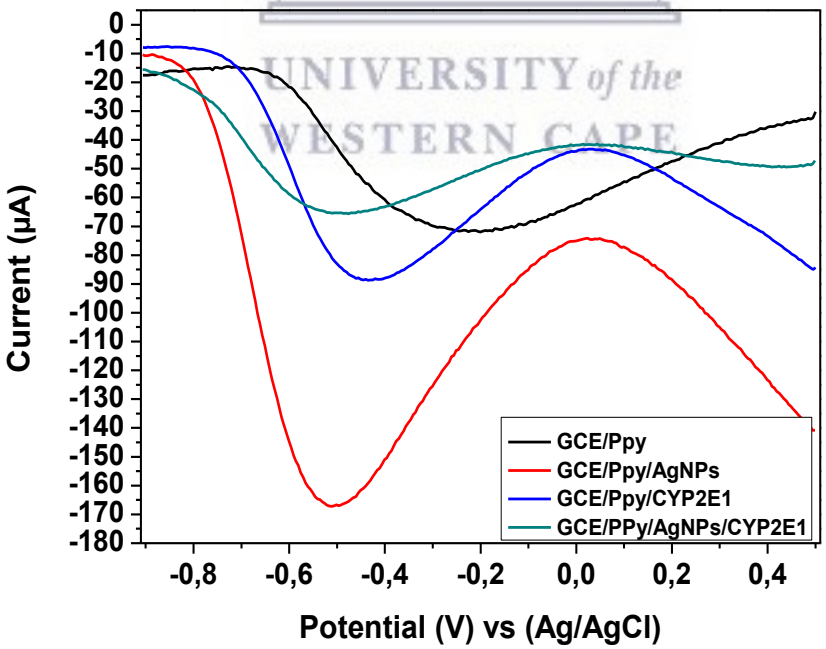

Figure 60: Differential pulse voltammograms of the immobilized CYP2E1 on GCE/PPy (blue curve) and GCE/PPy/AgNPs (green curve) in 0.1 M PBS at a scan rate of 50 mV/s

Table 8: Potential peaks of the GCE/PPy, GCE/PPy/AgNPs, GCE/PPy/CYP2E1 and GCE/PPy/AgNPs/CYP2E1 electrodes.

Electrode	Potential (mV)
GCE/PPy	-240
GCE/PPy/CYP2E1	-420
GCE/PPy/AgNPs	-510
GCE/PPy/AgNPs/CYP2E1	-479

4.4 Application of biosensors and sensors to ethambutol

The developed GCE/PAA/AgNPs/CYP2E1, GCE/PPy/AgNPs/CYP2E1 biosensors and GCE/PAA/AgNPs, GCE/PPy/AgNPs chemical sensors were further used to detect the anti-TB drug ethambutol using differential pulse voltammetry. All the experiments were done following the procedure in section ***A.2.5***. The GCE/PPy/AgNPs/CYP2E1 biosensor was able to detect ethambutol from a µg/mL range whereas the GCE/PAA/AgNPs/CYP2E1 biosensor was able to detect ETH from ng/mL range. PAA has an ability to bind specifically to biomolecules through its pendant carboxylic groups that are in close proximity to the transducer surface. Therefore, these characteristics of PAA can allow the design of electron transfer pathways between the immobilized CYP2E1 enzyme and the electrode surface. Polypyrrole is a biological compatible polymer matrix wherein number of drugs and enzyme can be incorporated by way of doping. It has gained tremendous recognition as a sophisticated electronic measuring device in the field of sensors and drug delivery and is highly efficient as a biosensor in presence of an enzyme. The two polymers were used as platforms to develop the enzymatic biosensors for the detection of anti-TB drugs due to their capabilities of being compatible with biomolecules. In addition, PAA is fairly a new polymer, therefore it was thought that PPy is a good candidate to compare its performance in biosensing since PPy is a conductive and well-studied polymer.

4.4.1 GCE/PAA/AgNPs/CYP2E1 biosensor

Figure 61 shows the GCE/PAA/AgNPs/CYP2E1 biosensor response to different concentrations of ethambutol using differential pulse voltammetry (DPV). The potentials were scanned from -1.0 to 1.5 V. A new oxidation peak on the first addition of ethambutol was detected at 810 mV. This was in agreement with the study of determining ethambutol in aqueous medium by Lima and co-workers [4,5]. The peak at 810 mV may be associated with the oxidation of –OH and secondary –NH groups in ethambutol. In addition, it was clearly observed that the current response increased as ethambutol concentrations were increased from 2.5 to 20.0 ng/mL. From the oxidation peak at 810 mV, current responses were measured with respect to each concentration of ethambutol. These current responses were used to construct a calibration curve in order to obtain the detection limit and sensitivity of GCE/PAA/AgNPs/CYP2E1 biosensor when detecting ethambutol (Figure 62). The limit of detection and sensitivity were evaluated within the linear range of the calibration curve, 2.5 to 12.5 ng/mL. The detection limit of ethambutol using GCE/PAA/AgNPs/CYP2E1 biosensor was calculated to be 0.75 ng/mL with a sensitivity of 5 μA/ng.mL^{-1}. The full profile response of GCE/PAA/AgNPs/CYP2E1 upon ethambutol addition yielded a parabolic calibration curve (Figure 62). This profile is called Michaelis-Menten whereby at low substrate concentrations of the enzymatic process will give a linear response, then level off to a flat plateau at high substrate concentrations. The plateau occurs when the enzyme is saturated, meaning that all available enzyme molecules are already tied up processing substrates. The point of saturation from the ethambutol response at GCE/PAA/AgNPS/CYP2E1 biosensor was reached at 14.9 ng/mL. The enzymatic reaction at the GCE/PAA/AgNPs electrode surface was considered as follows:

$$\text{CYP2E1} + \text{Ethambutol} \longrightarrow \text{CYP2E1} - \text{Ethambutol} \qquad K_1$$

$$\text{CYP2E1} - \text{Ethambutol} \longrightarrow \text{CYP2E1} + \text{Ethambutol Aldehyde} + H_2O \qquad K_2$$

Therefore, based on the Michaelis-Menten reaction, the enzymatic kinetics of CYP2E1 can be written as shown in Equation 3:

$V = K_2 [CYP2E1][Ethambutol]/K_m + [Ethambutol]$ Equation (3)

Where V is the rate, K_2 the equilibrium constant, K_m the Michaelis-Menten constant, [CYP2E1] the concentration of CYP2E1 enzyme and [Ethambutol] is the concentration of ethambutol. The lower K_m and higher V values indicates a high enzyme biocatalytic activity. The calibration curve in Figure 60 presents the entire enzymatic reaction where K_m and higher V parameters were studied. At lower concentrations, the rate of reaction was directly proportional to the ethambutol concentrations between 2.5 to 12.5 ng/mL. When $V = V_{max}$ (maximum rate), the K_m is numerically equal to half of the ethambutol concentration. Therefore, the value of K_m was found to be 6.25 ng/mL [6,7]. The Lineweaver-Burk (Equation 4) was further used to evaluate the K_m^{app} (apparent Mchaelis-Menten constant). The Michaelis constant is the substrate concentration at which the reaction rate is half of V_{max}. From Figure 63, the x-intercept of the graph represent $-1/K_m$ and y-intercept is equivalent to the inverse of V_{max}.

$$\frac{1}{Iss} = \frac{1}{Imax} + \frac{1}{Imax} K_m^{app} \frac{1}{[S]}$$

I_{ss} is the measured steady state current, I_{max} the maximum current under saturated substrate concentration, K_m^{app} is the apparent Michaelis-Menten and [S] is the concentration of ethambutol. From the above equation using the intercept and slope, the value of K_m^{app} was found to be 6.0 ng/mL and the I_{max} value was calculated to be 500 µA. The K_m^{app} value was in the same range 10^{-9} ng/mL as the study of Ngece et al and smaller than previously reported value by Costa et al [6,8]. The smaller value of K_m^{app} indicated that CYP2E1 enzyme at the GCE/PAA/AgNPs electrode has good affinity towards ethambutol and the I_{max} value shows that the biosensor was electroactive.

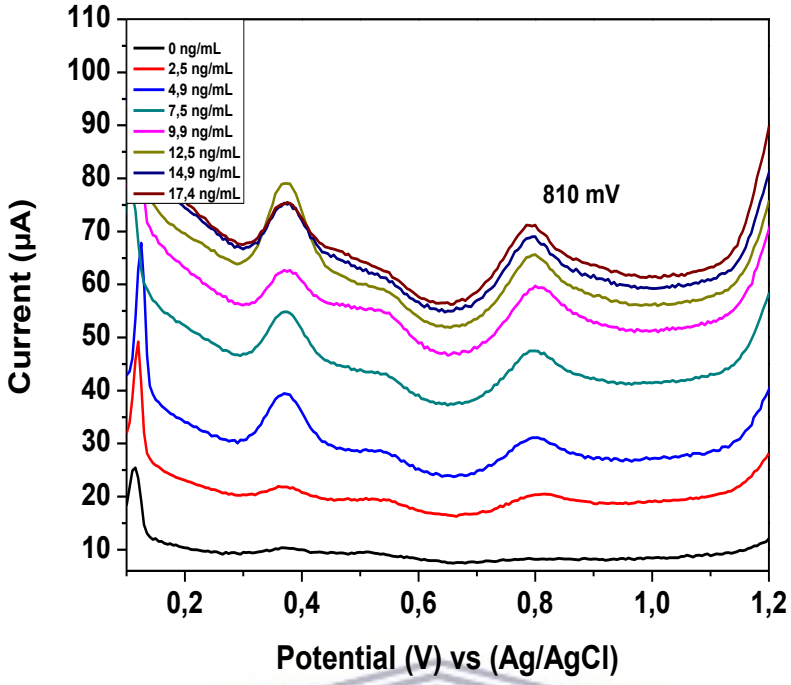

Figure 61: Differential pulse voltammograms of the GCE/PAA/AgNPs/CYP2E1 biosensor responding to different concentration of ethambutol in 0.1 M PBS at a scan rate of 50 mV/s

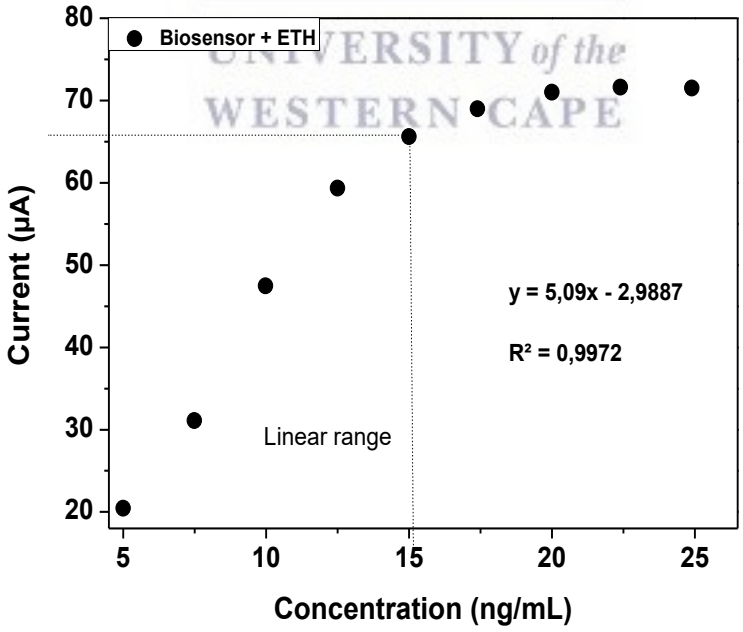

Figure 62: Calibration curve of Ip vs concentration of ethambutol at GCE/PAA/AgNPs/CYP2E1 biosensor in 0.1 M PBS

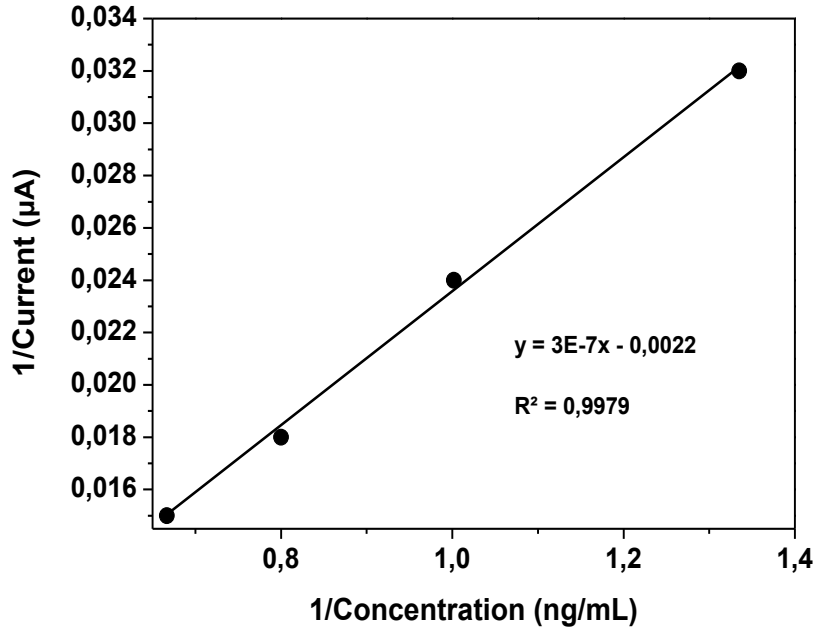

Figure 63: The linear inverse of the Ip vs concentration of ethambutol at GCE/PAA/AgNPs/CYP2E1 biosensor in 0.1 M PBS

4.4.2 GCE/PAA/AgNPs sensor

Considering the fact that the detection of ethambutol may be done in real samples (environmental water) where the concentration and the pH of the samples is not known and may not be compatible with enzyme CYP2E1, the use of GCE/PAA/AgNPs electrode as a chemical sensor was also investigated. Indeed, the enzyme is a biological compound that is active in a media of pH 7, therefore, when the enzyme is exposed to a concentrated medium (pH<7), the enzyme may denature or become less functional. In Figure 64, DPV response of GCE/PAA/AgNPs to different concentrations of ethambutol is presented. This figure also shows a peak at 810 mV after the first addition of ethambutol that was attributed to the oxidation of ethambutol molecule. However, when the concentration of ethambutol was increased, there was no increase in current similar to the GCE/PAA/AgNPs/CYP2E1 biosensor response. On the contrary, the current response decreased until 7.5 ng/mL. Hence, no linear response was obtained between the concentrations of 2.5 to 9.9 ng/mL. According to the proposed mechanism of GCE/PAA/AgNPs/CYP2E1 biosensor (Figure 65), the ethambutol was supposed to induce low-spin to high-spin states transition of the CYP2E1 ferri-heme which can be ascribed to strong interaction of CYP2E1 with surfaces. However, the

GCE/PAA/AgNPs chemical sensor suggests that the oxidation peak at 810 mV was the direct oxidation of ethambutol. In the GCE/PAA/AgNPs/CYP2E1 biosensor the same response was also observed, however it was clearly observed that the current response increased as ethambutol concentrations were increased from 2.5 to 20.0 ng/mL. Therefore, the presence of CYP2E1 enzyme promoted the surface interaction with ethambutol as a result of an increasing current response in the GCE/PAA/AgNPs/CYP2E1 biosensor.

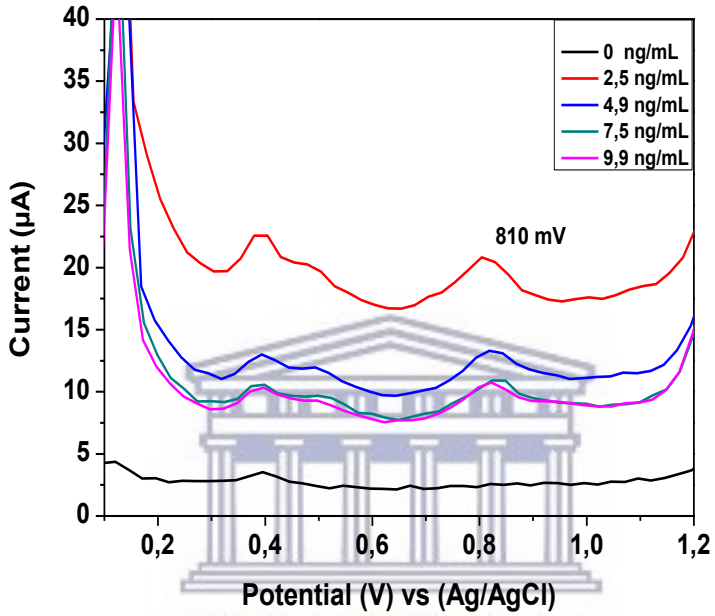

Figure 64: Differential pulse voltammograms of the GCE/PAA/AgNPs electrode responding to different concentration of ethambutol in 0.1 M PBS at a scan rate of 50 mV/s

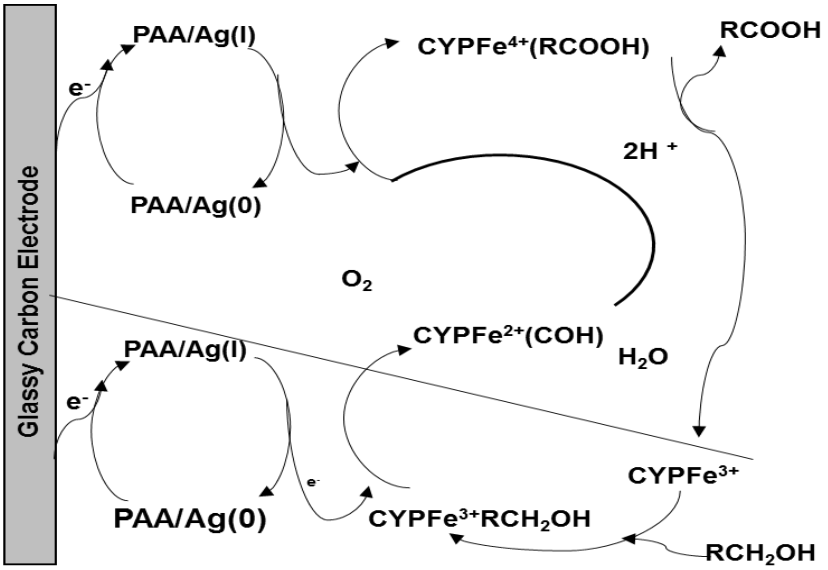

Figure 65: Reaction scheme for the proposed GCE/PAA/AgNPs/CYP2E1 biosensor

RCH_2OH – Ethambutol

RCOH – Ethambutol aldehyde intermediate

RCOOH – Dicarboxylic acid ethambutol

PAA/Ag – polyamic acid/silver nanoparticles

CYP – Cytochrome P450-2E1

4.4.3 GCE/PPy/AgNPs/CYP2E1 biosensor

The GCE/PPy/AgNPs/CYP2E1 biosensor was also applied for the detection of ethambutol at different concentrations (Figure 66) in order to compare the performance of the two biosensors GCE/PAA/AgNPs/CYP2E1 and GCE/PPy/AgNPs/CYP2E1. Polypyrrole was thought to be a good candidate to prepare the platform of the biosensor since PPy is a conductive polymer, and was assumed to have less background currents (capacitive current) than PAA. However, in the GCE/PAA/AgNPs/CYP2E1 biosensor and GCE/PAA/AgNPs sensor, ethambutol was oxidized at 810 mV. This potential was "too high" for the stability of polypyrrole (results not shown). Hence, the response of GCE/PPy/AgNPs/CYP2E1 to ethambutol was examined in another potential window. Thus, it was noticed by reductive DPV scans that the GCE/PPy/AgNPs/CYP2E1 biosensor is giving an indirect response at ethambutol detection.

This was the indirect response due to ethambutol causing a decrease in current at the de-doping of PPy around -470 mV. Therefore, the decrease in current at -470 mV was monitored as an indirect response of the biosensor when detecting ethambutol. The reduction peak decreased from the ethambutol concentrations of 2.5 µg/mL to 24.9 µg/mL and the linear range was observed between 2.5 µg/mL to 14.9 µg/mL (Figure 67). The limit of detection of the GCE/PPy/AgNPs/CYP2E1 biosensor was calculated to be 1.3 µg/mL, while the sensitivity of 2.6 µA/µg.mL^{-1} was determined from the calibration curve in Figure 67.

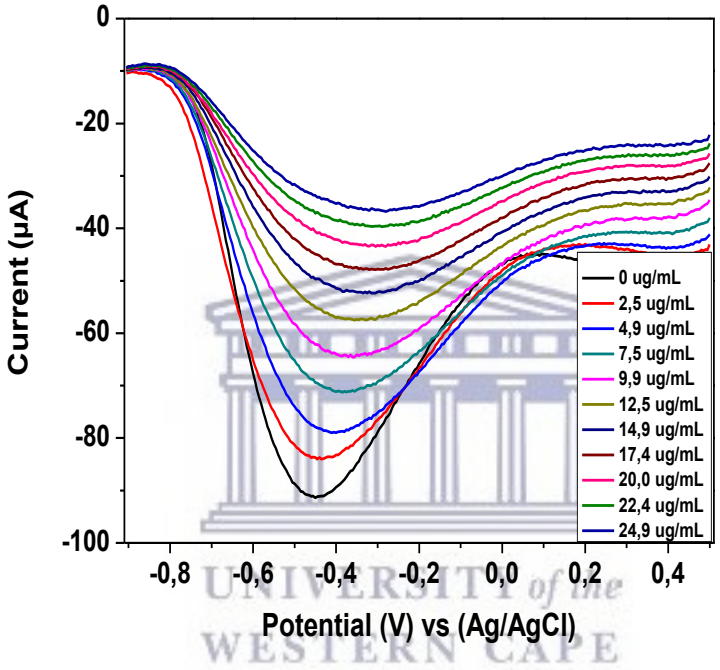

Figure 66: Differential pulse voltammograms of the GCE/PPy/AgNPs/CYP2E1 biosensor responding to different concentration of ethambutol in 0.1 M PBS at a scan rate of 50 mV/s

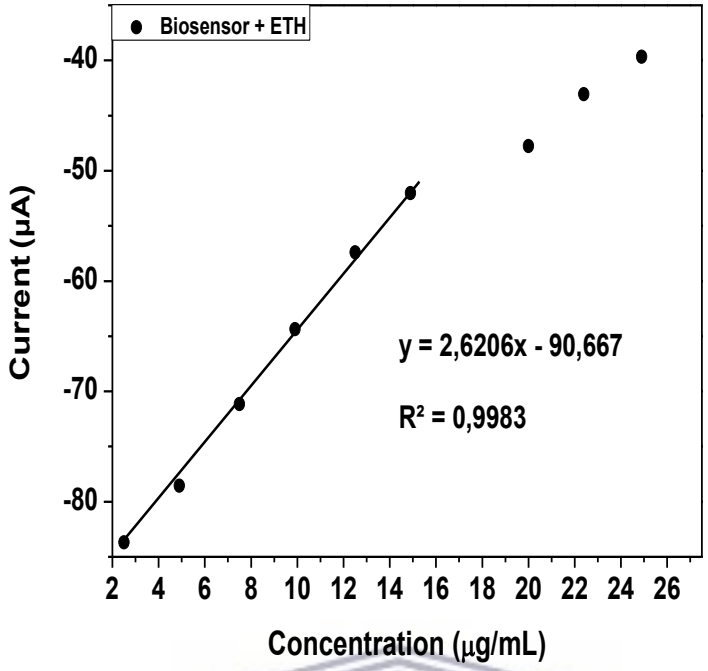

Figure 67: Calibration curve of Ip vs concentration of ethambutol at GCE/Ppy/AgNPs/CYP2E1 biosensor in 0.1 M PBS

4.4.4 GCE/PPy/AgNPs sensor

Without CYP2E1 enzyme, the response was the same as GCE/PPy/AgNPs/CYP2E1 biosensor. However, in the absence of CYP2E1 the reduction peak of PPy was at 360 mV (Figure 68). The linear range was observed between the concentrations of 2.5 µg/mL to 12.5 µg/mL. The GCE/PPy/AgNPs yielded a high sensitivity of 4.7 µA/µg.mL^{-1} (Figure 69) higher than the sensitivity of the GCE/PPy/AgNPs/CYP2E1 biosensor. The limit of detection was calculated to be 4.47 µg/mL and it was also higher than the one of the GCE/PPy/AgNPs/CYP2E1 biosensor.

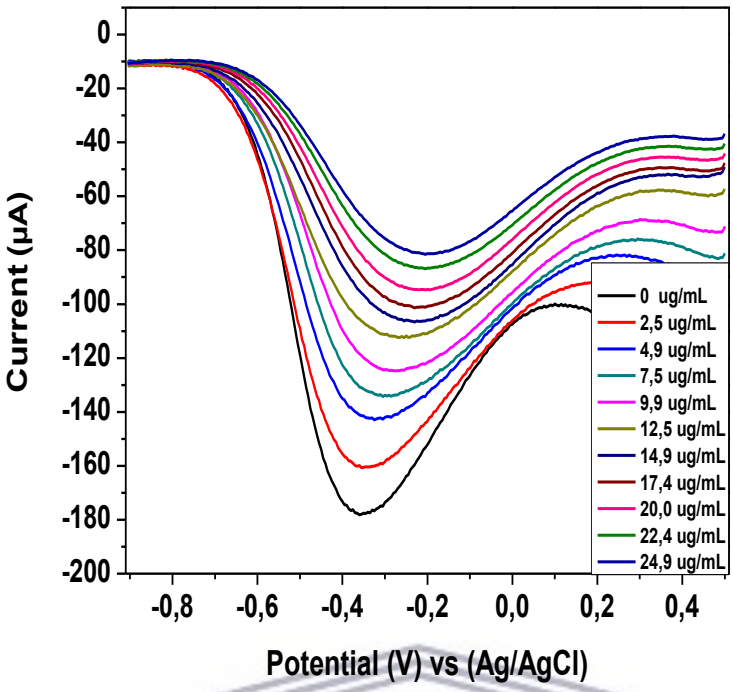

Figure 68: Differential pulse voltammograms of the GCE/PPy/AgNPs sensor responding to different concentration of ethambutol in 0.1 M PBS at a scan rate of 50 mV/s

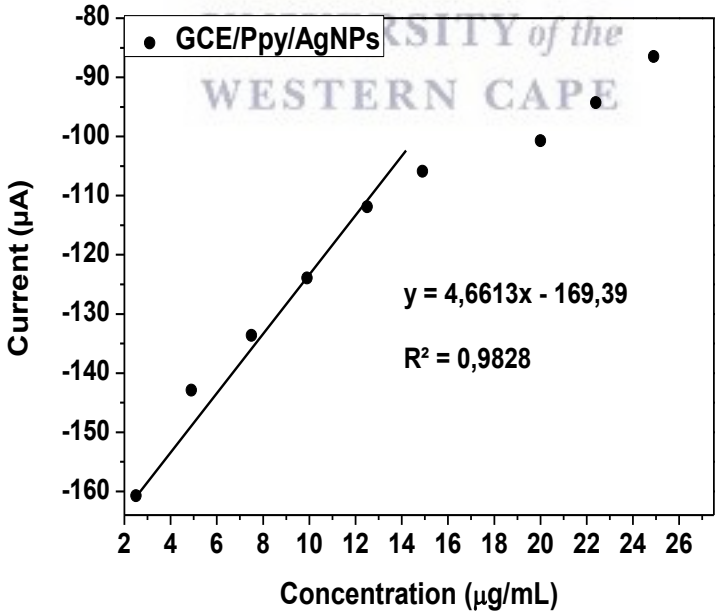

Figure 69: Calibration curve of Ip vs concentration of ethambutol at GCE/PPy/AgNPs electrode in 0.1 M PBS

4.5 Application of biosensor to rifampicin

Rifampicin is used for the treatment of TB in combination with other anti-TB drugs such as ethambutol. GCE/PAA/AgNPs/CYP2E1 and GCE/PPy/AgNPs/CYP2E1 biosensors and GCE/PAA/AgNPs and GCE/PPy/AgNPs chemical sensors were all used to detect rifampicin but only the GCE/PPy/AgNPs/CYP2E1 biosensor was able to detect rifampicin.

Figure 70 shows the GCE/PPy/AgNPs/CYP2E1 biosensor response to different concentrations of rifampicin. The potentials were scanned reductively from 0.5 to -0.9 V. The first addition of rifampicin (2.5 µg/mL) was observed by an increase in current response from -90 µA (0 µg/mL) to -109 µA. The GCE/PPy/AgNPs/CYP2E1 biosensor response of detecting rifampicin was contrary to the response of detecting ethambutol. The increase in current response showed that there was electron transfer across the PPy/AgNPs/CYP2E1 when different concentrations of rifampicin were detected. The linear response was obtained at a concentration range of 2.5 µg/mL to 9.9 µg/mL (Figure 71). The point of saturation was reached at 12.5 µg/mL with a limit of detection of 1.7 µg/mL.

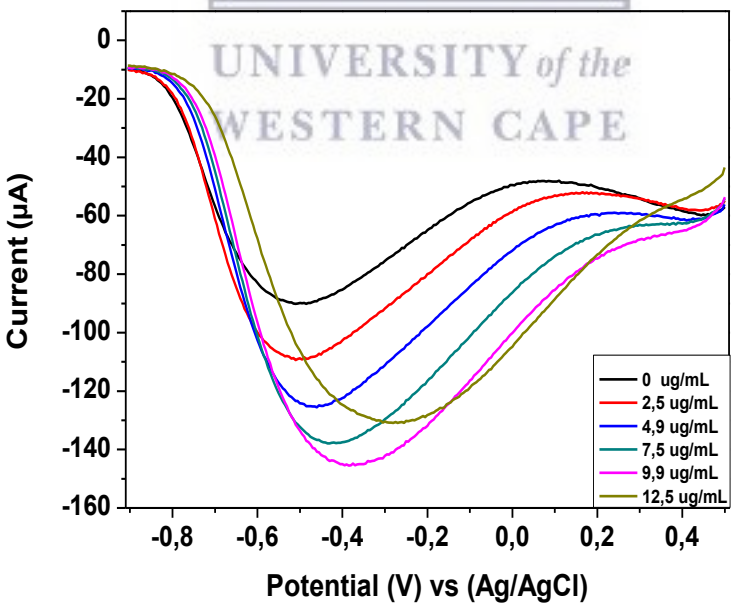

Figure 70: Differential pulse voltammograms of the GCE/PPy/AgNPs/CYP2E1 biosensor responding to different concentration of rifampicin in 0.1 M PBS at a scan rate of 50 mV/s

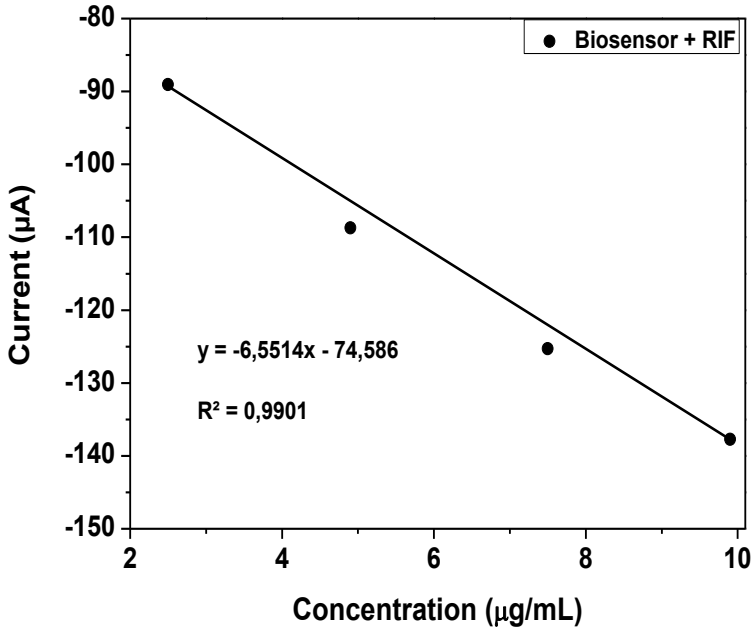

Figure 71: Calibration curve of Ip vs concentration of rifampicin at GCE/Ppy/AgNPs/CYP2E1 biosensor in 0.1 M PBS

4.6 Conclusion

4.6.1 Chemical sensors

The chemical sensors GCE/PAA/AgNPs and GCE/PPy/AgNPs were both used to detect ethambutol. The GCE/PAA/AgNPs chemical sensor gave a direct oxidation of ethambutol at 810 mV without obtaining a linear range since there was no good current response. This suggested that there was no good electron transfer between the surface of the sensor and ethambutol. On the other hand, the GCE/PPy/AgNPs gave an indirect response when ethambutol was detected. The linear range was observed between 2.5 μg/mL to 12.5 μg/mL, with a limit of detection of 4.47 μg/mL. Comparing the limits of detection and linear response of ethambutol with other studies in Table 9, the range of linear response forGCE/PPy/AgNPs sensor at ethambutol was better than the linear response of the other studies. The GCE/PPy/AgNPs limit of detection was better than the LODs of Parantoni and Sepehri studies. While with the study of Lima et al the LODs were at the same range 10^{-6} g/mL [4]. The efficiency of the GCE/PPy/AgNPs sensor demonstrates that the peak ethambutol serum level range which

is 2 – 6 µg/mL is within the linear response range of 2.5 µg/mL to 12.5 µg/mL, indicating that this sensor can be used with success in serum.

Table 9: Comparison of ethambutol limit of detection and sensitivities of chemical sensors

Chemical Sensor	Linear Range	Limit of detection	Reference
GCE/Gr-PRF	$2.04x10^{-4}$ – $2x10^{-3}$ g/mL	$3.1x10^{-4}$ g/mL	5
MEA	$1.02x10^{-5}$ - $4x10^{-4}$ g/mL	$9.6x10^{-6}$ g/mL	4
SPCE/MWCNT/Nafion	--	$8.4x10^{-7}$ g/mL	8
GCE/PMEL/AuNPs	$1.x10^{-4}$ - $3.1x10^{-2}$ g/mL	$4.3x10^{-5}$ g/mL	9
GCE/PPy/AgNPs	$2.5x10^{-6}$ - $12.5x10^{-6}$ g/mL	$4.5x10^{-6}$ g/mL	This work

4.6.2 Biosensors

The GCE/PAA/AgNPs served as suitable platform for CYP2E1 enzyme attachment promoting an oxidation of ethambutol facilitated by the mobility of electrons between the surface of the electrode and enzyme active sites. The GCE/PPy/AgNPs/CYP2E1 biosensor was able to detect anti-TB drugs at their peak serum levels (2 – 6 µg/mL). Whereas the GCE/PAA/AgNPs/CYP2E1 biosensor was able to detect ethambutol at concentrations lower than the serum level (2.5 ng/mL to 12.5 ng/mL). Therefore, GCE/PAA/AgNPs/CYP2E1 biosensor has an ability to detect ethambutol even at trace levels in aqueous systems. The sensitivity of GCE/PAA/AgNPs/CYP2E1 biosensor (5 µA/ng.mL^{-1}) was better than the sensitivity of the GCE/PPy/AgNPs/CYP2E1 biosensor (2.6 µA/µg.mL^{-1}). Therefore, GCE/PAA/AgNPs/CYP2E1 biosensors have a better efficiency both in sensitivity and limit of detection than the GCE/PPy/AgNPs/CYP2E1 biosensor. However on the other hand, both GCE/PAA/AgNPs/CYP2E1 and GCE/PPy/AgNPs/CYP2E1 biosensors have better sensitivities than the biosensor of Au/PANSA/PVP-AgNPs/CYP2E1 (1.13 µA/µg.mL^{-1}) [6] (Table 10).

Table 10: Comparison of detection limits of ethambutol and sensitivities of biosensors

Biosensor	Linear Range	Limit of detection (g/mL)	Reference
Au/PANSA/PVP-AgNPs/CYP2E1^{E}	$2.0x10^{-7}$ – $2.5x10^{-6}$ g/mL	$1.4x10^{-7}$	6
Au/PANSA/PVP-AgNPs/CYP2E1^{R}	$1.7x10^{-6}$ – $1.15x10^{-5}$ g/mL	$4.1x10^{-8}$	7
GCE/PPA/AgNPs/CYP2E1^{E}	$2.5x10^{-9}$ – $1.25x10^{-8}$ g/mL	$0.75x10^{-9}$	This work
GCE/PPy/AgNPs/CYP2E1^{E}	$2.5x10^{-6}$ – $1.5x10^{-5}$ g/mL	$1.3x10^{-6}$	This work
GCE/PPy/AgNPs/CYP2E1^{R}	$2.5x10^{-6}$ – $9.9\,x10^{-6}$ g/mL	$1.7x10^{-6}$	This work

Au/PANSA/PVP-AgNPs/CYP2E1^{E} = detection of ethambutol, Au/PANSA/PVP-AgNPs/CYP2E1^{R} = detection of rifampicin.

4.7 Stability and reproducibility study and interference studies

The proposed biosensor strategy was developed and evaluated. The biosensor of polyamic acid-based platforms was able to detected ethambutol by means of direct oxidation of –OH and secondary –NH. While the biosensor of polypyrrole-based platforms detected ethambutol and rifampicin by means of indirect response. GCE/PPy/AgNPS/CYP2E1 biosensor was able to yield a linear response that is within the peak serum levels of both drugs. However, the proposed mechanism response for both biosensors was not observed at ethambutol and rifampicin. The reproducibility of both biosensors was investigated. The linear response of ethambutol obtained at GCE/PPy/AgNPs/CYP2E1 was still within the peak serum level of ethambutol (2.5 to 14.9 µg/mL) (Figure 72). While at GCE/PAA/AgNPs/CYP2E1 biosensor the linear response was at 2.5 to 9.9 ng/mL (Figure 73 and Figure 74). The interference studies were not investigated for both biosensors. The last objective of the project was to do interference studies by means of evaluating the sensitivity and selectivity of the biosensors in detecting ethambutol and rifampicin concentrations in a cocktail or mixture form (rifampicin mixed with ethambutol). However, this was not evaluated due to the indirect response of ethambutol and rifampicin that was contrary to each other at GCE/PPy/AgNPs/CYP2E1 biosensor. On the other hand, the GCE/PAA/AgNPs/CYP2E1 biosensor has a background

current from PAA. To evaluate cross-reactivity and interfering species on the platform that enhances background current than enhancing the detection of the analyte may have made the system more complex.

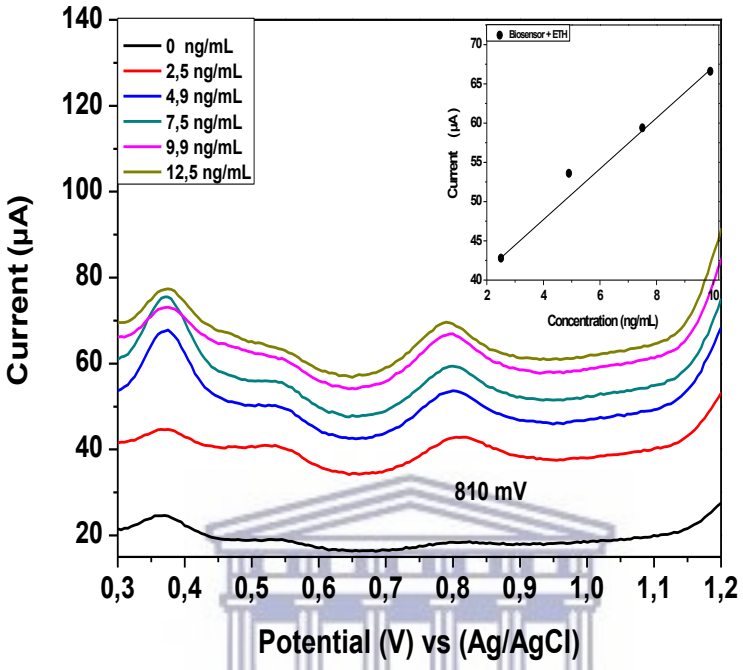

Figure 72: Differential pulse voltammograms of the GCE/PAA/AgNPs/CYP2E1 biosensor responding to different concentration of ethambutol in 0.1 M PBS at a scan rate of 50 mV/s with an inserted calibration curve Ip vs concentration of ethambutol

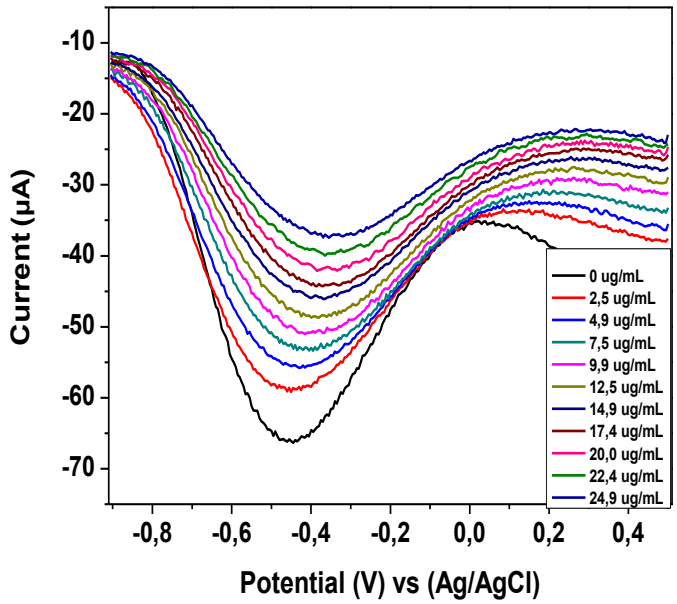

Figure 73: Differential pulse voltammograms of the GCE/PPy/AgNPs/CYP2E1 biosensor responding to different concentration of ethambutol in 0.1 M PBS at a scan rate of 50 mV/s

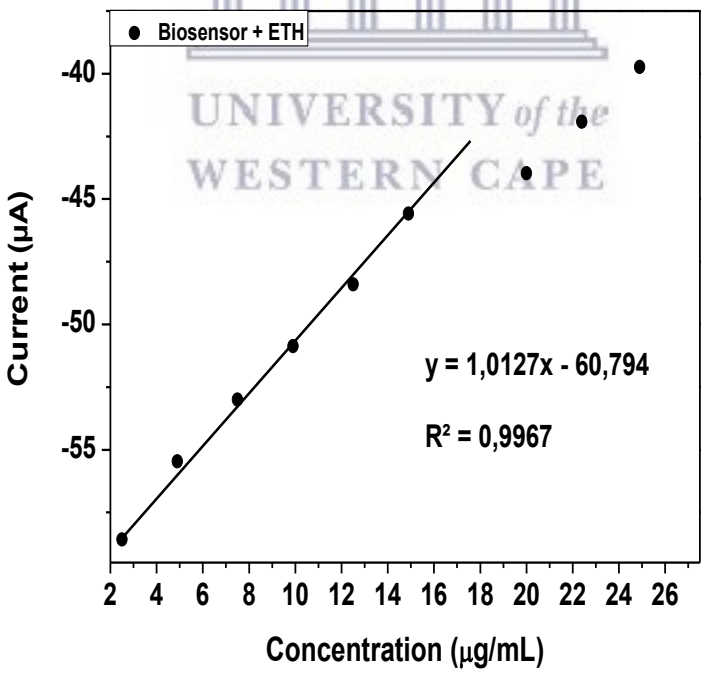

Figure 74: Calibration curve of Ip vs concentration of ethambutol at GCE/PPy/AgNPs/CYP2E1 biosensor in 0.1 M PBS

4.8 References

1. Macedo Cerqueira, P., Cesarino, E. J., Bertucci, C., Sueli Bonato, P. & Lanchote, V. L. Stereoselective metabolism of metoprolol: Enantioselectivity of ??-hydroxymetoprolol in plasma and urine. *Chirality* **15,** 542–549 (2003).

2. Guascito, M. R. *et al.* A new amperometric nanostructured sensor for the analytical determination of hydrogen peroxide. *Biosens. Bioelectron.* **24,** 1057–1063 (2008).

3. Baj-Rossi, C., de Micheli, G. & Carrara, S. Electrochemical detection of anti-breast-cancer agents in Human Serum by Cytochrome P450-coated Carbon nanotubes. *Sensors (Switzerland)* **12,** 6520–6537 (2012).

4. Lima, K. C. M. S., Santos, A. C. F., Fernandes, R. N., Damos, F. S. & de C??ssia Silva Luz, R. Development of a novel sensor for isoniazid based on 2,3-dichloro-5,6-dicyano-p-benzoquinone and graphene: Application in drug samples utilized in the treatment of tuberculosis. *Microchem. J.* **128,** 226–234 (2016).

5. Bellei Perantoni, C., Soares Carbogim, L. G., Silva Semaan, F., Camargo Matos, R. & Lowinsohn, D. Flow injection analysis of ethambutol in antituberculosis drugs using a graphite-paraffin electrode as amperometric detector. *Electroanalysis* **23,** 2582–2585 (2011).

6. Ngece, R. F. *et al.* A silver nanoparticle/Poly (8-anilino-1-naphthalene sulphonic acid) bioelectrochemical biosensor system for the analytical determination of ethambutol. *Int. J. Electrochem. Sci.* **6,** 1820–1834 (2011).

7. Ajayi, R. F. *et al.* Chemically amplified cytochrome P450-2E1 drug metabolism nanobiosensor for rifampicin anti-tuberculosis drug. *Electrochim. Acta* **128,** 149–155 (2014).

8. Costa, R. S., Machado, D., Rocha, I. & Ferreira, E. C. Hybrid dynamic modeling of Escherichia coli central metabolic network combining Michaelis-Menten and approximate kinetic equations. *BioSystems* **100,** 150–157 (2010).

9. Sepehri, Z. *et al.* Simultaneous electrochemical determination of isoniazid and ethambutol using poly-melamine/electrodeposited gold nanoparticles modified pre-anodized glassy carbon electrode. *Ionics (Kiel).* 1–11 (2017). doi:10.1007/s11581-017-2263-y

Chapter Five

Thesis conclusions and outlooks

In this work the feasibly study of the new point-of-care systems that are fast, reliable, ultra-sensitive and cheap was done for two issues related to tuberculosis. The first issue was the detection of tuberculosis disease while the second one was the detection of anti-TB drug to prevent multidrug-resistant tuberculosis. Hence, this work was divided in two parts.

Part I: Mycobacterium tuberculosis immunosensor

Mycobacterium tuberculosis was detected using the TB IgG ELISA principle. The indirect ELISA method of detecting *Mycobacterium tuberculosis* was adopted for *Mycobacterium tuberculosis* immunosensor. Polyamic acid was chemically synthesized as powder from monomers PMDA and ODA for the development of immunosensor platforms.

The FTIR analysis of PAA pallet using KBr confirmed the functional groups of carboxylic acid, amide and ether, proving that PAA was successfully synthesized.

PAA was soluble in ACN, DMF and PBS. PAA dissolved in three different solvents was electrodeposited and characterized in 0.1 M phosphate buffer solutions at a pH of 7.01. The electrochemical characterization of all three PAA solutions yielded the same electrochemical signals in terms of the number of oxidation and reduction peaks. PAA dissolved ACN and DMF proved to have a higher current response than PAA dissolved in PBS. However, a decrease in current response (peaks intensities) from PAA dissolved in PBS was an advantage for immunosensor development since a decrease in current response reduced background current and minimized the chances of electrical interference from PAA during the detection of *Mycobacterium tuberculosis antibodies.*

The antibody-antigen interaction on GCE/PAA platform was investigated by the square wave voltammetry. The immune-complex was formed and observed by a decrease of reduction peak at 810 mV. The immunosensor proved to be efficient with a limit of detection (LOD) of 0.08 mg/mL and high sensitivity of 700 μA/g.mL.$^{-1}$.

Part II: CYP2E1-based biosensor

Polyamic acid was chemically synthesized as powder from monomers PMDA and ODA. Drop coating and electrodeposition methods were used to deposit PAA on glassy carbon electrode. Drop coating method proved to be a better method of depositing PAA on GCE than electrodeposition method. Silver nanoparticles were synthesized by chemical reduction of $AgNO_3$ salt using $NaBH_4$. The size of the silver nanoparticles was found to be in a range of 2.5 to 20 nm and AgNPs absorbed visible light at 403 nm when the absorbance measurements were taken at a range of 200 – 800 nm. The electrochemical behaviour of silver nanoparticles was observed with an oxidation peak at 160 mV on GCE. When AgNPs were incorporated into PAA, their redox response was not observed but the current response of PAA was improved.

On the other hand, polypyrrple (PPy) was electrochemically synthesized from the Py monomer and characterized in 0.1 M phosphate buffer solutions at pH of 7.4. Electrochemical characterization of PPy showed the p-doping and de-doping of PPy proving that the polymer was successfully synthesized and attached on the surface of GCE. The incorporation of nanoparticles improved the electroactivity of PPy as the current response of PPy/AgNPs was higher than the current response of PPy. The polypyrrole platforms were more electroactive than the polyamic acid platforms.

Morphology studies of PAA and PAA/AgNPs (AFM) showed that PAA have a spherical structure whereas PAA/AgNPs composite showed the same structure but the size of the spheres were observed to be comparatively lager than of PAA. While PPy and PPy/AgNPs were both observed to have granular surface morphology. The presence of AgNPs in PPy/AgNPs increased the size of the grains in the polymer. PAA and PPy had surface features that were clearly distinguished by spherical and granular shape, respectively. SEM confirmed what was observed in AFM. PAA had a network-like structure with craks, while the PAA/AgNPs

composite had a smooth surface with some sphere-like patches that may have been caused by the incorpotration of silver nanoparticles. The surface morphology of PPy appeared to be a thick porous film with small white spots. The same morphology was observed with Ppy/AgNPs composite composing of sphere-like patches due to AgNPs. Both morphology studies (SEM and AFM) were able to show the difference when AgNPs was present in both polymers.

The immobilized CYP2E1 enzyme on GCE/PAA, GCE/PPy, GCE/PAA/AgNPs and GCE/PAA/PPy/AgNPs platforms was investigated by cyclic, square wave and differential pulse voltammetry. On the GCE/PAA and GCE/PAA/AgNPs platforms, the presense of the immobilized CYP2E1 enzyme was observed by a noticeable growth of the second oxidation peak of PAA when using cyclic voltammetry for characterization. While the characterization with the square wave voltammetry, there was a decrease in current response from both platforms (GCE/PAA and GCE/PAA/AgNPs) indicating the presence of CYP2E1 enzyme. On the GCE/PPy and GCE/PPy/AgNPs platforms, the presence of CYP2E1 was observed by a negative shift of the reduction peak of PPy.

Investigating the interfacial properties of CYP2E1 with ethambutol, the application of GCE/PAA/AgNPs/CYP2E1 and GCE/PPy/AgNPs/CYP2E1 biosensors to ethambutol was evaluated. The GCE/PAA/AgNPs/CYP2E1 biosensor was more sensitivity (5 $\mu A/ng.mL^{-1}$) than the GCE/PPY/AgNPs/CYP2E1 biosensor (2.6 $\mu A/\mu g.mL^{-1}$). The presence of CYP2E1 in GCE/PAA/AgNPs/CYP2E1 biosensor promoted the electron transfer between the electrode surface and ethambutol since when the GCE/PAA/AgNPs was used as a chemical sensor there was no good current response caused by the oxidation of ethambutol at different concentrations.

GCE/PAA/AgNPs/CYP2E1 biosensor had a lower limit of detection and was more sensitive than GCE/PPy/AgNPs chemical sensor and GCE/PPy/AgNPs/CYP2E1 biosensor.

Recommendations and future work

The GCE/PPy/AgNPs sensor and GCE/PAA/AgNPs/CYP2E1 and GCE/PPy/AgNPs/CYP2E1 biosensors were sensitivity enough to detect ethambutol at a concentration range between $2.5x10^{-9}$ to $1.5x10^{-5}$ g/mL. The follow up procedure should include the evaluation of the sensitivity and selectivity of the biosensors in detecting ethambutol and rifampicin concentrations in a cocktail or mixture form. Evaluate cross-reactivity with the intention of optimizing resolution, evaluate interfering species which may suppress to enhance detection of the analyte. Polyamic acid prepared as a composite film with polypyrrole can also be used as platform instead of using two different platforms since the molar ratio of polyamic acid and pyrrole monomer can be controlled during synthesis [1]. However, both of these polymers when AgNPs were incorporated, the AgNPs electrochemical behaviour was not observed. While on the other hand, the pair of redox peaks from the redox of the heme Fe centre of CYP2E1 attributed to the Fe^{2+}/Fe^{3+} transition was also not observed when immobilized on the two polymers. Therefore, a different transducer needs to be explored that can both give a distinguishable signal response of AgNPs and CYP2E1.

References

1. Hess, E. H., Waryo, T., Sadik, O. a., Iwuoha, E. I. & Baker, P. G. L. Constitution of novel polyamic acid/polypyrrole composite films by in-situ electropolymerization. *Electrochim. Acta* **128,** 439–447 (2014).

KEY WORDS

Cytochrome P450-2E1

Differential Pulse Voltammetry

Enzyme-linked immunosorbent assay

Ethambutol

First-line anti-TB drugs

Glassy carbon electrode

Immunosensor

Multidrug-resistance

Mycobacterium tuberculosis Ag85B

Polyamic acid

Polypyrrole

Rifampicin

Silver nanoparticles

Square wave voltammetry

Tuberculosis

ABSTRACT

Tuberculosis (TB) is an airborne disease caused by Mycobacterium tuberculosis (MTB) that usually affects the lungs leading to severe coughing, fever and chest pains. It was estimated that over 9.6 million people worldwide developed TB and 1.5 million died from the infectious disease of which 12 % were co-infected with human immunodeficiency virus (HIV) in the year 2015. In 2016 the statistics increased to a total of 1.7 million people reportedly died from TB with an estimated 10.4 million new cases of TB diagnosed worldwide. The development of the efficient point-of-care systems that are ultra-sensitive, cheap and readily available is essential in order to address and control the spread of the tuberculosis (TB) disease and multidrug-resistant tuberculosis. This work is the feasibly study on one part on the development of electrochemical immunosensor using a specific Mycobacterium tuberculosis Ag85B antigen to detect tuberculosis and on another part on the development of biosensors using cytochrome P450-2E1 (CYP2E1) enzyme to detect anti-TB drugs in aqueous systems. The immunosensor was developed by adopting the indirect ELISA method which was used for the detection of the IgG antibodies using the tuberculosis IgG ELISA. The development of immunosensor was achieved using glassy carbon electrode (GCE) modified with polyamic acid (PAA) in which Mycobacterium tuberculosis recombinant antigen Ag85B (Ag) was immobilized. PAA was electrodeposited on glassy carbon electrode (GCE) using cyclic voltammetry. The modified electrodes were characterized by cyclic and square wave voltammetry. The response profile of the immunosensor at Mycobacterium tuberculosis antibodies was studied by square wave voltammetry and the linear response was in a range of 0.3 to 1.6 mg/mL with a detection limit (LOD) of 0.08 mg/mL. On the other hand, two platforms for the development of biosensors for the detection of ethambutol and rifampicin (anti-TB drugs) were also prepared. Two platforms were prepared whereby polyamic acid-silver nanoparticles composite (PAA/AgNPs) was drop-coated on GCE to form GCE/PAA/AgNPs platform. While the other platform (GCE/PPy/AgNPs) was formed by electrodeposition of polypyrrole-silver nanoparticles composite (PPy/AgNPs) on GCE using chronopotentiometry. The GCE/PAA/AgNPs and GCE/PPy/AgNPs platforms were then characterized using cyclic voltammetry while their morphologies were obtained by atomic force microscopy (AFM) and scanning electron microscopy (SEM). The immobilization of cytochrome P450-2E1 enzyme (CYP2E1) on both platforms was achieved by means of drop coating. The efficiency of the GCE/PAA/AgNPs/CYP2E1 and GCE/PPy/AgNPs/CYP2E1 biosensors for the detection of ethambutol (ETH) and rifampicin (RIF) was studied by differential pulse voltammetry (DPV).

The GCE/PPy/AgNPs/CYP2E1 biosensor was able to detect anti-TB drugs at their peak serum levels (2 – 6 µg/mL). Whereas the GCE/PAA/AgNPs/CYP2E1 biosensor was able to detect ethambutol at concentrations lower than the serum level (2.5 ng/mL to 12.5 ng/mL). Therefore, GCE/PAA/AgNPs/CYP2E1 biosensor has an ability to detect ethambutol even at trace levels in aqueous systems. Thus, the GCE/PAA/AgNPs/CYP2E1 biosensor have lower limit of detecting ETH (0.75 ng/mL) than GCE/PPy/AgNPs/CYP2E1 biosensor (1.3 µg/mL). The sensitivity of GCE/PAA/AgNPs/CYP2E1 biosensor for ETH was 5 µA/ng.mL^{-1} while the sensitivity of GCE/PPy/AgNPs/CYP2E1 biosensor was 2.6 µA/µg.mL^{-1}. The GCE/PPy/AgNPs/CYP2E1 biosensor was the only biosensor that was able to detect RIF with a limit of detection of 1.7 µg/mL. The GCE/PPy/AgNPs/CYP2E1 biosensor is suitable for the detection of ETH and RIF at serum levels and in aqueous systems. While the GCE/PAA/AgNPs/CYP2E1 is suitable for only detecting anti-TB drugs at trace levels in water.

RESUME

La tuberculose (TB) est une maladie transmise par l'air causée par *Mycobacterium tuberculosis* (MTB) qui affecte habituellement les poumons, entraînant une toux sévère, de la fièvre et des douleurs thoraciques. En 2015, il a été estimé que plus de 9,6 millions de personnes dans le monde ont développé la tuberculose et que 1,5 millions sont morts de la maladie infectieuse dont 12% étaient co-infectés par le virus de l'immunodéficience humaine (VIH). En 2016, les statistiques ont atteint un total de 1,7 million de personnes décédées de la tuberculose avec environ 10,4 millions de nouveaux cas de TB diagnostiqués dans le monde. Le développement de systèmes de mesures rapides et fiables, ultra-sensibles, bon marché et facilement disponibles est essentiel pour lutter contre la tuberculose (TB) et la tuberculose multirésistante. Ce travail est une étude sur la faisabilité d'une part d'immunocapteurs électrochimique utilisant un antigène spécifique de *Mycobacterium tuberculosis* Ag85B pour détecter la tuberculose et d'autre part de biocapteurs utilisant l'enzyme cytochrome P450-2E1 (CYP2E1) pour détecter les médicaments antituberculeux dans le sérum ou l'eau.

L'immunocapteur a été développé en adoptant la méthode ELISA indirecte qui a été utilisée pour la détection des anticorps IgG dans les tests ELISA IgG contre la tuberculose. Il a été réalisé en électrodéposant par voltamétrie cyclique (CV) d'abord de l'acide polyamique (PAA) sur une électrode de carbone vitreux (GCE) puis des antigènes recombinants de *Mycobacterium tuberculosis* Ag85B (Ag). Les électrodes modifiées ont été caractérisées par CV et SWV. Le profil de réponse de l'immunocapteur à des anticorps de Mycobacterium tuberculosis a été étudié par SWV et la réponse linéaire était dans une gamme de 0,3 à 1,6 mg / mL avec une limite de détection (LOD) de 0,08 mg / mL.

D'autre part, deux plates-formes pour le développement de biocapteurs pour la détection de médicaments antituberculeux, l'éthambutol (ETH) et la rifampicine (RIF), ont également été préparées. L'une était un composite PAA/AgNPs (nanoparticules d'argent) déposé par goutte sur GCE pour former une plate-forme GCE/PAA/AgNPs. Alors que l'autre plate-forme (GCE/PPy/AgNPs) a été formée par électrodéposition de pyrrole en présence de nanoparticules d'argent (PPy + AgNPs) sur GCE en utilisant la chronopotentiométrie. Les plateformes GCE/PAA/AgNPs et GCE/PPy/AgNPs ont ensuite été caractérisées en utilisant la voltamétrie cyclique alors que leurs morphologies l'ont été par microscopie à force atomique (AFM) et microscopie électronique à balayage (MEB). L'immobilisation de l'enzyme cytochrome P450-2E1 (CYP2E1) sur les deux plates-formes a été réalisée par dépôt de gouttes. L'efficacité des

biocapteurs GCE/PAA/AgNPs/CYP2E1 et GCE/PPy/AgNPs/CYP2E1 pour la détection de ETH et de RIF a été étudiée par DPV. Le biocapteur GCE/PPy/AgNPs/CYP2E1 a été capable de détecter les médicaments antituberculeux à leur concentration sérique maximale (2 à 6 μg/mL). Alors que le biocapteur GCE/PAA/AgNPs/CYP2E1 était capable de détecter l'ETH à des concentrations inférieures au taux sérique (2,5 ng/mL à 12,5 ng/mL). Par conséquent, le biocapteur GCE/PAA/AgNPs/CYP2E1 a la capacité de détecter ETH même à l'état de traces dans les systèmes aqueux. Ainsi, le biocapteur GCE/PAA/AgNPs/CYP2E1 a une limite inférieure de détection de l'ETH (0,75 ng/mL) par rapport au biocapteur GCE/PPy/AgNPs/CYP2E1 (1,3 μg/mL). La sensibilité du biocapteur GCE/PAA/AgNPs/CYP2E1 pour l'ETH était de 5 $\mu A/ng.mL^{-1}$ alors que celle du biocapteur GCE/PPy/AgNPs/CYP2E1 était de 2,6 $\mu A/\mu g.mL^{-1}$. Le biocapteur GCE/PPy/AgNPs/CYP2E1 était le seul biocapteur capable de détecter le RIF avec une limite de détection de 1,7 μg/mL. Le biocapteur GCE/PPy/AgNPs/CYP2E1 convient à la détection de l'ETH et du RIF aux taux sériques et aux systèmes aqueux. Alors que le GCE/PAA/AgNPs/CYP2E1 ne convient que pour la détection des médicaments antituberculeux à des niveaux traces dans l'eau.

Annex

This section presents the information on all the materials used to perform all the experiments. A general overview of all the sequential steps taken in order to accomplish the aim of the study is also discussed. These sequential steps are divided into two experimental parts: (i) immunosensors and (ii) biosensors. The experimental section of immunosensor presents the chemical and reagents, ELISA protocols, modification of electrodes and the preparation of immunosensor platforms. While the biosensor section presents preparation of electrodes, modification of glassy carbon (GCE) with polyamic acid (PAA), silver nanoparticles (AgNPs), polypyrrole (PPy), composites (PAA/AgNPs, PAA/AgNPs and PPy/AgNPs/AgNPs) and an enzyme cytochrome P450-2E1 (CYP2E1). It also presents the instrumental techniques that are used for the characterization of the materials and detection of selected tuberculosis drug.

A. Experimental

A.1 Part I: Imumunosensor experimental preparations

A.1.1 Chemicals and Reagents

Tuberculosis IgG ELISA Kit was supplied by Creative Diagnostics (BioSciences Inc, New York, United States of America). Pyromellitic dianhydride 99 % (1,2,4,5-benzenetetracarboxilic anhydride), 4,4-oxydianiline 99 %, sodium chloride 99%, potassium chloride 99%, di-potassium hydrogen phosphate and potassium phosphate monobasic were purchased from Sigma–Aldrich (Johannesburg, South Africa). Anti-Mycobacterium tuberculosis Ag85B antibody (Ab) and recombinant Mycobacterium Ag85B protein (Ag) were obtained from Biocom Biotech (abcam, Germany) and cytochrome P450 2E1 enzyme was obtained from Fisher Scientific (France). HPLC grade acetonitrile (ACN) was procured from Sigma–Aldrich. Pure water was obtained from a water purification unit (Elga Ltd., Bucks, England). All other chemicals such as pyrrole, ethambutol and rifampicin were of analytical-reagent grade.

A.1.2 ELISA Protocols

ELISA indirect methods were performed using the tuberculosis IgG ELISA Kit and absorbance measurements were taken using the UV visible spectroscopy. The UV visible spectroscopy that was used to take absorbance measure was the multilabel plate reader. Whereby the plate reader was calibrated with the blank well and the absorbance was measured at 630nm. The ELISA kit consisted of polystyrene microwells that were pre-coated with IgG antigens. The first step was to add 100 µL diluent in the wells except for the blank. The specimens, 10 µL of positive and negative controls were added in their respective wells. The plate was covered and incubated for 30 minutes at 37°C. After the incubation, each well was washed 5 times with washing buffer and allowed to soak for 30-60 seconds between each washing, the plate was then turned onto blotting paper and tapped to remove remainders. In the second step, 100 µL of HRP-conjugated anti-IgG antibodies were added in each well except the blank, incubated and washed the same way as in the first step. The HRP-conjugated anti-IgG antibodies bind to the IgG antibodies in this step and the excess was washed again. Two chromogen solutions of 50 µL containing TMB and hydrogen peroxide were then added in each well. Their reaction was catalyzed by HRP to

produce a blue color. The plate was covered and incubated for 15 minutes at 37°C avoiding light. The positive control and MTB IgG positive sample wells were colored in blue. The reaction was finally stopped with addition of sulfuric acid and the positive solutions turned in color yellow color.

A.1.3 Preparation of electrodes

The GCE/PAA modified electrode was prepared by in-situ electrochemical deposition using the following procedure. Initially, the solid polyamic acid (PAA) was synthesized using a famous procedure by Andreescu et al. 2005: the solid PAA was synthesized in organic medium using 4,4-oxydianiline (ODA) and 1,2,4,5-benzenetetracarboxylic anhydride (pyromellic dianhydride, PMDA) precursors. 2.0220 g (0.01 mol) of ODA and 157 ml of acetonitrile (ACN) were added to a round bottom flask, stirred until solvation. Then, 50 ml of ACN containing 2.2121 g of PMDA (0.01 mol) was added drop by drop for more over 1 hour, and the solution was stirred for 24 h. The resulting yellowish precipitates (polyamic acid) were filtered through a membrane under suction and dried them at room temperature. The slight yellow organic product was obtained and its mass was 3.3897 g. For the preparation of the GCE/PAA electrode; a PAA solution was prepared by dissolving 5 mg of PAA into a 0.1 M phosphate buffer pH 7.04 solution (3 mL) and sonicated for 10 minutes to ensure homogeneity. The mixture of 500 µL was then transferred to the electrochemical cell (3 mL of PBS as an electrolyte) system containing GCE, Ag/AgCl, and a platinum wire as the working, reference, and counter electrodes, respectively. The deposition was carried out using a cyclic voltammetry technique with a potentiostat (PalmSens, Compact Electrochemical Interfaces) using five cycles in a potential window -1.0 V to +1.0 V at a scan rate of 50 mV/s. The PAA-deposited GCE electrode was then washed with de-ionized water in order to remove unbound materials. For the deposition experiments with PAA dissolved in other solvents, the standard solutions were prepared by dissolving 5 mg of PAA into of each solvent (acetonitrile or dimethylformamide). Then 500 µL of the dissolved PAA was transferred into a cell containing 3 mL of PBS electrolyte and the deposition of PAA was done in the same way as the deposition of PAA that was dissolved in PBS. The characterization of the PAA that was dissolved in DMF and ACN solvents was done in a potential window of -1.0 to +1.0 V. The potential sweeps were done at different scan rates between 10, 30.., 90 mV/s.

A.1.4 Immunosensor platforms preparation

The prepared GCE/PAA electrode was further modified with the recombinant *Mycobacterium tuberculosis* antigen Ag85B (Ag). The GCE/PAA electrode was immersed in ta 0.1 g/mL antigen (Ag85B) solution and incubating for 24 h at 4 °C. After incubation, the modified electrode (GCE/PAA/Ag) was used to detect different concentrations of anti-Mycobacterium tuberculosis Ag85B (Ab) using square wave voltammetry. The electrochemical signals were measured by sweeping the potential reductively from +1.0 to -1.0 V at scan rate of 50 mV/s.

A.2 Part II: Biosensor experimental preparations

A.2.1 Synthesis of silver nanoparticles

All glassware used in the synthesis of silver nanoparticles (AgNPs) were washed with a solution of 1 M potassium hydroxide/ethanol. Firstly, 10 mM silver nitrate ($AgNO_3$) and 20 mM sodium borohydride ($NaBH_4$) were prepared in ultra-pure water and diluted ten times to obtain 1 mM $AgNO_3$ and 2 mM $NaBH_4$. Figure 75 shows the Schematic procedure of the synthesis of silver nanoparticles. In a 50 mL flask containing 15 mL of aqueous sodium borohydride solution at concentration of 2 mM, 5 mL of silver nitrate was added (1 mM) drop-wisely (1 drop per second) while stirring the solution strongly at 0^0C. After the addition of $AgNO_3$, 60 mg of sodium citrate was added in the solution and stirred at room temperature for 30 seconds. The resulting yellow solution was then covered with aluminium foil since AgNPs are susceptible to oxidation when exposed to light. The properties of AgNPs were studied using UV-visible spectroscopy and diffraction light scattering (DLS).

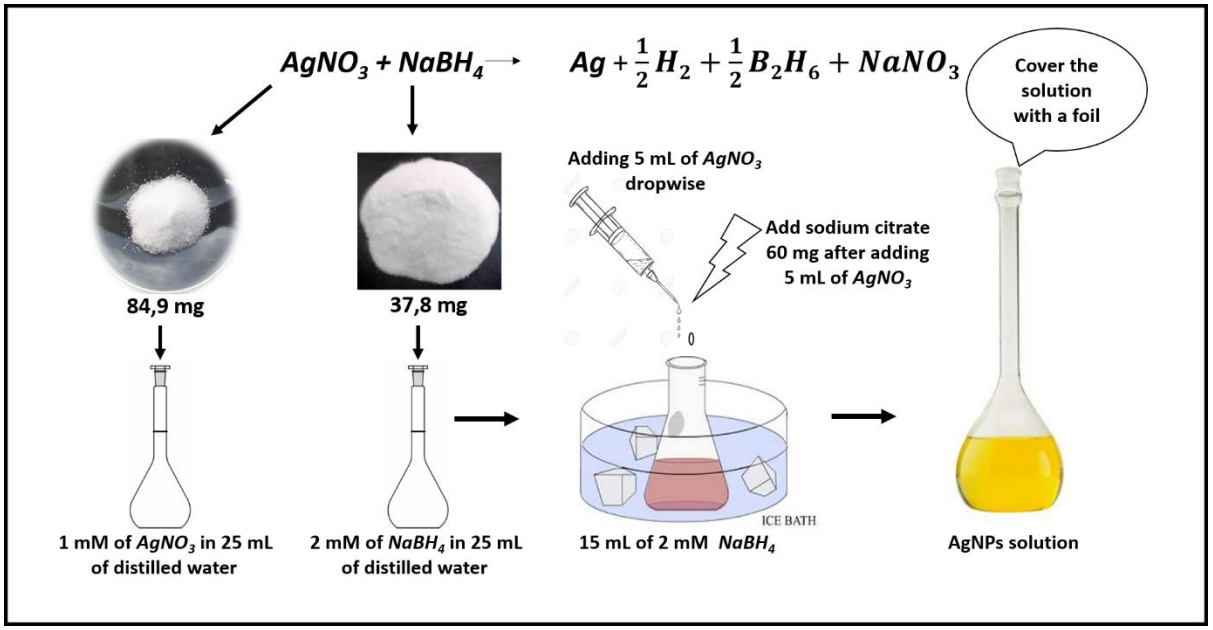

Figure 75: Schematic procedure of the synthesis of silver nanoparticles

A.2.2 Preparation of electrodes

A.2.2.1 Modification of GCE with PAA

The modification of electrodes was achieved by using electrodeposition and drop coating methods. The modification of glassy carbon electrode (GCE) using electrodeposition method was achieved using the previous procedure in section ***A.1.3***. While the modification of GCE with PAA using the drop coating method was achieved by preparing a solution of PAA whereby 5 mg of PAA was dissolved into a 5 mL of 0.1 M phosphate buffer pH 7.4 solution and sonicated for 60 minutes to ensure homogeneity. The PAA mixture of 3 µL was then drop-coated on the surface (0.071 cm^2) of GCE and dried at room temperature (25^0C). The Ag/AgCl, and a platinum wire were used as a reference and counter electrodes, respectively. The drop-coated PAA on the surface of GCE was then characterized using a cyclic voltammetry technique from a potentiostat (Volta Lab, EC-Lab) at different scan rates between (10, 20... 100, 150 mV/s), in a potential window of -1.0 V to +1.0 V. Figure 76 shows the schematic modification of GCE with PAA.

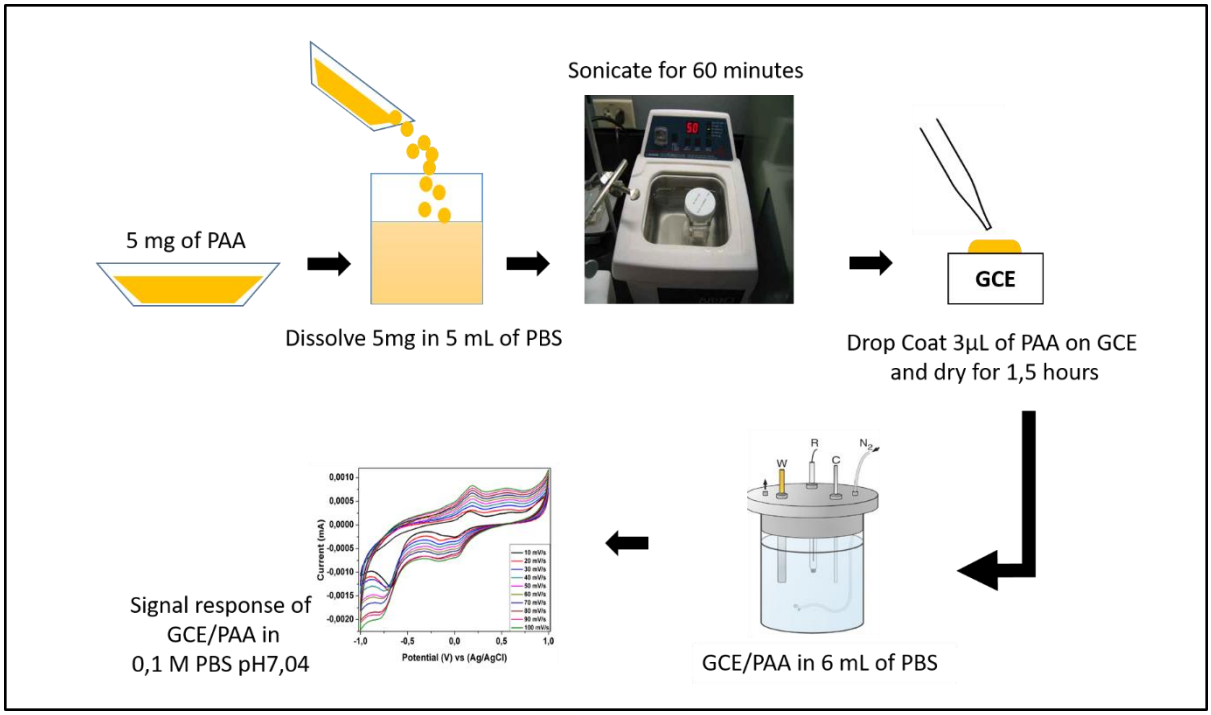

Figure 76: Schematic procedure of modifying glassy carbon electrode with polymic acid

A.2.2.2 Modification of GCE with AgNPs

The electrodeposition of AgNPs was performed using AgNPs suspension prepared by diluting 1 mL of 1mM silver nanoparticles (from the synthesis) in 6 mL of the phosphate buffer electrolyte. The deposition was then carried out using a cyclic voltammetry technique from a potentiostat (Volta Lab, EC-Lab) in 10 cycles, on a potential window ranging between -1.0 V to +1.0 V at a scan rate of 50 mV/s. The modified electrode GCE/AgNPs was further characterized at different scan rates in a 20 mL cell containing a fresh 6 mL phosphate buffer electrolyte in a potential window of -1.0 V to +1.0 V.

A.2.2.3 Modification of GCE with PAA/AgNPs

For the modification of the glassy carbon electrode (GCE) with PAA/AgNPs, a solution was prepared by dissolving 5 mg of PAA into a 5 mL of silver nanoparticles solution and sonicating for 60 minutes to ensure homogeneity. 3 µL of PAA/AgNPs solution was drop coated onto a GCE and dried at room temperature. The characterization of GCE/PAA/AgNPs was done same as the characterization of GCE/PAA indicated in section ***A.2.2.1***.

A.2.2.4 Modification of GCE with PPy

Pyrrole (Py) was distilled to get rid of all the impurities prior to electropolymerization. In a cell containing 10 mL of PBS, 70 µL of Py was added. The chronopotentiometry was used as a method of electropolymerization whereby a current of 0.071 $\mu A/cm^{-2}$ was fixed over time of 600s. A dark polypyrrole (PPy) film was formed on the surface of the GCE. The PPy was characterized using a cyclic voltammetry technique with a potentiostat (VoltaLab, EC-Lab) at different scan rates (20, 30 .... 80 mV/s), in a potential window of -0.9 V to +0.5 V.

A.2.2.5 Modification of GCE with PPy/AgNPs

The same procedure as in section ***A.2.2.4*** was adopted for Py/AgNPs electropolymerization. However, in this procedure 70 µL of Py and 150 µL of AgNPs were transferred into the electrolyte and the PPy/AgNPs film was formed and characterized accordingly.

A.2.4 GCE/PAA/AgNPs/CYP2E1 and GCE/PPy/AgNPs/CYP2E1 biosensors

The same procedure of modifying GCE with PAA/AgNPs was followed as indicated in section ***A.2.2.3*** section and for the GCE/PPy/AgNPs was also done as indicated in section ***A.2.2.5***. On the electrodes of GCE/PAA/AgNPs and GCE/PPy/AgNPs, cytochrome P450-2E1 (CYP2E1) was immobilized on the surface of the electrodes by drop-coating a volume of 1 µL. The new electrodes (GCE/PPy/AgNPs/CYP2E1 and GCE/PAA/AgNPs/CYP2E1) were then dried at 4 ^0C for approximately 3 hours. The characterization was done using cyclic, square wave and differential pulse voltammetry.

A.2.5 Ethambutol and rifampicin detection

The standard solution of both drugs; ethambutol (ETH) and rifampicin (RIF) was prepared by dissolving each drug in a phosphate buffer solution (PBS) to the desired concentrations (5 mg/mL). Different concentrations of each anti-TB drug were prepared in a 4 mL reaction cell containing PBS. The voltammetric/analytical response of the GCE/PAA/AgNPs/CYP2E1 and GCE/PPy/AgNPs/CYP2E1 biosensors for the standard ETH and RIF solutions were measured using the following parameters: cyclic voltammetry, in a window -1.0 V to +1.5 V

(GCE/PAA/AgNPS) and -0.9 V to +0.5 V (GCE/PPy/AgNPs), with a sensitivity of 100µA at 50 mV/s; and the same window for differential pulse voltammetry were used, respectively. The parameters used for differential pulse voltammetry; the pulse height was 50 mV, pulse width 20 mV and step time was 100 ms.

A.3 UV-visible absorbance analysis

A.3.1 UV-visible absorbance analysis of AgNPs

From the stock solution of the synthesized 1 mM AgNPs, the absorbance of the nanoparticles was measured using Jasco V570 UV-visible spectroscopy. The Jasco V570 spectroscopy is a simple double beam spectrometer. One beam illuminates the reference cell holder and the other illuminates the sample. This configuration enables reference correction to be applied continually throughout a measurement. The absorbance was measured at a range of 200 to 800 nm. An 800 µL of the 1 mM silver nanoparticles was mixed with 3 mL of phosphate buffer solution in a 4 mL quartz cuvette (1cm path), while in the other cuvette containing PBS was used as a reference/blank solution.

A.3.2 UV-visible absorbance analysis of AgNPs/PAA

1 µL of 5mg/mL PAA and 800 µL of the 1 mM silver nanoparticles were mixed with 3 mL of phosphate buffer solution in a 4 mL quartz cuvette (1cm path) and the absorbance measurements were taken similarly to section ***A.3.1***.

A.3.4 UV-visible absorbance analysis of PAA

1 µL of 5mg/mL PAA was diluted with 3 mL of phosphate buffer solution in a 4 mL quartz cuvette (1cm path and the absorbance measurements of PAA were taken similarly to section ***A.3.1***.

A.4 Scanning electron microscopy analysis

The procedure for the preparation of the GCE/PAA, GCE/PAA/AgNPs, GCE/PPy and GCE/PPy/AgNPs electrodes for scanning electron microscopy (SEM) analysis was done in the same way as the preparation of these electrodes for electrochemical analysis. The only difference in preparing the electrodes for SEM analysis was that the screen printed carbon electrodes (SPCE) were used instead of glassy carbon electrode in order to accommodate the configuration of SEM instrument. After the electrodeposition and drop coating of the materials respectively, the modified screen printed carbon electrodes were thoroughly dried overnight and kept in a sealed Petri dish container in readiness for SEM analysis. The SEM analysis was performed on a GeminiSEM 300, ZEISS scanning electron microscopy.

A.5 Atomic force microscopy analysis

The preparation of the electrodes for atomic force microscopy (AFM) analysis was the same as the preparation of electrodes for SEM analysis in section ***A.4***. The AFM analysis was performed on the Dimension Icon Bruker's high-resolution atomic force microscopy.

B. Description of the techniques used

B.1 Electrochemical techniques

B.1.1 Electrodes

Two electrodes are enough to measure analyte response, but usually three electrode devices are used. The current or electrochemical phenomena is measured at the working electrode (glassy carbon electrode for this study with a surface area of 0.071 cm^2). In order to establish a desired voltage between the working electrode and the reference electrode solution (analyte), electrical contact must be made with the solution using a reference electrode (Ag/AgCl) and counter electrode (platinum wire). A reference electrode maintains a fixed, reproducible electrical potential between the metal contact and the solution allowing a known voltage to be applied. The counter electrode serves as a sink for electrons so that current can be passed from the external circuit through the cell. To maintain the observed current, this electrode will often

oxidize or reduce the solvent/electrolyte, though reactions occur over short period of time and rarely produce any appreciable changes in bulk concentrations.

B.1.2 Cyclic voltammetry

Cyclic voltammetry is the most widely used electrochemical technique for studying the nature of electrochemical reactions in detail. During cyclic voltammetry measurements (potential sweep are conducted linearly between two potentials at a scan rate of ν (mV/s)) the solution is kept stationary and the data obtained can be represented as a current-potential plot known as cyclic voltammogram. It has wide application in the study of redox processes, electrochemical properties of analytes in solution and for the understanding reaction intermediates. The data obtained from cyclic voltammetry measurements can be plotted as shown in Figure 77.

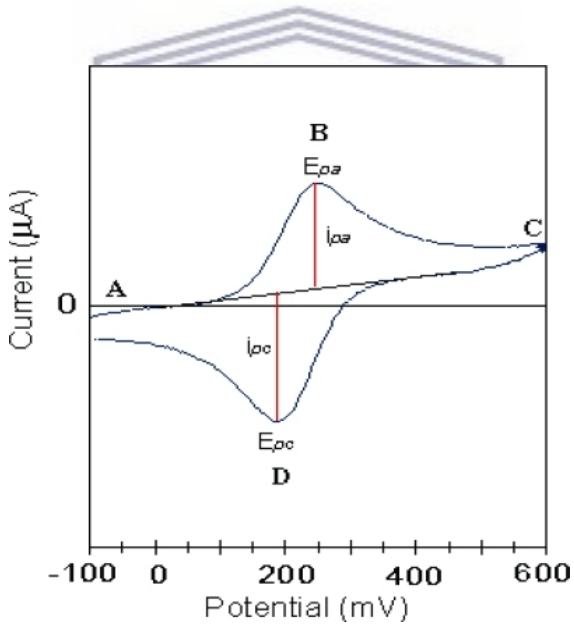

Figure 77: Parameters in cyclic voltammogram are the peak potentials (Epa, Epc) and peak currents (Ipa, Ipc) of the anodic and anodic peaks

The forward scan produces a current peak for any analytes that can be oxidized through the range of the potential scanned. The current increases as the potential reaches the oxidation potential of the analyte, but decreases as the concentration of the analyte is depleted close to the electrode. The information about the redox potential and the electrochemical reaction rates of compounds can be obtained. The Randles-Sevcik expression or equation can be used to

calculate diffusion coefficient, which is the measure of how fast charge can be transported through the material on the surface of the working electrode, i.e., polymer layer.

Randles-Sevcik expression:

$Ip = 2.69x10^5 n^{3/2} ACD^{1/2} \nu^{1/2}$ Equation (1)

where: n = number of electrons transferred per molecule

A = electrode surface area (cm^2)

C = concentration ($mol.cm^{-3}$)

D = diffusion coefficient ($cm^2\ s^{-1}$)

B.1.3 Square wave voltammetry

Square wave voltammetry (SWV) has proved to be a suitable form of potential sweep to investigate redox reactions with overlapping waves. The excitation signal in SWV consists of a symmetrical square wave pulse of amplitude superimposed on staircase wave form of step height ΔE. The forward pulse coincides with the staircase step. The net current (i_{net}) is obtained by taking the difference between the forward and the reverse currents ($i_f - i_r$) and is centred on the redox potential (Figure 78). In SWV, the peak height is directly proportional to the concentration of the electroactive species and direct detection limit as low as 10^{-8} M is possible. SWV is associated with some advantages over cyclic voltammetry. These advantages include excellent sensitivity and rejection of background currents. The scanning speed in SWV is also high. The high speed coupled with computer control and signal averaging allows for experiments to be performed repetitively and increases the signal to noise ratio. SWV is also applied to study electrode kinetics with regard to preceding, following or catalytic homogeneous chemical reactions and determination of species at trace levels.

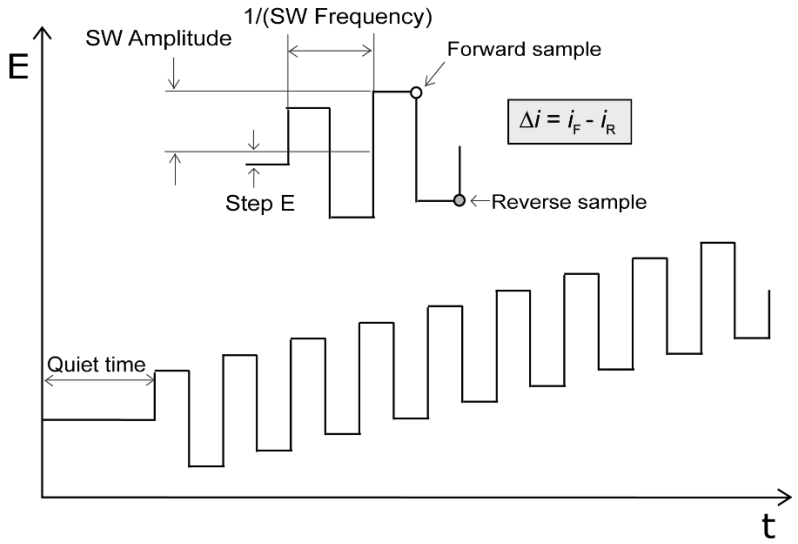

Figure 78: Potential wave form for square wave voltammetry

B.1.4 Differential pulse voltammetry

The basis of differential pulse voltammetry (Figure 79) is the difference in the rate of the decay of the charging and faradaic currents following a potential step. Each potential pulse is fixed at an amplitude between 10 to 100 mV (depending on the range available in the potentiostat) and superimposed on a slowly changing base potential. Current is measured at two points for each pulse, first point is before the application of the pulse and the second point is at the end of the pulse. The difference between current measurements at these two points for each pulse is determined and plotted against the base potential. DPV have similar advantages as SWV over cyclic voltammetry. However, DPV has proved to be a suitable to detect drug at trace level. The study of square wave and differential pulse voltammetric methods for the analysis of olivetol at gold electrode also proved DPV is a better tool than SWV to detect drugs as the linear response and limit of quantification (LOQ) was better than the LOQ and linear response of the SWV [2]. The linearity was between 0.1 - 1.3 µM (SWV) and 0.1 – 1.5 µM (DPV). While the LOQ was found to be 6.45×10^{-9} M using DPV and 1.59×10^{-8} M when SWV was used.

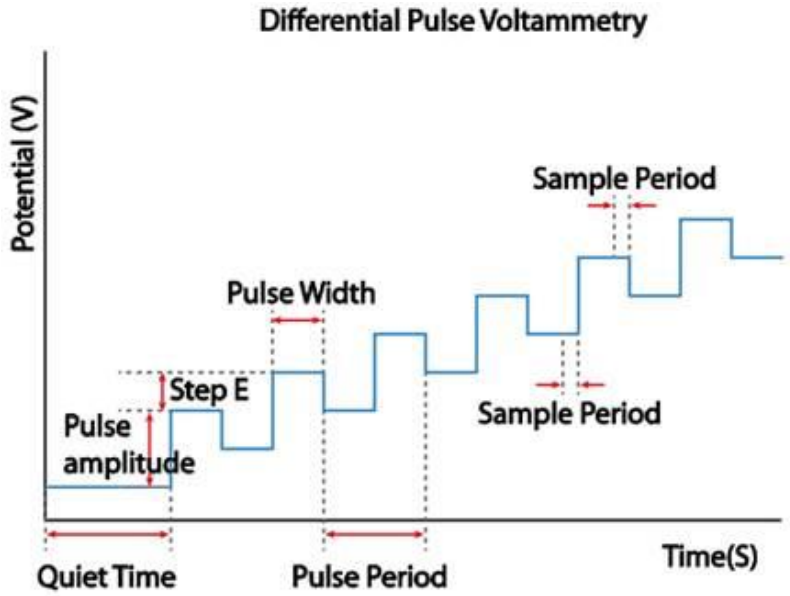

Figure 79: Potential wave form for differential pulse voltammetry

B.2 Analytical techniques

B.2.1 Ultraviolet visible spectroscopy

Ultraviolet and visible spectrometers have been in general use for more than 4 decades and over this period have become the most important analytical instrument in the modern day laboratory. In many applications other techniques could be employed but none rival UV-Visible spectrometry for its simplicity, versatility, speed, accuracy and cost-effectiveness. The UV-visible range is only a small part of the total electromagnetic spectrum, and is generally defined from wavelengths of 190 nm at the high energy ultraviolet (UV) end to about 750 nm at the low energy red end of the spectrum. A vast number of molecules absorb ultraviolet or visible light. Different molecules absorb radiation of different wavelengths. A number of absorption bands can be obtained from absorption spectrum that corresponds to function or structural groups within the molecule. The absorbance of a solution increases as attenuation of the beam increases. Hence the absorbance is directly proportional to the path length, *b*, and the concentration, *c*, of the absorbing species. Beer's law states that: A = *ebc* where *e* is a constant proportionality called absorptivity. Light of other regions of the spectrum gives rise to different types of transitions and hence different types of spectroscopy.

B.2.1.1 Chromophore

A chromophore (literally colour-bearing) group is a functional group, not conjugated with another group, which exhibits a characteristic absorption spectrum in the ultraviolet or visible region.

Table 11: List of common chromophores and their transitions

Chromophore	Compound	Transition	λ_{max} (nm)
C=O	Carboxylic acid	$\pi \rightarrow \pi^*$	200
C=O	Ester	$\pi \rightarrow \pi^*$	210
C=O	Amide	$\pi \rightarrow \pi^*$	205
N=O	Nitromethane	$n \rightarrow \pi^*$	200/275

B.2.2 Scanning electron microscopy

A scanning electron microscopy (SEM) is a powerful microscopy that uses electrons rather than light to form an image of objects such as fractured metal components, foreign particles and residues, polymers, electronic components and biological samples among others. It uses a focused beam of high energy electrons to generate a variety of signals at the surface of solid specimens. The signal derive from electron sample interaction and reveal information about the sample including external morphology (surface of the material; the smoothness or roughness), chemical composition, crystalline structure and orientation of materials making up the sample. The advantages associated with SEM include among others its ability to perform analyses of selected point locations on the sample. Areas ranging from approximately 1 cm to 1 microns can also be imaged in a scanning mode using conventional SEM techniques (magnification ranging from 20X to approximately 80,000X and a spatial resolution of 20 to 200 nm).

B.2.3 Atomic force microscopy

The Dimension Icon AFM is an atomic force microscopy system that enables to make measurements at nanoscale resolution of topography and other properties of the sample such as electrical characterization depending on the choice of mode. This Dimension Icon AFM has a Nanoscope V controller that is able to display and capture up to eight images simultaneously. Different modes of AFM such as ScanAsyst, PeakForce Tapping, TappingMode, Contact Mode, Nanolithography allows to obtain different information about the sample of interest and they also can allow a researcher to choose the mode that is suitable for the sample that is to be analysed/characterized. The XYZ closed-loop head delivers high scan speed, without loss of image quality, to enable greater throughput for data collection. To perform manipulation and lithography at the nanometer and molecular scales, the XYZ closed-up scanner provides probe positioning with no piezo creep and extremely low noise for the best positioning of the sample. This XYZ position noise must at be less or equal to 0.15 nm with an RMS typical imaging bandwidth up to 625 Hz. While for heating and cooling characterization of the samples, the execute temperature control and thermal analysis on samples must range from -35^{0}C to 250^{0}C while scanning in various AFM modes. Alternatively, thermal probe can be used to perform sub-100 nm local heating to 400^{0}C. The material mapping is the imaging mode that was used for this study, it allows to map and distinguish between nanochemical properties while simultaneously imaging the topography at high resolution. This mode operates over an extremely wide range (1MPA to 50 GPA for modulus and 10pN to 10μN) to characterize large variety of sample types.

B.3 References

1. Andreescu, D., Wanekaya, A. K., Sadik, O. a. & Wang, J. Nanostructured polyamic acid membranes as novel electrode materials. *Langmuir* **21,** 6891–6899 (2005).

2. Bagalkoti, J. T., Pattar, V. P. & Nandibewoor, S. T. Square wave and differential pulse voltammetric methods for the analysis of olivetol at gold electrode. *J. Electrochem. Sci. Eng.* **7,** 77 (2017).

3. Strik, D. P., Ter Heijne, A., Hamelers, H. V. M., Saakes, M. & Buisman, C. Feasibility Study on Electrochemical Impedance Spectroscopy for Microbial Fuel Cells: Measurement Modes & Data Validation. *ECS Trans.* **13,** 27–41 (2008).